Oncogenic KRAS renders cells resistant to ferroptosis by upregulating FSP1

Inaugural-Dissertation

zur

Erlangung des Doktorgrades

Dr. rer. nat

der Mathematisch-Naturwissenschaftlichen Fakultät

der Universität zu Köln

Köln, 2022

vorgelegt von

Fabienne Müller

aus Lauterbach

First reviewer and examiner:

Prof. Dr. Silvia von Karstedt

Department of Translational Genomics and

CECAD Research Center

University of Cologne

Second reviewer and examiner:

Prof. Dr. Manolis Pasparakis

CECAD Research Center

Institute for Genetics

University of Cologne

Chair of the thesis defense committee:

Prof. Dr. Jan Riemer

Biochemistry - Redox Metabolism

Institute of Biochemistry

University of Cologne

Day of thesis defense: 13.02.2023

INDEX

FIGURE INDEX III

LIST OF ABBREVIATIONS IV

ABSTRACT VII

ZUSAMMENFASSUNG IX

1 INTRODUCTION 1

1.1 CELL DEATH 1

1.2 FERROPTOSIS 2

1.2.1 INDUCTION OF FERROPTOSIS 3

1.2.2 REGULATORS OF FERROPTOSIS 5

1.2.2.1 FSP1 (FERROPTOSIS SUPPRESSOR PROTEIN 1) 5

1.2.2.2 GPX4 AND SYSTEM XC- 6

1.2.2.3 ANTIOXIDANT DEFENSE SYSTEMS OF FERROPTOSIS 7

1.2.2.4 NRF2 (THE MASTER FACTOR FOR ANTIOXIDANT RESPONSE IN FERROPTOSIS) 8

1.2.3 CHEMICAL FERROPTOSIS INDUCERS 10

1.2.4 FERROPTOSIS INHIBITORS 11

1.2.5 RELEVANCE OF FERROPTOSIS *IN VIVO* 11

1.2.6 GENETIC EVIDENCE FOR FERROPTOSIS IN CANCER 13

1.2.7 INFLUENCE OF RAS ON FERROPTOSIS SENSITIVITY 13

1.3 INFLUENCE OF CELL DENSITY ON FERROPTOSIS RESISTANCE 16

1.4 RAS GTPASES 17

1.4.1 RAS STRUCTURE 18

1.4.2 DOWNSTREAM SIGNALING PATHWAYS OF RAS 19

1.4.3 RAS MUTATIONS IN HUMAN CANCER 21

1.4.4 TARGETING RAS / ANTI-RAS THERAPY 25

1.5 KRAS-MEDIATED REWIRING OF CELL DEATH 26

1.6 AIM OF THIS STUDY 27

2 PUBLICATION / MANUSCRIPT 28

2.1 ELEVATED FSP1 PROTECTS KRAS-MUTATED CELLS FROM FERROPTOSIS DURING TUMOR INITIATION 28
2.2 SUPPLEMENTARY INFORMATION 45
3 RESULTS 53
4 DISCUSSION 67
4.1 FERROPTOSIS RESISTANCE IN KRAS-MUTATED CELLS 67
4.2 ONCOGENIC KRAS-MEDIATED PROTECTION OF LIPID PEROXIDATION 68
4.3 FSP1 AS AN ANTIOXIDANT DEFENSE MECHANISM 69
4.4 UPREGULATION OF FSP1 VIA NRF2 AND THE MAPK PATHWAY IN KRAS-MUTATED CELLS 72
4.5 FSP1 EXPRESSION IN KRAS-MUTATED CANCERS 74
4.6 FERROPTOSIS RESISTANCE IS DENSITY DEPENDENT 75
5 CONCLUDING REMARKS AND FUTURE PERSPECTIVES 77
6 REFERENCES 79
EIDESSTATTLICHE ERKLÄRUNG ZUR DISSERTATION 100
ACKNOWLEDGEMENT 101

FIGURE INDEX

Figure 1: Different types of regulated cell deaths (RCDs) 2
Figure 2: Ferroptosis pathway 4
Figure 3: KEAP1-NRF2 pathway 9
Figure 4: Hippo-YAP pathway.....17
Figure 5: RAS effector pathways 21
Figure 6: RAS isoforms and mutation occurrence in all human cancers 22
Figure 7: Diagrams of hotspot mutations in RAS oncogenes 24
Figure 8: Cells expressing $KRAS^{G12D}$ are the most resistant to ferroptosis induction 54
Figure 9: Expression of oncogenic $KRAS^{G12D}$ protects cells from cell growth inhibition during ferroptosis induction.....56
Figure 10: $KRAS^{G12D}$-mutated human pancreatic cancer cell lines are more resistant to ferroptosis induction 57
Figure 11: G12C-inhibition enhances sensitivity to ferroptosis induction.....58
Figure 12: Ferroptosis resistance is density dependent 59
Figure 13: $KRAS^{G12D}$ protects cells from ferroptosis in middle density 60
Figure 14: FSP1 upregulation is density dependent.....61
Figure 15: General ROS accumulation is density dependent.....62
Figure 16: Analogues of CoQ10 protect cells from ferroptosis 64
Figure 17: NRF2 upregulation via siKEAP1 knockdown or TBHQ treatment protects cells from ferroptosis.....65
Figure 18: Ferroptosis inhibition suppresses spheroid growth.....66
Figure 19: The KRAS-NRF2-FSP1-axis 72

LIST OF ABBREVIATIONS

A549	Adenocarcinoma Human Alveolar Basal Epithelial Cells
AA	Arachidonic Acid
ACC	Acetyl-CoA Carboxylase
ACD	Accidental Cell Death
ACSL4	Acyl-CoA Synthetase Long Chain Family Member 4 (ACSL4)
AdA	Adrenic Acid
ADCD	Autophagy-Dependent Cell Death
ADP	Adenosine Diphosphate
AIFM1	Apoptosis Inducing Factor Mitochondria Associated 1
AIFM2	Apoptosis Inducing Factor Mitochondria Associated 2
AML	Acute Myeloid Leukemia
ARE	Antioxidant Response Element
ART	Artesunate
ATP	Adenosine Triphosphate
BJeLR	Human Foreskin Fibroblasts
BSO	Buthionine Sulfoximine
Calu-1	Lung Carcinoma Cell Line
CBS	Cystathionine Beta-Synthase
CoA	Coenzyme A
CoQ10	Ubiquinone or Coenzyme Q10
COSMIC	Somatic Mutations in Cancer
CSE	Cystathionine γ-Lyase
CUL3	Cullin3
D-PUFAs	Deuterated Polyunsaturated Fatty Acids
DFO	Deferoxamine
DLBCL	Diffuse Large B-Cell Lymphoma
DMT1	Divalent Metal Transporter 1
DPIs	Diverse Pharmacological Inhibitors
EGF	Epidermal Growth Factor
EGFR	Epithelial Growth Factor Receptor
ER	Endoplasmic Reticulum
Erastin	Eradicator of RAS and ST-Expressing Cells
ERK	Extracellular Signal-Regulated Protein Kinases 1/2
FAD	Flavin Adenine Dinucleotide
Fe^{2+}	Ferrous Iron, heme iron
Fe^{3+}	Ferric Iron, non-heme iron
Fer1	Ferrostatin-1
FOXO	Forkhead Box O
FSP1	Ferroptosis Suppressor Protein 1
FTI	Farnesyltransferase Inhibitor
GAP	GTPase-Activating Protein

GCL	Glutamate-Cysteine Ligase
GCLC	Glutamate-Cysteine Ligase Catalytic Subunit
GCLM	Glutamate-Cysteine Ligase Modifier Subunit
GDP	Guanosine Diphosphate
GEF	Guanine Nucleotide Exchange-Factor
GPCR	Protein–Coupled Receptor
GPX	Glutathione Peroxidase
GSH	Glutathione
GSR	Glutathione-Disulfide Reductase
GSS	Glutathione Synthetase
GSSG	Glutathione Disulfide
GTP	Guanosine Triphosphate
H_2O_2	Hydrogen Peroxide
HCC	Hepatocellular Carcinoma Cells
HL-60	Acute Myeloid Leukemia Cells harboring a $NRAS^{Q61L}$ Mutation
HME	Human Mammary Epithelial
HMOX1, HO-1	Heme oxygenase-1
HO·	Hydroxal Radical
HRAS	Harvey Rat Sarcoma Virus
HVR	Hypervariable Region
ICD	Immunogenic Cell Death
IKE	Imidazole Ketone Erastin
JNK	C-Jun N-Terminal Kinase
KEAP1	Kelch-Like ECH-Associated Protein 1
KO	Knockout
KRAS	Kirsten Rat Sarcoma Virus
LDCD	Lysosomal-Dependent Cell Death
LIP	Labile Iron Pool
Lip1	Liproxstatin-1
LOX	Lipoxygenase
LPCAT3	Lysophosphatidylcholine Acyltransferase 3
MAPK	Mitogen-Activated Protein Kinase
MEF	Mouse Embryonic Fibroblast
MLKL	Mixed Lineage Kinase Domain-Like Protein
MMP	Mitochondrial Membrane Potential
MMPs	Matrix Metalloproteinases
MPT	Mitochondrial Permeability Transition
mTOR	Mammalian Target Of Rapamycin
NAC	N-Acetyl Cysteine
NADP+	Nicotinamide Adenine Dinucleotide Phosphate
NADPH	Nicotinamide Adenine Dinucleotide Phosphate Hydrogen
NETs	Neutropil Extracellular Traps
NFκB	Nuclear Factor Kappa-Light-Chain-Enhancer Of Activated B Cells

NMD	Nonsense-Mediated Decay
NOX	NADPH Oxidase
NQO1	NAD(P)H Quinone Oxidoreductase 1
NRAS	Neuroblastoma RAS Viral Oncogene Homolog
NRF1	Nuclear Factor Erythroid-2–Related Factor 1
NRF2	Nuclear Factor Erythroid 2-Related Factor 2
O_2	Oxygen
OXPHOS	Oxidative Phosphorylation
PDAC	Pancreatic Ductal Adenocarcinoma
PE	Phosphatidylethanolamine
PI3K	Phosphoinositide-3-Kinase
PKB / AKT	Protein Kinase B / Gene AKT
PL	Phospholipid
PRDX	Peroxireductase
PUFA	Polyunsaturated Fatty-Acid
PUFA-PL	Polyunsaturated Fatty-Acid-Containing Phospholipid
RBX1	Ring Box Protein 1
RCD	Regulated Cell Death
RIPK	Receptor-Interacting Protein Kinase
RMS13	Rhabdomyosarcoma Cells
ROS	Reactive Oxygen Species
RSL3	RAS-Selective Lethal 3
RTA	Radical Trapping Antioxidant
RTK	Receptor-Tyrosine Kinase
shRNA	short hairpin RNA
SLC7A11	Solute Carrier Family 7 Member 11
SLC7A11	Solute Carrier Family 3 member 2
SOD	Superoxid-Dismutase
STEAP3	Six-Transmembrane Epithelial Antigen Of Prostate 3
System Xc-	Glutamate-Cysteine Antiporter System Xc-
TAZ	paralog WW domain containing transcription regulator 1 (WWTR1,also called TAZ)
TCA	Mitochondrial Tricarboxylic Acid
TCGA	The Cancer Genome Atlas
TFRC	Transferrin Receptor
TMEM173/STING	Transmembrane Protein 173/Stimulator Of Interferon Genes
TNF	Tumor Necrosis Factor
TRAIL	TNF-Related Apoptosis-Inducing Ligand
VDAC	Voltage-Dependent Anion Channel
VEGF	Vascular Endothelial Growth Factor
WT	Wild Type
xCT	Solute Carrier Family 7 Member 11 (SLC7A11)
YAP1/YAP	Yes-Associated Protein 1

ABSTRACT

RAS genes are the most frequently mutated oncogenes across human cancers and mutations in RAS lead to malignant transformation, tumor initiation and tumor maintenance. Mutant KRAS is the most common and most aggressive isoform and occurs in the deadliest cancers worldwide. One key feature of oncogenic KRAS expression is the upregulation of reactive oxygen species (ROS). Moderate ROS levels activate several cancer cell progressions and promote cellular transformation, whereas increased ROS levels result in cell death. The exact mechanism how cells with elevated ROS levels due to oncogenic KRAS expression escape cell death remains still unknown.

Here, we identified in an isogenic cellular system that expression of oncogenic KRAS compared to wild type renders cells more resistant to ferroptosis, a recently recognized form of regulated cell death. In this study, we found that $KRAS^{G12D}$-expressing cells exhibit basal higher general and lipid ROS levels and are protected from lipid peroxidation upon ferroptosis induction. Moreover, our study revealed that KRAS-mutant cells increase ferroptosis suppressor protein 1 (FSP1) expression to protect cells from lipid peroxidation. In particular, we discovered that FSP1 is upregulated upon NRF2 activation. Additionally, we ascertained that FSP1 is enhanced as a consequence of KRAS mediated activation of mitogen-activated protein kinase (MAPK) pathway. Strikingly, for the first time we showed that elevated FSP1 expression in $KRAS^{WT}$ cells *in vitro* promotes cellular transformation in soft agar assays and spheroid growth in spheroid assays. Furthermore, our study revealed that FSP1 overexpression in $KRAS^{WT}$ tumors accelerates tumor onset – in the absence of oncogenic $KRAS^{G12D}$ – *in vivo*. Additionally, this study demonstrated that only pharmacological induction of ferroptosis in combination with FSP1 inhibition decreases pancreatic organoids derived from LsL-$KRAS^{G12D}$ expressing mouse models. Interestingly, we determined that in cancer types with high KRAS mutational frequencies such as non-small cell lung cancer (NSCLC), colorectal cancer (CRC) and pancreatic ductal adenocarcinoma (PDAC) FSP1 expression is increased compared to the respective original tissue. Moreover, FSP1 upregulation correlates with NRF2 expression in PDAC patient datasets.

Taken together, our work contributes to the understanding of oncogenic KRAS induced ferroptosis resistance and FSP1 regulated ferroptosis protection. Hence, we propose

that KRAS mutant cells upregulate FSP1 to overcome ferroptosis during cellular transformation and tumor establishment. Therefore, we suggest considering FSP1 suppression in combination with ferroptosis inhibition as a clinical therapy option to treat cancer patients harboring a KRAS-mutation.

ZUSAMMENFASSUNG

RAS-Gene sind die am häufigsten mutierten Onkogene bei menschlichen Krebserkrankungen und RAS-Mutationen führen zu bösartiger Transformation, Tumorentstehung und Tumorerhaltung. Mutiertes KRAS ist die häufigste und aggressivste Isoform und kommt bei den tödlichsten Krebsarten weltweit vor. Ein Hauptmerkmal der onkogenen KRAS-Expression ist die Hochregulierung von reaktiven Sauerstoffspezies (ROS). Moderate ROS-Konzentrationen aktivieren mehrere Krebszellen und fördern die Zelltransformation, während erhöhte ROS-Konzentrationen zum Zelltod führen. Der genaue Mechanismus, wie Zellen mit erhöhten ROS-Werten aufgrund einer onkogenen KRAS-Expression dem Zelltod entgehen, ist noch unbekannt.

Wir haben in einem isogenen Zellsystem festgestellt, dass die Expression von onkogenem KRAS im Vergleich zum Wildtyp die Zellen resistenter gegen Ferroptose macht, eine kürzlich anerkannte Form des regulierten Zelltods. In dieser Studie fanden wir heraus, dass $KRAS^{G12D}$-exprimierende Zellen basal höhere allgemeine und Lipid-ROS-Werte aufweisen und bei Ferroptose-Induktion vor Lipidperoxidation geschützt sind. Außerdem zeigte unsere Studie, dass KRAS-mutierte Zellen die Expression des Ferroptose-Suppressor Proteins 1 (FSP1) erhöhen, um die Zellen vor Lipidperoxidation zu schützen. Wir entdeckten, dass FSP1 bei NRF2-Aktivierung hochreguliert wird. Darüber hinaus konnten wir feststellen, dass FSP1 durch die KRAS-vermittelte Aktivierung des Mitogen-aktivierten Proteinkinase (MAPK)-Signalwegs verstärkt wird. Bemerkenswert ist, dass wir zum ersten Mal zeigen konnten, dass eine erhöhte FSP1-Expression in $KRAS^{WT}$-Zellen *in vitro* die Zelltransformation in Soft-Agar-Experimenten und das Sphäroidwachstum in Sphäroid-Experimenten fördert. Darüber hinaus zeigte unsere Studie, dass die Überexpression von FSP1 in $KRAS^{WT}$-Tumoren das Auftreten von Tumoren – in Abwesenheit von onkogenem $KRAS^{G12D}$ – *in vivo* beschleunigt. Weiterhin konnte in dieser Studie gezeigt werden, dass nur die pharmakologische Induktion der Ferroptose in Kombination mit der FSP1-Inhibition die Pankreasorganoide aus LsL-$KRAS^{G12D}$-exprimierenden Mausmodellen reduziert. Wir haben interessanterweise festgestellt, dass bei Krebsarten mit hoher KRAS-Mutationshäufigkeit wie dem nicht-kleinzelligen Lungenkrebs (NSCLC), dem kolorektalen Karzinom (CRC) und dem duktalen Adenokarzinom der Bauchspeicheldrüse (PDAC) die FSP1-Expression im Vergleich

zum jeweiligen Ausgangsgewebe erhöht ist. Außerdem korreliert die Hochregulierung von FSP1 mit der NRF2-Expression in PDAC-Patientendatensätzen.
Insgesamt trägt unsere Arbeit somit zum Verständnis der onkogenen KRAS-induzierten Ferroptose-Resistenz und des durch FSP1 regulierten Ferroptose-Schutzes bei. Wir gehen davon aus, dass KRAS-mutierte Zellen FSP1 hochregulieren, um die Ferroptose während der Zelltransformation und der Tumorbildung zu überwinden. Daher schlagen wir vor, die Unterdrückung von FSP1 in Kombination mit der Ferroptosehemmung als klinische Therapieoption zur Behandlung von Krebspatienten und Krebspatientinnen mit einer KRAS-Mutation in Betracht zu ziehen.

1 INTRODUCTION

1.1 CELL DEATH

Cell death is a critical and active process in multicellular organisms. Controlling cell death is crucial to maintain tissue homeostasis, to eliminate potentially harmful cells and to regulate development [1], [2]. Abnormal cell death plays a major role in several human diseases including cancer, autoimmune diseases, organ failure, neurodegeneration and infection [2]–[5].

There are two different ways by which cells can undergo cell death: accidental cell death (ACD) and regulated cell death (RCD). ACD can be triggered by physical, chemical or mechanical stimuli to the cell and RCD is characterized by a complex molecular machinery [6]. RCD can be pharmacologically or genetically modulated [6] and activated when intracellular or extracellular perturbations of the microenvironment are unrecoverable and cellular homeostasis restoration fails after stress response [7]. Based on macroscopic morphological alterations, historically three major different forms of RCD have been described: type I cell death (apoptosis), type II cell death (autophagy) and type III cell death (necrosis) [8], [9]. Over the past years multiple novel cell death modalities have been classified and characterized through distinct morphologies caused by different mechanisms [6]. In Figure 1 several different types of regulated cell death are pictured. Two of the most common and well-studied RCD types are apoptosis and necroptosis. Apoptosis and Necroptosis can be triggered either by extracellular stimuli or within a signaling cascade in the cell. Apoptosis is enabled by caspases activation, while necroptosis is activated via caspases suppression [10]. However, in the following chapters, this work will focus on another type of regulated cell death called ferroptosis.

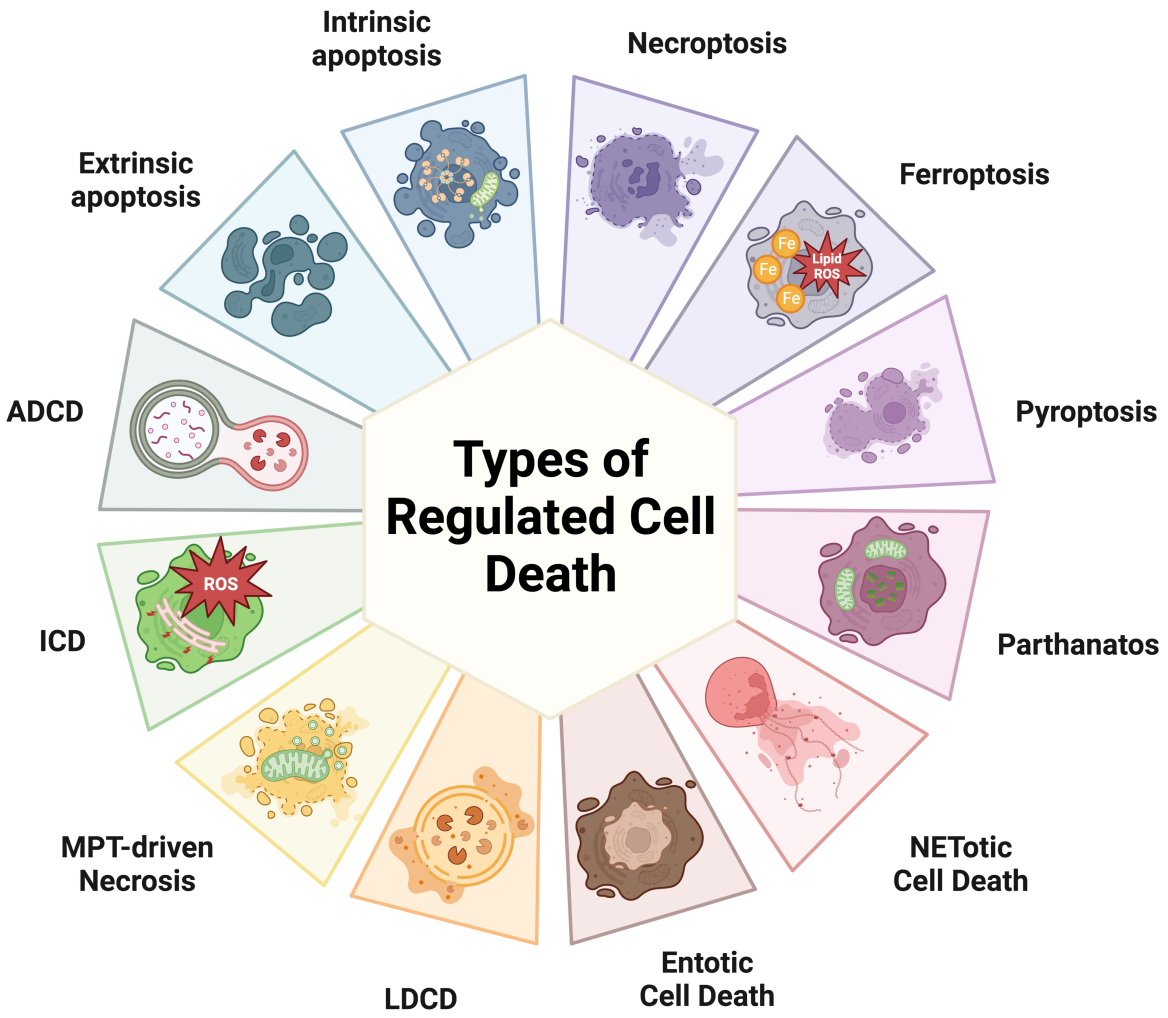

Figure 1: Different types of regulated cell deaths (RCDs)
Schematic illustration of different types of regulated cell death, which are mediated by specific intra- or extracellular molecular triggers and characterized by unique cell responses and conducts. ADCD: autophagy-dependent cell death, ICD: immunogenic cell death, NET: neutrophil extracellular trap, LDCD: lysosome-dependent cell death, MPT: mitochondrial permeability transition. Adapted from Galluzzi et al. 2018 [6]. Scheme was drawn by using licensed biorender.com.

1.2 FERROPTOSIS

(ADOPTED FROM BEBBER, MÜLLER ET AL. 2020)

Ferroptosis is an iron and lipid peroxidation dependent type of regulated cell death (RCD). This type of cell death is characterized by increased levels of lipid reactive oxygen species (ROS) and its dependency on intracellular iron, which gives ferroptosis its name [11].

Ferroptosis was first discovered in 2003 in a synthetic lethal chemical screening for genotype-selective antitumor agents in which a novel compound named erastin (for eradicator of RAS and ST-expressing cells) was described to target rat sarcoma

(RAS)-mutant cells and lead to a non-apoptotic form of cell death [12]. Later, it was described that ferroptosis is an oxidative related iron-dependent type of cell death by Yagoda et al. and Yang and Stockwell, who ascertained small molecules erastin and RAS-selective lethal 3 (RSL3) to induce oxidative species resulting in a non-apoptotic cell death in cells harboring oncogenic RAS [13], [14]. In contrast to other types of RCD such as apoptosis or necroptosis, ferroptosis is independent from caspases and receptor-interacting protein kinase (RIPK) activities [6].

1.2.1 INDUCTION OF FERROPTOSIS

Ferroptosis requires redox-active iron. Iron is an essential nutrient and comes in two different forms: heme iron and non-heme iron. Non-heme iron (Fe^{3+}) is binding to transferrin and then transported into the cell through the membrane protein transferrin receptor (TFRC/CD71). Endosomal six-transmembrane epithelial antigen of prostate 3 (STEAP3) reduces Fe^{3+} to Fe^{2+} in endosomes and releases it into a labile iron pool (LIP) in the cytoplasm through a divalent metal transporter 1 (DMT1) [15], [16]. Interestingly, DMT1 has been shown to be upregulated upon ferroptosis-induction [17]. Once divalent iron (Fe^{2+}) is in the cytoplasm the Fenton reaction catalyzes hydroxyl radicals (HO·) when Fe^{2+} and hydrogen peroxides (H_2O_2) react, resulting in damage of cellular DNA, proteins or lipids [16], [18]. Therefore, one major hallmark of ferroptosis is iron which donates electrons to generate ROS leading to lipid peroxidation and the initiation of cell death [19]. Of note, ferroptosis can be inhibited by iron chelator deferoxamine (DFO) or genetic inhibition of cellular iron uptake [11].
Besides intracellular iron accumulation another hallmark of ferroptosis is lipid peroxidation. Lipid peroxidation destabilizes the lipid bilayer, which leads to oxidative damage of the biomembrane or other lipoproteins [20]. The main targets of lipid peroxidation are the polyunsaturated fatty-acid-containing phospholipids (PUFA-PLs) [21]. It has been identified that arachidonic acid (AA)- and adrenic acid (AdA)-containing phosphatidylethanolamine (PE) species were the top lipid targets of lipid peroxidation during ferroptosis [22]. Peroxidation of PUFAs in membranes results in lethal lipid radicals generated from toxic lipid hydroperoxides, which induce ferroptosis [23]. PUFA-PLs are oxidized in two different ways: non-enzymatically and enzymatically. In the non-enzymatical free-radical chain reaction hydroxyl radicals (HO·) generated from Fenton reactions can react directly with PUFAs and thereby trigger lipid ROS production [24]. The enzymatic way is more complex: Ferroptosis

induction is activated via the accumulation of oxygenated PUFAs arachidonic acid - containing PE (AA-PE) - specifically AA-OOH-PE - and its elongated version adrenoyl (AdA-PE). The formation of AA-OOH-PE requires three enzymes: acyl-CoA synthetase long chain family member 4 (ACSL4), lysophosphatidylcholine acyltransferase 3 (LPCAT3) and lipoxygenases (LOXs) [16], [22], [25]. More precisely the AA-OOH-PEs is produced via the ACSL4-catalyzed formation of AA and AdA with Coenzyme A (CoA) into acyl-CoA, followed by the LPCAT3-controlled esterification of AA-CoA into AA-PE and completed by the LOX-oxidized form of AA-PE into AA-OOH-PE [22], [25]. Interestingly, ACSL4 was described as one of the first essential regulatory proteins in the ferroptotic cell death process [26]. Moreover, it has been found that ACSL4 and LPCAT3 were significantly enriched in ferroptosis-sensitive cells [26]–[28]. Taken together these findings demonstrate that peroxidation of PUFAs is an essential process in the ferroptosis pathway.

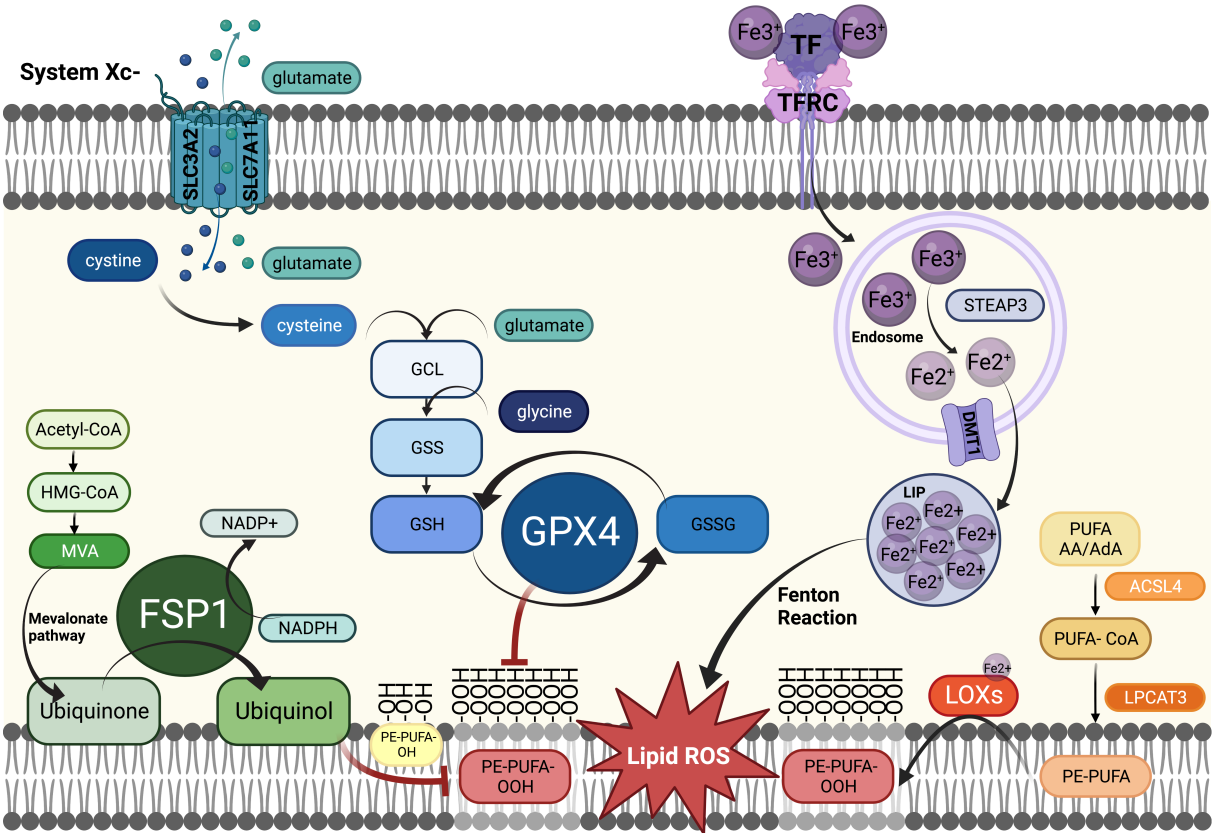

Figure 2: Ferroptosis pathway

Schematic illustration of the ferroptosis pathway. Ferroptosis is characterized by the iron-dependent lipid peroxidation. Main peroxidation targets are polyunsaturated fatty-acids (PUFAs)-containing phospholipids. Peroxidation (-OOH) of phosphatidylethanolamine (PE)-PUFAs (PE-PUFA-OOH) mediates membrane destabilization and rupture, which induce ferroptosis [23]. PE-PUFA-OOH are generated from PUFA-arachidonic acid and -adrenic acid (PUFA-AA/AdA), which acyl-CoA synthetase long chain family member 4 (ACSL4) catalyzes into Coenzyme A (PUFA-CoA). Next, esterification of PUFA-CoA into PE-PUFA is controlled

by lysophosphatidylcholine acyltransferase 3 (LPCAT3). In a final step, lipoxygenase (LOX) oxidizes PE-PUFAs into PE-PUFA-OOH [22], [25]. Lipid peroxidation can be triggered by the intracellular iron accumulation [19]. Through the membrane protein transferrin receptor (TFRC) none-heme iron (Fe^{3+}) is transported into the cell. In an endosome, six-transmembrane epithelial antigen of prostate 3 (STEAP3) reduces Fe^{3+} to Fe^{2+} and releases Fe^{2+} through a divalent metal transporter 1 (DMT1) into a labile iron pool (LIP) in the cytoplasm [15], [16]. Once divalent iron (Fe^{2+}) is in the cytoplasm the Fenton reaction catalyzes hydroxyl radicals ($HO\cdot$) when Fe^{2+} and hydrogen peroxides (H_2O_2) react, resulting in lipid peroxidation [16], [18]. Glutathione peroxidase 4 (GPX4) can prevent cells from lipid ROS. By using glutathione (GSH) as a redox equivalent GPX4 reduces lipid hydroperoxides (PE-PUFA-OOH) to their corresponding lipid alcohols (PE-PUFA-OH) and thereby protecting cells from lipid peroxidation [29], [30]. Oxidized glutathione disulfide (GSSG) is recycled by glutathione-disulfide reductase (GSR) and nicotinamide adenine dinucleotide phosphate hydrogen/hydrogen (NADPH/H+) back into GSH [30]. GSH is synthesized by GSH synthetase (GSS) and glutamate-cysteine ligase (GCL). GSH synthesis is dependent on the availability of cysteine, glutamate and glycine [22], [31]. Cysteine is reduced from cystine, which is shuttled into the cell via the glutamate-cysteine antiporter system Xc- (System Xc-). System Xc- is an amino acid antiporter and consists of two subunits: the functional unit SLC7A11 (solute carrier family 7 member 11) and the regulatory subunit SLC3A2 (solute carrier family 3 member 2), which exchange extracellular cystine into and intracellular glutamate out of the cell [32]–[34]. Another way to protect cells from ferroptosis is the ferroptosis suppressor protein 1 (FSP1), which reduces ubiquinone to ubiquinol by using NAD(P)H. Ubiquinol mediates as a lipophilic radical trapping antioxidant (RTA) by trapping lipid peroxyl radicals thereby preventing lipid peroxidation [35], [36]. Ubiquinone is produced by the mevalonate pathway. For the mevalonate pathway the synthesis of 3-hydroxy-3-methylglutaryl-CoA (HMG)-CoA from acetyl-CoA through acetoacetyl-CoA is required to catalyze mevalonate (MVA), which is essential for the mevalonate pathway to generate ubiquinone [37], [38]. Scheme was drawn by using licensed biorender.com.

1.2.2 REGULATORS OF FERROPTOSIS

1.2.2.1 FSP1 (FERROPTOSIS SUPPRESSOR PROTEIN 1)

One key regulator, which protects cells from lipid ROS, is apoptosis inducing factor mitochondria associated 2 (AIFM2). AIFM2 was newly identified as an anti-ferroptotic gene and therefore renamed into ferroptosis suppressor protein 1 (FSP1). AIFM2 was described as a flavoprotein, which was believed to trigger caspase-independent apoptosis because of its sequence similarity to apoptosis-inducing factor mitochondria-associated 1 (AIFM1), another initially postulated pro-apoptotic gene [39]. However, recently in 2019, FSP1 was discovered as a ferroptosis protective gene. It was shown in two separate studies that FSP1 can compensate loss of GPX4 activity and is independent on ACSL4 expression and oxidizable fatty acids. In one study they identified FSP1 in a screen for genes in ferroptosis resistant cells complementing GPX4 loss and in another study they found FSP1 as a potent ferroptosis resistance factor in a CRISPR-Cas9 knockout screen for synthetic lethality with GPX4 inhibition using small molecule inhibitor RSL3 [35], [36].

FSP1 contains a short N-terminal hydrophobic sequence and a canonical flavin adenine dinucleotide (FAD)-dependent oxidoreductase domain [36]. Both studies revealed that N-terminal myristylation recruits FSP1 to the plasma membrane, where it functions as an oxidoreductase to reduce ubiquinone (also known as coenzyme Q10 (CoQ10)) to ubiquinol [35], [36]. Ubiquinone is produced by the mevalonate pathway. For the mevalonate pathway the synthesis of 3-hydroxy-3-methylglutaryl (HMG)-CoA from acetyl-CoA through acetoacetyl-CoA is required to catalyze mevalonate (MVA). MVA is essential for the mevalonate pathway, which is an important anabolic pathway synthesizing different metabolites such as ubiquinone [37], [38]. Ubiquinone exists in three redox states: fully oxidized (ubiquinone), partially reduced (semiquinone or ubisemiquinone), and fully reduced (ubiquinol). Ubiquinol functions as a lipophilic radical trapping antioxidant (RTA) by trapping lipid peroxyl radicals that mediate lipid peroxidation [35], [36]. FSP1 uses nicotinamide adenine dinucleotide (phosphate) hydrogen (NAD(P)H) *in vitro* for the reduction of CoQ10 [40]. Interestingly, it was shown that FSP1 expression correlates with ferroptosis resistance in hundreds of cancer cell lines. Specifically, it was demonstrated that FSP1 mediates resistance to ferroptosis in lung cancer cell lines and in mouse tumor xenografts. These data suggest that cancer cells upregulate FSP1 as a strategy to escape ferroptosis cell death [35], [36]. Of note, deletion of NAD(P)H quinone oxidoreductase 1 (NQO1), a quinone/CoQ oxidoreductase, did not affect sensitivity to RSL3, but FSP1 and NQO1 knockout cells ($FSP1^{KO}/NQO1^{KO}$) were more sensitive than $FSP1^{KO}$ cells. These findings reinforce the data that FSP1 alone is capable to suppress ferroptosis [36]. In another just recently published study, it was investigated that dihydroorotate dehydrogenase (DHODH) inhibitors including brequinar used at higher concentrations also inhibit FSP1 and thereby sensitize cancer cells to ferroptosis [41]. Moreover, the same group just published another study in which they discovered that vitamin K, fully reduced by FSP1, functions as an anti-ferroptotic player [42]. The FSP1-mediated reduction of vitamin K results in a form, which operates as a potent RTA and inhibits (phospho)lipid peroxidation, and thereby protect cells from ferroptosis [42].

1.2.2.2 GPX4 AND SYSTEM XC-

Another important regulator to inhibit and block lipid peroxidation is glutathione peroxidases 4 (GPX4). GPX4 is a selenoprotein and a member of the glutathione peroxidases (GPXs). Interestingly, inhibition of GPX4 using small molecule

compounds such as RSL3 or Molecular Libraries 162 and 210 (ML210 and ML162) results in ferroptosis induction [11], [30], [43], [44]. By using glutathione (GSH) as a redox equivalent, GPX4 reduces lipid hydroperoxides (PE-PUFA-OOH), also called lipid ROS, to their corresponding lipid alcohols (PE-PUFA-OH) thereby protecting cells from lipid peroxidation [29], [30]. After reduction of hydroperoxides by GPX4, oxidized glutathione disulfide (GSSG) is recycled by glutathione-disulfide reductase (GSR) using NADPH/H+ [30]. GSH, one of the most abundant cellular antioxidants, is synthesized by GSH synthetase (GSS) and glutamate-cysteine ligase (GCL). Of note, buthionine sulfoximine (BSO) binding to GCL pharmacologically inhibits GSH biosynthesis and results in ferroptosis [11], [45]. GSH synthesis is dependent on the availability of cysteine, glutamate and glycine [22], [31]. Cysteine is reduced from cystine, which is shuttled into the cell via the glutamate-cysteine antiporter system Xc- (System Xc-). System Xc- is an amino acid antiporter and consists of two subunits: the functional unit SLC7A11 (solute carrier family 7 member 11) and the regulatory subunit SLC3A2 (solute carrier family 3 member 2), which imports extracellular cystine in exchange of intracellular glutamate export [32]–[34]. Therefore, system Xc- is another important regulator of ferroptosis. Interestingly, inhibition of SLC7A11 (xCT) by the small molecule erastin results in cystine depletion, followed by reduced GSH levels and decreased GPX4 activity, which leads to ferroptosis [46].

1.2.2.3 ANTIOXIDANT DEFENSE SYSTEMS OF FERROPTOSIS

Moreover, it was shown that xCT inhibition induces mitochondrial fragmentation, mitochondrial ROS production, loss of the mitochondrial membrane potential (MMP) and adenosine triphosphate (ATP) depletion [13], [16], [45], [47]–[49]. These findings demonstrate that mitochondrial metabolism plays a major role in ferroptosis. Additionally, it is known that mitochondria depletion *in vitro* or oxidative phosphorylation (OXPHOS) inhibition rescued cells from cystine depletion or erastin-induced ferroptosis [47]. Mitochondria generate adenosine triphosphate (ATP) through the metabolic pathway OXPHOS. During this mitochondrial process ROS are produced, which can cause aberrant oxidation of proteins, lipids and DNA [50]. Therefore, cells have evolved different antioxidant defense systems to survive. One defense system is converting two superoxides, which are generated during OXPHOS, into water (H_2O) and hydrogen peroxide (H_2O_2) by the superoxide dismutase (SOD) [51]. To further protect the cell, H_2O_2 is reduced to water (H_2O) by different antioxidant

enzymes such as GPXs or peroxireductases (PRDXs) [52]. Another antioxidant defense system to guard cells from oxidative stress caused by lipid peroxidation is the activation of the key regulator of the antioxidant response – Nuclear factor erythroid 2-related factor 2 (NRF2) [53].

1.2.2.4 NRF2 (THE MASTER FACTOR FOR ANTIOXIDANT RESPONSE IN FERROPTOSIS)

Nuclear factor erythroid 2-related factor (NRF2), also known as NFE2L2, is induced upon oxidative or electrophilic stress in the cell and transcriptionally activates an antioxidant defense program including anti-ferroptotic genes. Under basal condition NRF2 is kept in the cytoplasm by a kelch-like ECH-associated protein 1-cullin3-ring box protein 1 (KEAP1-CUL3-RBX1), an E3 ubiquitin ligase complex. KEAP1 facilitates the NRF2 ubiquitination by CUL3. After NRF2 is ubiquitinated it is transported to the proteasome and degraded [54], [55]. However, increased oxidative stress conditions disrupt the KEAP1-CUL3 ubiquitination system of NRF2, which leads to increased levels of newly translated NRF2 in the cytoplasm. Also, mutations of KEAP1, CUL3 or NRF2 can prevent NRF2 ubiquitination [54]. NRF2 translocates to the nucleus, where it heterodimerizes with small musculoaponeurotic fibrosarcoma oncogene homolog (Maf), which leads to transcription of antioxidant response element (ARE)-containing genes [56], [57]. AREs induce the expression of antioxidant and metabolic genes such as SLC7A11, GPX4, glutamate-cysteine ligase catalytic subunit (GCLC) and glutamate-cysteine ligase modifier subunit (GCLM) [54], [58]. GCLC and GCLM are two subunits of the GCL, an enzyme which plays a major role in the GSH synthesis [59]. Moreover, NQO1 and Heme oxygenase-1 (HMOX1, HO-1) are target genes of NRF2. NQO1 catalyzes the reduction and detoxification of highly reactive quinones, which lead to oxidative stress, to hydroquinones [60]. Interestingly, NQO1 has a preference for short-chain acceptor quinones such as ubiquinone [61]. HO-1 cleaves heme into antioxidant biliverdin, carbon monoxide and iron [62]. Of note, an increased labile iron pool (LIP) (Fe^{2+}) due to excessive activation of HO-1 enhances ferroptosis [63], [64]. Also, inhibition or silencing of HO-1 induced by withaferin A, erastin and BAY 11-7085 leads to resistance to ferroptosis [63]–[65].

Controversially to these findings it was published that knockdown of NQO1 and HO-1 in hepatocellular carcinoma cells (HCC) promotes ferroptosis when treated with ferroptosis inducers erastin and sorafenib [66]. It seems that excessive upregulation of

HO-1 has a cytotoxic effect while a moderate upregulation could have a cytoprotective effect [67]. Nevertheless, HO-1 and its effect on ferroptosis needs to be further investigated. Interestingly, there are other genes known to be transcriptionally activated by NRF2 such as FSP1, which seem to expand the role of NRF2 in regulating oxidoreductases [68]. Moreover, recently it has been discovered, that the CoQ-FSP1 axis is a key downstream effector and transcriptional target of the KEAP1-NRF2 pathway [69]. This study indicates that mutation or deficiency of KEAP1 in lung cancer cells mediates ferroptosis- and radiation-resistance due to upregulation of FSP1 through NRF2 [69]. Additionally, pharmacological inhibition of FSP1 and ferroptosis sensitizes lung cancer cells or patient-derived xenograft tumors to radiation [69]. These findings highlight the need of novel therapeutic strategies which target ferroptosis in KEAP1 mutant lung cancers. Of note, mutations in the KEAP1-NRF2 complex occur in almost 23% of lung adenocarcinomas (LUAD) and 34% of squamous cell carcinomas [70], [71]. High levels of NRF2 lead to a shorter overall survival with poor prognosis and to resistance of most available standard-of-care therapies [72].

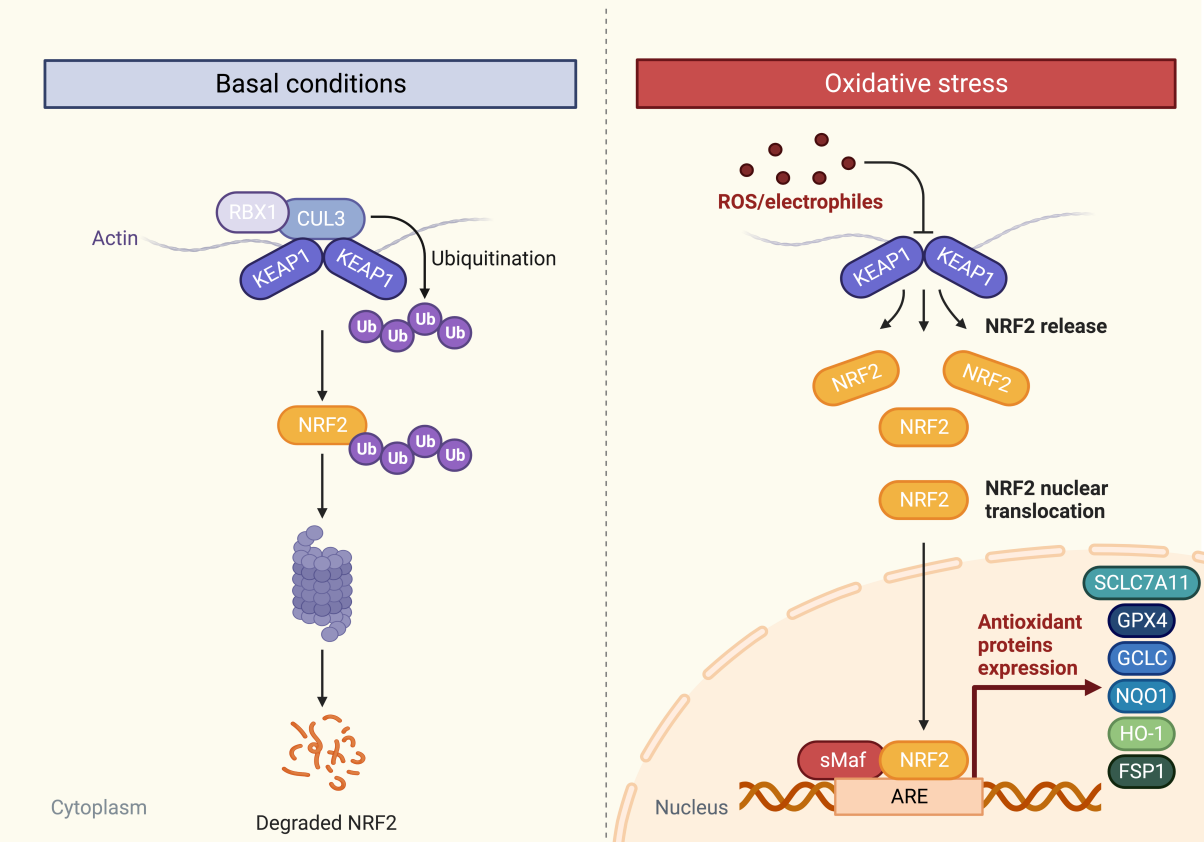

Figure 3: KEAP1-NRF2 pathway
Schematic illustration of the KEAP1-NRF2 pathway. Nuclear factor erythroid 2-related factor 2 (NRF2) is kept in the cytoplasm by a kelch-like ECH-associated protein 1-cullin3-ring box protein 1 (KEAP1-CUL3-RBX1), an E3 ubiquitin ligase complex. Under basal conditions NRF2 is ubiquitinated by CUL3, while KEAP1 facilitates the reaction. After NRF2 is ubiquitinated it is

transported to the proteasome, where it degrades [54], [55]. Under oxidative stress conditions the ubiquitination of NRF2 is impaired due to disrupted KEAP1-CUL3 complex. NRF2 levels increase in the cytoplasm and translocate to the nucleus. Once in the nucleus NRF2 forms a heterodimer with small Maf proteins and binds to antioxidant response elements (ARE). AREs initiate the expression of antioxidant proteins such as solute carrier family 7 member 11 (SLC7A11), glutathione peroxidase 4 (GPX4), glutamate-cysteine ligase catalytic subunit (GCLC), NAD(P)H quinone oxidoreductase 1 (NQO1), Heme oxygenase-1 (HO-1) and ferroptosis suppressor protein 1 (FSP1), to protect the cell from oxidative stress [54], [58], [73]. Scheme was drawn by using licensed biorender.com.

1.2.3 CHEMICAL FERROPTOSIS INDUCERS

There are currently four different chemical strategies to induce ferroptosis. The main two groups contain compounds inhibiting the system Xc-/GSH/GPX4 axis and are referred to as Class I ferroptosis-inducing compounds (FIN I) and Class II ferroptosis-inducing compounds (FIN II) [14], [30]. Class I FINs block system Xc- thereby preventing cystine import into the cell leading to GSH depletion. Due to the ensuing drop in GPX4 activity, this leads to increased lipid ROS levels resulting in ferroptotic cell death. Compounds such as erastin (and analogs as for instance imidazole ketone erastin (IKE)), glutamate, the tyrosine kinase inhibitor sorafenib (e.g. BAY 43-9006), and the antirheumatic drug sulfasalazine are system Xc- inhibitors [11], [46]. Of note, erastin also functions through the mitochondrial voltage-dependent anion channel (VDAC). Consequently, VDAC2 and VDAC3 knockdown results in erastin resistance [23]. Class II FINs such as (1S,3R)-RSL3, ML162, ML210, altretamine and other diverse pharmacological inhibitors (DPIs) inactivate GPX4 directly through covalently binding of its active selenocysteine site and thereby inhibiting its enzymatic activity resulting in ferroptosis [21], [30]. Another small molecule FIN56 induces ferroptosis via two different pathways: it promotes degradation of GPX4 and reduces the abundance of CoQ10 via the mevalonate pathway [74]. It is unknown how GPX4 degradation is promoted, but the enzymatic activity of acetyl-CoA carboxylase (ACC) plays a role in this pathway [74]. The fourth group inhibits GPX4 indirectly by directly oxidizing iron and stimulating lipid peroxidation and thereby leading to ferroptosis [75], [76]. Moreover, several other reagents can induce ferroptosis via different ways. Depletion of GSH can be induced by inhibition of GCL via BSO which results in ferroptotic death [30]. Additionally, cystine starvation leads to GSH depletion triggering ferroptosis. In pancreatic cancer cells artesunate may induce ferroptosis [77]. Furthermore, cisplatin can induce ferroptosis and apoptosis in several tissues [78], [79]. Moreover, recently iFSP1 has been discovered to trigger ferroptosis in RSL3 resistant cells [36].

Although Class I FINs have been used *in vivo* in cancer cells to induce ferroptosis, there is a need of analog developments with greater potency [17], [30], [80]. Class II FINs so far show no effects *in vivo*, which demonstrate necessity of further investigation of potential ferroptosis inducers *in vivo* for cancer treatments.

1.2.4 FERROPTOSIS INHIBITORS

Several compounds capable of specifically blocking ferroptotic cell death exist. These include iron chelators, which suppress the Fenton reaction by chelating iron from the labile iron pools (LIPs), preventing thereby lipid peroxidation [81]. Iron chelators are deferoxamine, ciclopirox or deferiprone [82]. Other compounds such as vitamin E, trolox, deuterated polyunsaturated fatty acids (D-PUFAs), butylated hydroxytoluene, Ferrostatin-1 (Fer-1) and Liproxstatin-1 block lipid peroxidation directly [23]. Fer-1 is one main ferroptosis inhibitor whose activity was described to function via direct scavenging of lipid ROS [11].

Moreover, as mentioned before ubiquinol generated by FSP1 seems to inhibit ferroptosis and functions as an endogenous radical trapping agent functionally equivalent to the described small-molecule lipophilic radical scavengers Fer-1 and Liproxstatin-1 [11]. Furthermore, it was shown that the metabolic derivates tetrahydrobiopterin / dihydrobiopterin (BH4/BH2) of GTP cyclohydrolase-1 (GCH1) also suppress ferroptosis by depleting phospholipids with two PUFA tails [83]. Additionally, it was discovered that BH4 acts as a potent RTA, which can protect cells alone and in synergy with vitamin E from lipid peroxidation [84]. Another study just recently revealed, that hydropersulfides scavenge free radicals and thereby prevent cells from lipid peroxidation and ferroptosis [85].

1.2.5 RELEVANCE OF FERROPTOSIS *IN VIVO*

xCT plays an important role in the ferroptosis pathway by importing cystine, which is needed for the GSH synthesis to protect cells from lipid ROS. xCT is highly expressed in neurons and brushes border membranes of the kidney and duodenum as well as in the thyroid gland [34], [86].

It was shown that xCT-deficient mice show increased cystine concentration extracellular and decreased GSH levels intracellular in comparison to wild type (WT) mice. However, *in vitro*, cellular cysteine levels in embryonic fibroblasts derived from

knockout (KO) mice were similar compared to cells derived from WT mice. Moreover, these isolated mouse embryonic fibroblasts (MEFs) from xCT KO mice die in cell culture and only survive when 2-mercaptoethanol or N-acetyl cysteine (NAC) is supplemented, both serve as alternative cystine sources. These data suggest that *in vitro* in 2 D culture cells compensate the cysteine synthesis via the transsulfuration pathway [86]. The transsulfuration pathway metabolizes methionine to homocysteine and cystathionine beta-synthase (CBS) further processes it to cystathionine. CBS is acted on by cystathionine γ-lyase (CSE) to generate cystathionine to cysteine [33], [87]. In Cbs deleted mice elevated levels of homocysteine in plasma lead to homocystinuria which results in death of the mice after 5 weeks [88], [89]. Interestingly, a newly discovered CBS inhibitor induces ferroptosis in different cancer cell lines [90]. Another key regulator of ferroptosis is GPX4. It has been reported that GPX4 is necessary for embryogenesis since GPX4 KO mice die in utero at E7.5 [91]. Mice die at the same embryonic development when harboring a mutation in the enzymatically active selenocysteine of Gpx4, whereas a heterozygous loss of selenocysteine in Gxp4 leads to defect spermatogenesis in born mice [92], [93]. Also, it was shown that Gxp4 is essential for mitochondria integrity due to the fact that whole-body inducible Gpx4 knockout mice exhibited increased mitochondrial damage and decreased activity of the electron transport chain members complex I and IV [94]. Moreover, Gpx4 is important for tissue homeostasis and survival of adult mice since Gpx4 KO mice lost body weight and died within two weeks after [29], [94].

GSH is necessary for GPX4 to prevent cells from lipid peroxides. GSH is produced during GSH synthesis, where GCL is needed to form GSH precursor γ-glutamylcysteine. GCL consists of two subunits: the catalytic subunit GCLC and the regulatory subunit GCLM [59]. Deletion of Gclc, which leads to blockade of Gsh synthesis, is embryonically lethal at E8.5. Furthermore, Gclc knockout in embryos results in increased cell death assayed by TUNEL staining and gastrulation failure [95], [96]. Interestingly, Gclm KO compared to WT leads to normal development but less GSH production in mice [97]. Also, deletion in glutathione synthetase (GSS), which generates GSH, results in death of the mice at E.7.5, whereas heterozygous mice survive [98]. These data reinforce how important GSH-synthesis as well as GCLC are for embryonic development. To sum up, these findings support that ferroptosis protection plays a crucial role in embryonic development and tissue homeostasis.

1.2.6 GENETIC EVIDENCE FOR FERROPTOSIS IN CANCER

It was demonstrated that GSH, driven by GCLM, is required for cancer initiation. Harris et al. 2015 showed that in different mice models of mammary tumors, lymphomas, thymomas and sarcomas loss of Gclm impaired tumor initiation and progression. Interestingly, the same results were observed when PyMT-Gclm+/+ mice, which exhibited mammary tumors, were treated prior to cancer onset with BSO, an inhibitor of GSH synthesis. Of note, when mice were treated with BSO upon mammary tumor onset, tumor burden was unchanged. These results indicate that at later stages of tumor progression there must be an alternative antioxidant mechanism to protect malignant tumors from ROS levels due to the fact that BSO fails to impact tumor growth [99]. Moreover, upregulation of GCLM across multiple human tumor types and data showing high GCLM mRNA expression in human tumors results in lower relapse-free survival and overall survival of the patients [99]. Furthermore, specific deletion of xCT in tumor cells impairs tumor growth in murine cancer models, caused by defective cystine uptake, which initiates decreased GSH levels and accumulation of ROS [100]. However, although it was shown that cysteine depletion in a PDAC xenograft model had little effect on tumor growth [101], whole body xCT deletion in a PDAC genetically engineered mouse model induced ferroptosis and was sufficient to reduce tumor growth [102]. These results assume that deletion of xCT could be an effective cancer treatment. Moreover, depletion of Gpx4 in the pancreas of an oncogenic Kras-driven murine model resulted in macrophage infiltration and activation by stimulating transmembrane protein 173/stimulator of interferon genes (TMEM173/STING)-dependent DNA sensor pathway. Furthermore, Gpx4 depletion promoted Kras-driven tumorigenesis in PDAC [103]. In contrast, treatment with Liproxstatin-1 suppressed Kras-driven pancreatic tumorigenesis in mice [103]. These findings propose that Gpx4 depletion accelerates tumorigenesis upon ROS upregulation or oxidative damage. Recently, in subcutaneous tumor studies it was shown that GPX4 KO tumors also significantly impair tumor size, while $GPX4^{KO}/FSP1^{KO}$ tumors, where ferroptosis was inhibited with Fer1, reduced tumor growth [36].

1.2.7 INFLUENCE OF RAS ON FERROPTOSIS SENSITIVITY

Ferroptosis was firstly named in 2012, when erastin and RSL3 were discovered to induce an iron-dependent form of non-apoptotic cell death [11]. Not known at that time

ferroptosis was firstly described in 2003 in a synthetic lethality screen for small molecules targeting Harvey rat sarcoma viral oncogene homolog (HRAS)^{G12V}-mutant human foreskin fibroblasts (BJeLR), in which erastin was found to initiate cell death and therefore named for eradicator of RAS and ST-expressing cells (erastin) [12]. Moreover, in 2008 two other compounds RSL3 and RSL5 were detected in a synthetic lethal screening to increase lethality in cells expressing oncogenic RAS. It was shown that HRAS^{G12V} cells upregulate TFRC and downregulate ferritin, which enriches the cellular iron pool [14]. Additionally, lung carcinoma cell line (Calu-1) harboring a Kirsten sarcoma viral oncogene homolog (KRAS)^{G12C} mutation were more sensitive to erastin treatment then cells expressing two different short hairpin RNAs (shRNAs) targeting KRAS. Furthermore, A-673 cells, with an activating BRAF^{V600E} but no KRAS mutation become more resistant to erastin treatment after BRAF shRNA induction [13].

To investigate ferroptosis sensitivity in the context of the mutational status of RAS in cancer cells, 117 cancer cell lines from different tissues were treated with erastin. From 117 different cancer cell lines 38 were harboring oncogenic RAS mutations. It was determined that independent of the mutational RAS status, the tissue origin was the stronger predictor for ferroptosis sensitivity. In this study it was shown, that diffuse large B-cell lymphoma (DLBCL) cell lines were revealed as the most sensitive cell lines to ferroptosis induction via erastin treatment [30].

Furthermore, it was described that human mammary epithelial (HME) cells expressing mutant epithelial growth factor receptor (EGFR) and BRAF mutant cells are sensitive to ferroptosis by mitogen-activated protein kinase (MAPK) signaling activation via cystine deprivation leading to hydrogen peroxides. Moreover, it was shown that ferroptosis induced by cystine deprivation inhibits tumor growth *in vivo* in an EGFR mutant non-small cell lung cancer (NSCLC) xenograft model [104].

Activated RAS is known to upregulate superoxide and hydrogen peroxide production. Regarding these findings, cells expressing neuroblastoma RAS viral oncogene homolog (NRAS)^{G12D} and HRAS^{G12V} mediate an oxidative stress response via the p38 MAPK activation and ROS production [105]. Moreover, ROS production was stimulated by activation of NADPH-oxidases (NOX), which is regulated by the phosphoinositide-3-kinase/Ras-related C3 botulinum toxin substrate 1 (PI3K/Rac1) and RAF/MEK/ERK pathways in NIH-3T3 cells expressing HRAS^{G12V}. Also, pretreatment with antioxidant N-acetylcysteine (NAC) or a NADPH oxidase inhibitor (diphenyleneiodonium (DPI)) decreased DNA repair capacity in these cells [106], [107].

Interestingly, activation of NADPH oxidase 1 (NOX1) through oncogenic KRAS increases ROS generation. NOX1 induces cellular and causes malignant transformation [108]. Additionally, it was shown that tumor suppressor inactivation of p16 and KRAS activation through $KRAS^{G12V}$ upregulates NADPH oxidase 4 (NOX4) [109]. Since oncogenic KRAS elevates ROS-generating NOX activity and GSH biosynthesis, targeting of NOX and GPX4 with a combination treatment of DPI and BSO resulted in lethality of cancer cells harboring oncogenic RAS mutations [110]. These data suggest that oncogenic RAS isoforms regulate lipid peroxidation and ferroptosis through ROS generation, which may support cellular transformation *in vitro*. Still, it remains unknown how oncogenic RAS handles tumor initiation *in vivo* after ROS induction.

ROS plays a pivotal role in biological processes. Interestingly, different ROS concentrations influence tumor microenvironment, cancer progression, metastasis and survival. To date it is known that moderate ROS levels activate several cancer cell progression and growth cascades such as mitogen-activated protein kinase/extracellular signal-regulated protein kinases 1/2 (MAPK/ERK1/2), p38, c-Jun N-terminal kinase (JNK), and phosphoinositide-3-kinase/protein kinase B (PI3K/AKT), nuclear factor kappa-light-chain-enhancer of activated B cells (NF-κB), matrix metalloproteinases (MMPs) and vascular endothelial growth factor (VEGF) [111]. However, high levels of ROS can induce apoptosis [112], [113]. Therefore, it is important for tumor cells to deal with high ROS levels to survive. One way to accommodate with increased ROS levels is activation of the NRF2-antioxidant response element signaling pathway [114]. Notably, it is known that NRF2 is activated upon expression of $KRAS^{G12D}$, $BRAF^{V619E}$ and MYC^{ERT2} oncogenes, which leads to an antioxidant defense and thereby lower intracellular ROS levels and enhancing tumorigenesis [115], [116].

Knowing that oncogenic RAS increases ROS levels, it is still controversially discussed how sensitive or resistant cells expressing oncogenic RAS are to lipid ROS and thereby ferroptosis. As mentioned before it was shown that mutant RAS cells are sensitive to erastin or RSL3 treatment [11]. Intriguingly, it was demonstrated that independent of the KRAS status, artesunate (ART) was inducing an iron and ROS-dependent cell death in pancreatic ductal adenocarcinoma (PDAC) cell lines [77]. Moreover, another study discovered that erastin treatment enhanced sensitivity of acute myeloid leukemia (AML) cells harboring a $NRAS^{Q61L}$ mutation (HL-60), but not

in other cell lines expressing $NRAS^{G12D}$ or $KRAS^{A18D}$ or even RAS wild type [117]. These data suggest that not only oncogenic RAS, but also other genetic or non-genetic factors may influence ferroptosis sensitivity. Of note, rhabdomyosarcoma cells (RMS13) expressing either $NRAS^{G12V}$, $HRAS^{G12V}$ or $KRAS^{G12V}$ were indeed more resistant to ferroptosis induction via erastin or RSL3 treatment then cells expressing empty vector, suggesting oncogenic RAS may also protect cells from ferroptosis [118]. Furthermore, it has recently been published that oncogenic $KRAS^{G12V}$ cells upregulate xCT to protect cells from H_2O_2-induced cell death and that xCT supports RAS-induced transformation and tumorigenicity [119]. Interestingly, cells expressing homozygous $KRAS^{G12D/G12D}$ exhibit a metabolic rewiring in which they increase among other things glutathione biosynthesis, assuming these cells are more resistant to ferroptosis, because they are better protected from lipid ROS [120]. In this study they also show that these cells upregulate glucose-derived metabolites for the TCA cycle, which lead to glutathione-mediated detoxification. Correspondingly, it is known that the mitochondrial tricarboxylic acid (TCA) cycle plays an important role in ferroptosis [47]. Also, other studies demonstrate that in KRAS-driven cancers metabolic changes in glycolysis or glutaminolysis can increase and thereby affect the TCA cycle [121].

1.3 INFLUENCE OF CELL DENSITY ON FERROPTOSIS RESISTANCE

Apart from oncogenic RAS- and ROS-ferroptosis dependency, it was unexpectedly discovered that HCT116 cells become more resistant to ferroptosis when seeded in higher density. The protooncogenic transcriptional co-activator yes-associated protein 1 (YAP1/YAP) transcriptionally upregulates ACLS4 and TFRC, two ferroptosis modulators, which usually promote ferroptosis. When cells seeded in high confluence YAP is inhibited, resulting in ferroptosis resistance of these cells [122]. In general, the Hippo-YAP pathway is involved in several biological functions such as cell proliferation, differentiation and organ size control [123], [124]. Mechanistically, this pathway is characterized by cell-cell contacts mediated by E-cadherin, activating the Hippo phosphorylation signaling pathway by inactivating YAP and its paralog WW domain containing transcription regulator 1 (WWTR1,also called TAZ) through mammalian Ste20-like kinases 1/2 (MST1/2) and large tumor suppressor 1/2 (LATS1/2) [123]. When Hippo pathway is off due to low density, YAP/TAZ can shuttle into the nucleus

and act as a transcription co-regulator leading to upregulation of ACSL4 and TFRC resulting in ferroptosis sensitivity [125]. Furthermore, Mishima et al. just recently reiterated how important cell density is in ferroptosis studies [41]. These data should be considered when testing ferroptosis sensitivity in different cells.

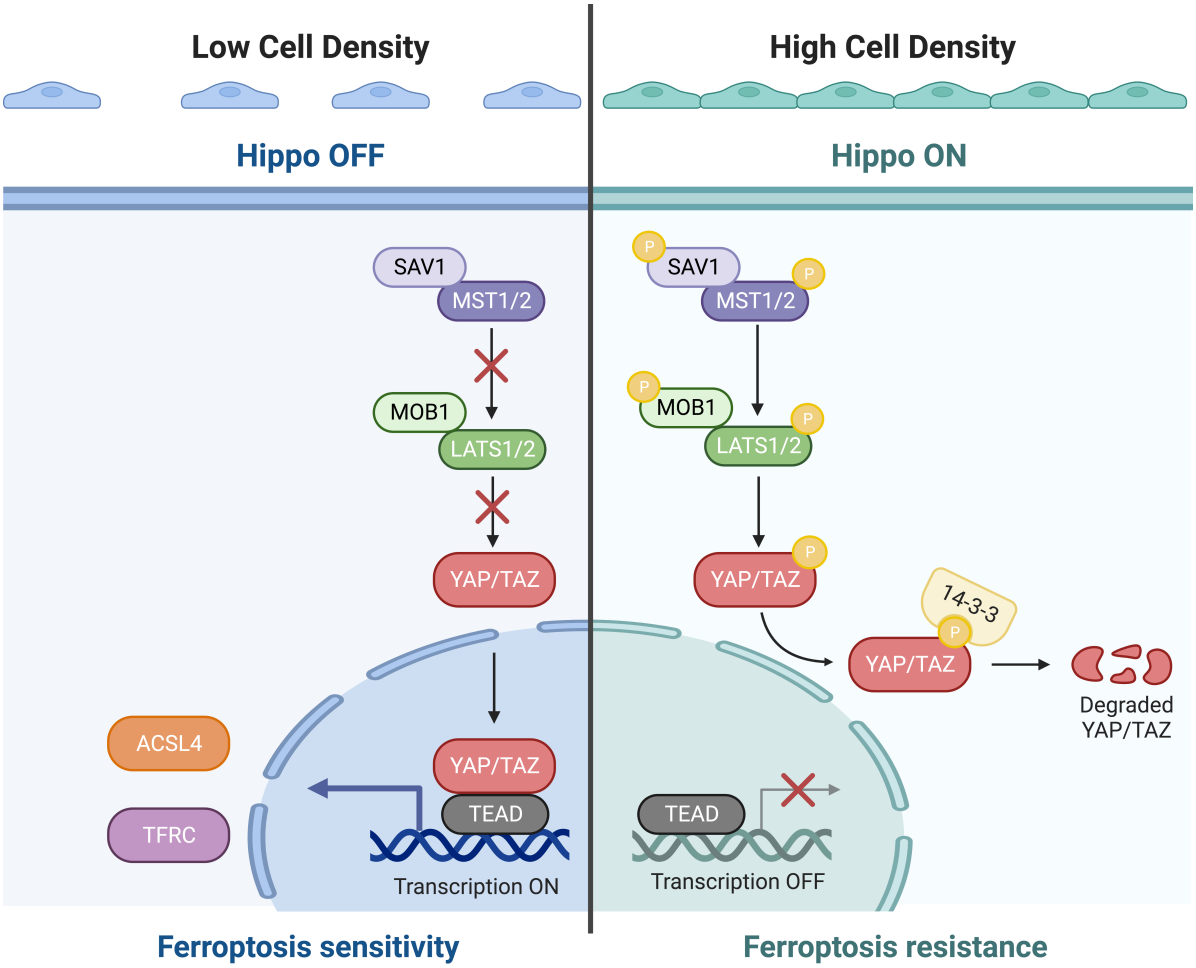

Figure 4: Hippo-YAP pathway
Schematic illustration of the Hippo-YAP pathway. This pathway is characterized by cell-cell contacts mediated by E-cadherin, activating the Hippo phosphorylation signaling pathway by inactivating yes-associated protein 1 (YAP) and its paralog WW domain containing transcription regulator 1 (TAZ) through mammalian Ste20-like kinases 1/2 (MST1/2) and large tumor suppressor 1/2 (LATS1/2) [123]. When Hippo pathway is off due to low density, YAP/TAZ can shuttle into the nucleus and act as a transcription co-regulator leading to upregulation of ACSL4 and TFRC resulting in ferroptosis sensitivity [125]. Therefore, adherent cells seeded in low density are ferroptosis sensitive while adherent cells seeded in high density are ferroptosis resistant. Scheme was drawn by using licensed biorender.com.

1.4 RAS GTPASES

Two of the three RAS genes were originally identified as cellular counterparts of the viral oncogenes of cellular transformation through the retroviruses Harvey and Kirsten sarcoma in rodents [126]. After Kirsten rat sarcoma virus (KRAS) and Harvey Rat

sarcoma virus (HRAS) in 1983 another human transforming oncogene was discovered and found to be a member of the RAS gene family. It was named neuroblastoma RAS viral (v-ras) oncogene homolog (NRAS), because it was initially detected in human neuroblastoma cell lines [127], [128]. Since then, there has been an intense focus on studying the biology, biochemistry and structure of these three RAS oncogenes. KRAS, HRAS and NRAS encode for four different 21 kDA long RAS proteins, in which KRAS has two isoforms that arise from alternative exon 4 splicing (KRAS4A and KRAS4B respectively), in which KRAS4B is the predominantly splicing variant [129], [130]. RAS protein family members belong to small GTPases which bind to guanosine triphosphate (GTP) and guanosine diphosphate (GDP). RAS GTPases cycle between two conformations: the inactive GDP-bound conformation, called switched-off, and the active GTP-bound conformation, called switch-on. Conversion from the inactive GDP-bound state to the active GTP-bound state is mediated by guanine nucleotide exchange-factors (GEFs). The switch back to inactive RAS is promoted by GTPase-activating proteins (GAPs), which catalyze GTP hydrolysis [131]. Cycling between the two states ON and OFF controls key cellular processes. Once switched on, RAS GTPases activate a spectrum of downstream signaling effectors which regulate cellular growth, proliferation, survival and differentiation [132], [133].

1.4.1 RAS STRUCTURE

RAS contains two domains, the C-terminal and the G domain, and exists of six beta strands and five alpha helices. The C-terminal consists of 24-25 residues and is characterized by a membrane targeting region (CAAX-COOH, also known as CAAX box) and a hypervariable region (HVR). The CAAX motif is required for posttranslational lipid modifications and controls subcellular localization. The HVR dictates membrane localization and is responsible for downstream signaling pathway activations facilitated by prenylation and palmitoylation of cysteine residues.

The G domain approximately consists of 170 residues and binds to guanosine nucleotides. It consists of five G motifs (G1-G5). G1, also called P-loop (GxxxxGKS/T), is a glycine-rich phosphate-binding loop, which wraps around the phosphates of GDP/GTP. G2, called “Switch I”, contains a threonine on position 35, which is crucial for terminal phosphate (γ-phosphate) binding of GTP and also contacts the divalent magnesium ion bound in the active site. The G3 motif, also called “Switch II”, consists of a DxxGQ motif, where glutamine (Q) activates a catalytic water molecule for

hydrolysis of GTP to GDP and the aspartate (D) is essential for guanine versus adenine binding. G4 is the NT/KxD motif, which specifically interacts with guanine. Also, the G5 motif provides a specificity for guanine due to the interaction of alanine in the SAK consensus sequence. Switch I and Switch II are the main responsible parts of the G-domain, which lead to conformational change of the GDP to GTP cycle and therefore to effector binding [130], [134]–[137].

1.4.2 DOWNSTREAM SIGNALING PATHWAYS OF RAS

RAS GTPases regulate several cellular processes such as cell division, proliferation, migration and cellular differentiation through direct interactions with various effectors [132], [133]. Different stimuli, such as receptor-tyrosine kinases (RTKs) or G protein–coupled receptors (GPCRs) can activate RAS proteins. RAS activation occurs when growth factors bind to their receptor tyrosine kinases (RTKs) (e.g. epidermal growth factor (EGF) binding to epidermal growth factor receptor (EGFR)) and initiate dimerization and autophosphorylation of the receptor. Upon growth factor stimulation, SOS interacts with GRB2 and is recruited to the plasma membrane. The SH2 domain of GRB2 binds to phosphotyrosine residues of the autophosphorylated receptors. Once SOS is translocated to the plasma membrane it initiates the GDP/GTP exchange on RAS, which leads to further downstream effector signaling pathway activation [138], [139]. More than ten proteins with distinct functions including e.g., RAF, PI3K, RALGDS, TIAM, PLCε have been identified as RAS effectors [140], [141].

Two of the main RAS downstream effectors are the RAF/MEK/ERK cascade and the PI3K/AKT pathway. The RAS/RAF/MEK/ERK signaling pathway (also known as the MAPK/ERK pathway) controls key cellular functions such as proliferation, differentiation, angiogenesis, migration and survival. RAS stimulates the protein kinase activity of RAF family kinases, which consists of 3 different RAF kinases, A-RAF, B-RAF and c-RAF (also called RAF-1) [142]. The RAF family kinases were described as one of the first oncoproteins almost 40 years ago [143]. Once RAS is activated, RAF dimerizes and changes conformationally, which leads to phosphorylation of its activation sites and dephosphorylation of its deactivation sites [144]. The activation site of RAF phosphorylates and activates two MAPKs, called MEK1 and MEK2. MEK1 and MEK2 in turn phosphorylate and activate ERK1 and ERK2, two extracellular signal-regulated kinases (ERKs) or classical MAP kinases. Once activated, ERK translocates to the nucleus where it controls and activates several cell cycle proteins and

transcription factors [145]. Another well-known downstream effector pathway of RAS is the PI3K/AKT signaling cascade. It is also involved in several cellular events such as cell growth, proliferation, differentiation, protein synthesis, metabolism and survival [146]. Four different classes of intracellular lipid PI3Ks exist, which can also be activated via RTKs or GPCRs. PI3K phosphorylates phosphoinositides leading to formation of phosphatidylinositol 3,4,5-triphosphate (PIP3) [145]. PIP3 is a secondary messenger which recruits pyruvate dehydrogenase kinase 1 (PDK1) and serine/threonine protein kinase B (PKB/AKT) to the plasma membrane and thereby activates AKT. AKT comprises three subtypes: AKT1, AKT2, AKT3, which further phosphorylate several substrates such as mammalian target of rapamycin (mTOR), forkhead box O (FOXO) or NF-κB. Therefore, activated AKT plays a major role in cell proliferation, apoptosis, glucose metabolism, transcription and cell migration. Interestingly, the lipid phosphatase PTEN can negatively regulate the PI3K/AKT pathway by dephosphorylating PIP3 and converting it into phosphatidylinositol 4,5-bisphosphate (PIP2) [145], [147].

Due to the important role of RAS signaling pathways in cellular processes, gene mutations in RAS signaling players such as receptor tyrosine kinases (e.g. EGFR), RAS regulators (e.g., GAP, GEF) and RAS effectors (e.g., PI3Kα, BRAF) have an immense effect in human cancers. Therefore, therapies should target and inhibit these signaling cascades.

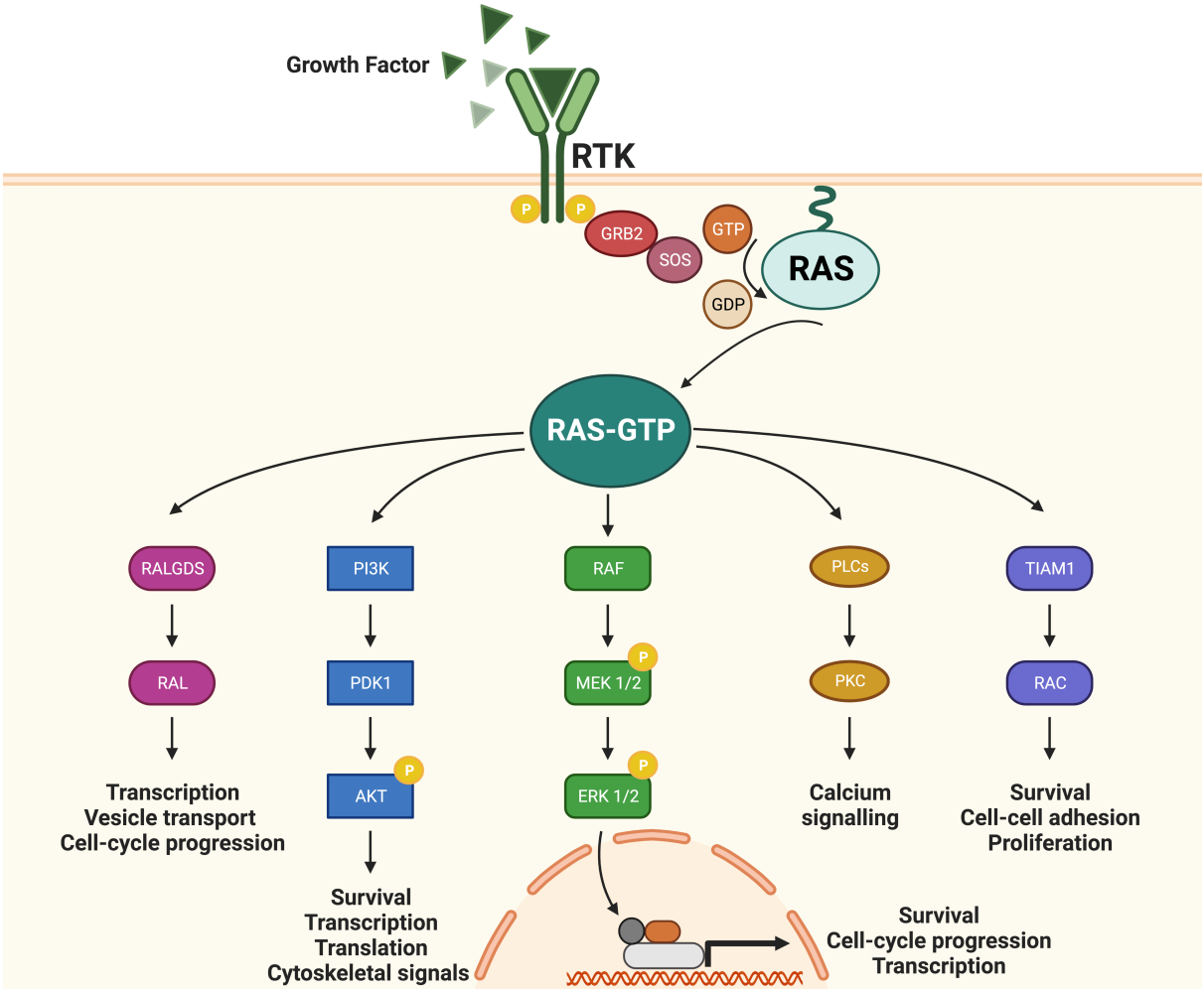

Figure 5: RAS effector pathways
Schematic illustration of the RAS effector pathway. RAS activation can occur through different stimulations. One example is when growth factors bind to their receptor tyrosine kinases (RTKs) and thereby initiate dimerization and autophosphorylation of the receptor. Through the SH2 domain GRB2 binds to the phosphotyrosine residues of the autophosphorylated receptors. With its SH3 domain GRB2 is interacting with SOS. SOS is recruited from the cytosol to the plasma membrane and initiates the GDP/GTP exchange on RAS. Once RAS is bound to GTP it activates further downstream effector signaling pathways [138], [139]. Some of these RAS effectors are e.g., RALGDS, PI3K, RAF, PLCε and TIAM, which control and regulate cellular processes such as survival, proliferation and transcription [140], [141]. Scheme was drawn by using licensed biorender.com.

1.4.3 RAS MUTATIONS IN HUMAN CANCER

40 years ago, in 1982, the first mutationally activated RAS gene was identified in human cancer [126]. Since then, there has been an intense focus on studying RAS mutations and validating mutant RAS as a key driver for malignant transformation and tumor initiation and maintenance. Overall, RAS is the most commonly mutated oncogene in all human cancers, with KRAS being the most frequently mutated isoform. RAS mutations occur in the deadliest cancers worldwide, which are predominantly lung, pancreatic and colon cancer. As a consequence, there is an urgent need of

elusive “anti-RAS” therapy for cancer treatment, since RAS mutations exist so frequently [133], [145].

The frequency and distribution of RAS mutations varies due to the fact that for analysis different databases with distinct patient numbers are used, including diverse cancer types and divergent RAS isoforms. Prior et al. cross-referenced in 2020 all major published cancer mutation databases, with the two largest ones being Catalogue of Somatic Mutations in Cancer (COSMIC) and The Cancer Genome Atlas (TCGA), to define general mutation frequencies of RAS isoforms from different cancer types. They determined that almost 3.4 million (19%) of cancer patients per year worldwide harboring a RAS mutation [148]. Due to high discrepancy of the different databases, data based on the COSMIC databank will be used in the following to give an overview of the different frequencies of KRAS, NRAS and HRAS in various cancer types. Overall, in all human cancers the most prevalent mutations do occur in KRAS (~23%), followed by mutations in NRAS (~8%) and mutations are less found in HRAS (~3%) [133]. Moreover, KRAS is commonly mutated in 85%, NRAS is less commonly mutated in 11% and HRAS, being rarely mutated in 4% of all RAS driven cancers [129].

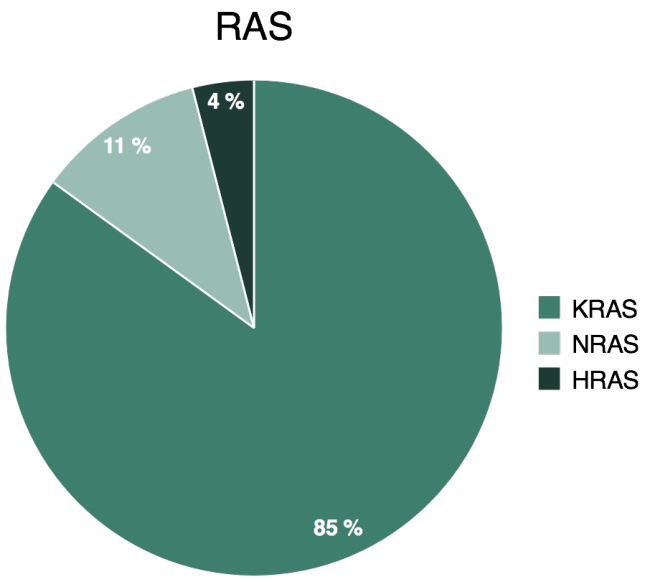

Figure 6: RAS isoforms and mutation occurrence in all human cancers
KRAS is commonly mutated in 85%, NRAS in 11% and HRAS is barely mutated in 4% of all RAS driven cancers. Data is analyzed from COSMIC. Data was adapted from Hobbs et al. 2016 [129].

Interestingly, KRAS mutations have the highest incidence in pancreatic cancer (57%). Also, in malignancies of the large intestine (35%), biliary tract (28%), small intestine (17%), lung (16%) and endometrium (15%) KRAS mutations do occur [133]. NRAS

mutations commonly appear in malignant melanomas (17%) as well as in malignancies of hematopoietic and lymphoid tissue (10%) and thyroid cancer (7%) [133]. HRAS mutations have been found prevalently in salivary gland tumors (15%) and in cervical tissue, as well as in the upper aero-digestive tract and urinary tract (all 9%) [133].

Although RAS mutations are widely distributed all over the gene, there is a so called "hotspot" for commonly occurring mutations in three amino acid residues, which are G12, G13 and Q61 and representing 98% of all RAS mutations [129]. Gain-of-function single base missense mutations in these hotspots lead to intrinsic GTP activity of RAS proteins, since GAP is impaired to promote hydrolysis of GTP, resulting in constantly activation of further downstream signaling. Therefore, RAS mutations lead to uncontrolled activation of cellular processes consequent in tumorigenesis and cancer [133], [149].

Interestingly, the frequency of every RAS gene mutation also occurs differently in each of the three hotspots. G → A transitions at the second base of codon 12 or 13 resulting in G12D or G13D mutations, whereas G → T transversions at the same spot resulting in G12V mutations [150]. G12 mutations appear in 83% of KRAS isoforms, followed by 14% of G13 mutations and only 2% of Q61 mutations. In contrast, in NRAS isoforms Q61 is the most mutated hotspot. Surprisingly, HRAS has no predominant mutated hotspot and G12, G13 and Q61 mutations do occur in the same frequency [129]. G12D is the predominant substitution of codon G12 in KRAS (41%) and NRAS (52%). In HRAS it is G12V (65%). For codon G13, G13D is the most common mutation in KRAS (89%), followed by NRAS (53%), but only less mutated in HRAS (13%). In contrast, in HRAS G13R (49%) is the favored substitution. For Q61 codon mutations, Q61R is the predominant version in NRAS (80%) and HRAS (41%), whereas Q61K is the preferred substitution in KRAS (39%), but rare in NRAS (2%) and HRAS (17%) [133].

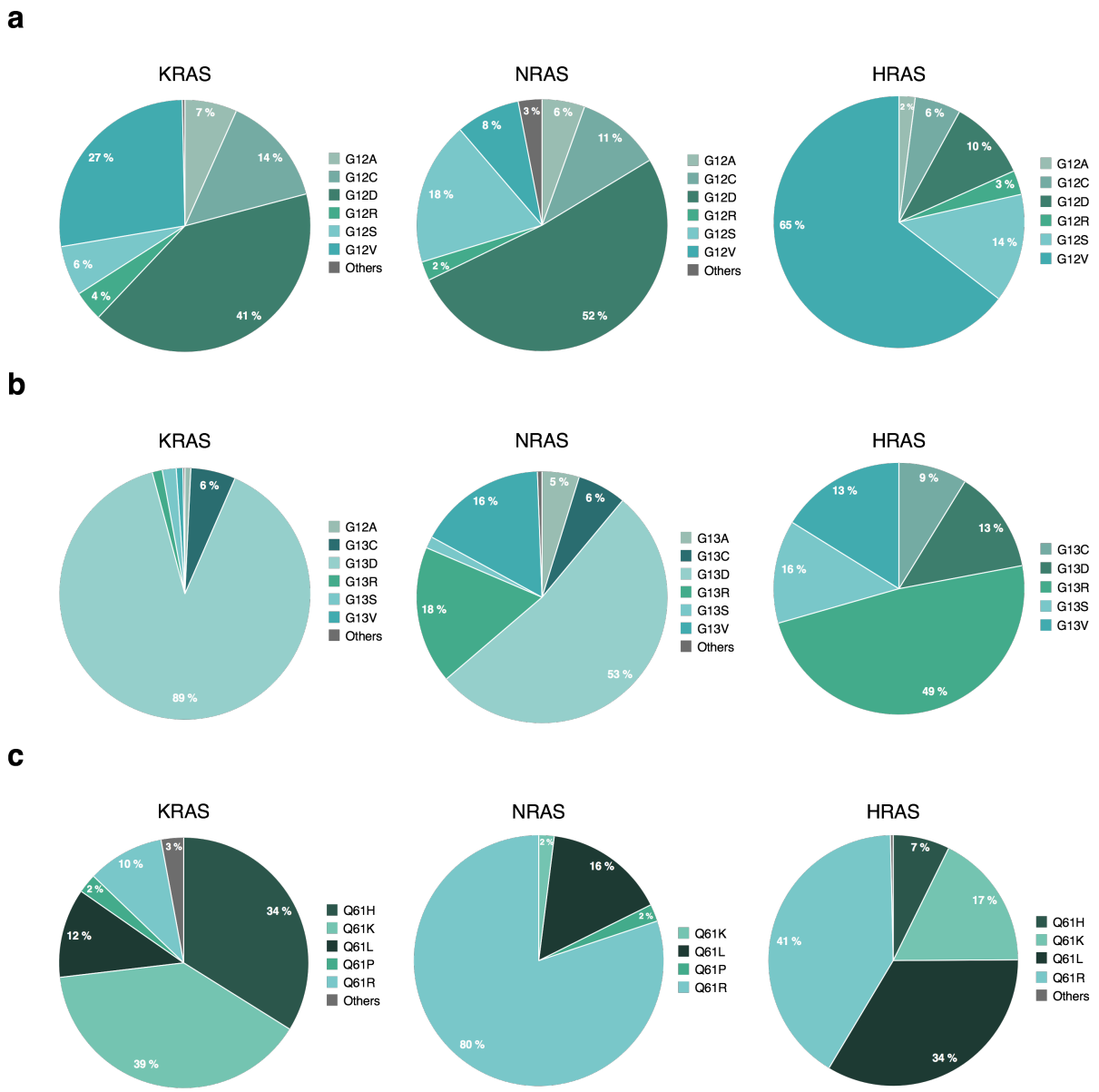

Figure 7: Diagrams of hotspot mutations in RAS oncogenes
a Schematic diagram of G12 mutations in KRAS, NRAS and HRAS. **b** Schematic diagram of G13 mutations in KRAS, NRAS and HRAS. **c** Schematic diagram of Q61 mutations in KRAS, NRAS and HRAS. Shown are various oncogenic somatic mutations identified in various human cancers. Data was analyzed from COSMIC. Data is adapted from Murugan et al. 2019 [133].

Moreover, RAS isoforms exhibit significantly different base mutations in specific cancers. For instance, in PDAC G12 is the favored hotspot mutation area in KRAS, where the G → A transition at the second base of codon 12 resulting in G12D is the most frequent mutation in this cancer type [129]. Suspensefully, in lung cancer the G → T transversion at the first base in the codon leading to a G12C mutation is predominantly seen in smoker cancer patients, while patients who never smoked more often exhibit a G → A transition mutation [151]. In contrast, in melanoma the predominant mutations are NRAS Q61, whereas NRAS G12 mutations are more

common in acute myeloid leukemia. Additionally, G13 mutations are relatively often mutated in colorectal adenocarcinoma (CRC) [129], [150], [152].
These patterns assume that each different RAS mutation has a different outcome on the oncogenic functions. It needs to be further investigated, which factors play a key role in preferences of mutation patterns occurring in different cancer types [150]. However, there is evidence that each particular mutation of the hotspots (G12, G13, Q61) has different oncogenic effects and functional consequences on the tumor outcome, which means that anti-RAS therapy needs to address several approaches to target RAS mutant cancers [129].

1.4.4 TARGETING RAS / ANTI-RAS THERAPY

RAS-driven cancers comprise the majority of all human cancers. RAS hyperactivation is observed in the deadliest types of cancer, such as PDACs, LUAD, colorectal myelomas and endometrial carcinomas [145]. KRAS mutations predominantly occur in pancreatic, colorectal and LUAD cancers and the clinical outcome of KRAS-driven cancers is really poor [133]. Interestingly, in leukemia or melanomas NRAS and HRAS mutations are more common [145].
In the past years there has been a big effort to develop new therapeutic approaches to indirectly or directly target RAS. One approach to target RAS is to inhibit the SOS-mediated RAS activation catalyzed by RAS-GEF with targeted small compounds [153], [154]. Also, small molecules to inhibit the RAS GTP interaction with its effectors such as RAF and PI3K have been identified [155]. Another approach for an anti-RAS therapy are farnesyltransferase inhibitors (FTI), which target the RAS CAAX motif to prevent membrane association of RAS [156]. Moreover, several compounds exist to inhibit downstream signaling pathway regulators such as RAF or PI3K [157], [158].
Furthermore, it is possible to silence KRAS expression with RNA interference siRNA (RNAi) [159], [160]. Interestingly, cancer vaccines, which induce immunogenicity in patients, have been developed to treat KRAS-driven cancers [161]. However, although RAS is often designated as the “undruggable”, potential anti-RAS drugs were recently developed: the G12C-inhibitors. These inhibitors, such as ARS-1620 and the newer molecules sotorasib (AMG-510) and adagrasib (MRTX849), bind to the thiol of mutant cysteine in $KRAS^{G12C}$ and therefore prevent SOS1-RAF-GEF interaction, which inhibits KRAS activation [162]–[165]. However, these inhibitors only target cancer patients harboring $KRAS^{G12C}$ mutations. Moreover, another small molecule was discovered,

which covalently targets the $KRAS^{G12S}$ mutation. Irreversible binding of the small molecule leads to an acylation of the noncatalytic serine in $KRAS^{G12S}$ resulting in oncogenic signaling suppression [166]. Surprisingly, more recently, MRTX1133, a potent, selective and non-covalent $KRAS^{G12D}$ inhibitor has been developed. It inhibits $KRAS^{G12D}$ signal transduction and leads to tumor regression in $KRAS^{G12D}$-mutant cell-line-derived and patient-derived xenograft models [167]. Due to the fact that $KRAS^{G12D}$ is the most prevalent KRAS mutant in all human cancers, this therapy gives hope for treating more cancer patients resulting in a better clinical outcome.
With the arrival of the new precise personalized targeted therapies, there is optimism that the “undruggable” RAS might be rendered druggable.

1.5 KRAS-MEDIATED REWIRING OF CELL DEATH

Another therapeutic approach to target KRAS-mutated cancers could be the inhibition of tumor necrosis factor (TNF)-related apoptosis-inducing ligand (TRAIL) and other TRAIL-receptors (TRAIL-Rs). Essentially, TRAIL is known to induce apoptosis, a form of programmed cell death, and to kill tumor cells *in vivo* [168], [169]. Moreover, activation of death receptors on tumor cells can suppress metastasis formation [170]–[173]. Therefore, death receptor-stimulating agents have been developed as anti-tumor therapeutics [174]. However, many cancer cell lines are resistant to TRAIL-induced apoptosis and it is known that TRAIL and CD95, another death receptor, can also stimulate cell proliferation, survival and invasion in tumors [175]–[180]. In addition, TRAIL can also activate several signaling pathways such as the MAPKs JNK, p38 and ERK [181], [182]. Surprisingly, it has been shown that in KRAS-mutated colorectal cancer (CRC) cell lines oncogenic KRAS and its effector RAF1 influence TRAIL and CD95, which stimulate the invasion of colorectal tumor cells and liver metastases [183]. Moreover, another study revealed that endogenous TRAIL/TRAIL-Rs induce cancer progression, invasion, and metastasis in KRAS-mutated cancers, thereby leading to apoptosis resistance [184]. Therefore, inhibition of the interaction of TRAIL/TRAIL-Rs could be a therapeutic approach to treat patients harboring KRAS-mutations. However, since TRAIL-R signaling in KRAS mutant cancers results in apoptosis resistance, the induction of another type of cell death could be investigated to overcome resistance mechanism of oncogenic KRAS.

1.6 AIM OF THIS STUDY

KRAS is the most frequently mutated oncogene in the deadliest cancers worldwide including PDAC and LUAD [129]. Mutations in KRAS lead to constitutively activated downstream effector pathway signaling, which results in uncontrolled cell division, proliferation, migration, cellular differentiation and resistance to cell death [133]. Although RAS has been immensely studied for almost 40 years and molecular therapies to target mutant RAS have reached the clinic, there is still an urgent need to improve knowledge about how oncogenic forms of KRAS rewire cell death. Moreover, it is established that KRAS-mediated tumorigenesis is ROS dependent and cells expressing mutant KRAS deal with higher ROS levels [105], [108]. Additionally, it was shown that cells expressing oncogenic KRAS upregulate NRF2 – the antioxidant machinery – to induce ROS detoxification [115] . Controversially, it is known that high ROS levels will result in apoptosis [113] and high lipid ROS levels will lead to ferroptosis [19]. Therefore, it still needs to be further investigated how KRAS mutant cells cope with high ROS levels and how they deal with lipid ROS induced cell death.

Therefore, the following aims of this study were determined:

1. Characterization of various independent isogenic cellular models expressing near-endogenous levels of oncogenic or wild type (WT) KRAS in regard to ferroptosis sensitivity/resistance *in vitro*
2. Identification of the resistance mechanism in cells expressing mutant KRAS *in vitro*
3. Validation of the resistance mechanism and its regulation through oncogenic KRAS *in vitro*
4. Investigation of the impact of the resistance mechanism on cellular transformation in 2D vs 3D *in vitro* assays and on tumor initiation *in vivo*

Taken together, these aims were designed to shed light into ferroptotic cell death resistance mechanisms in KRAS-mutated cancer cells.

2 PUBLICATION / MANUSCRIPT

2.1 ELEVATED FSP1 PROTECTS KRAS-MUTATED CELLS FROM FERROPTOSIS DURING TUMOR INITIATION

Fabienne Müller, Jonathan K. M. Lim, Christina M. Bebber, Eric Seidel, Sofya Tishina, Alina Dahlhaus, Jenny Stroh, Julia Beck, Fatma Isil Yapici, Keiko Nakayama, Lucia Torres Fernández, Johannes Brägelmann, Gabriel Leprivier & Silvia von Karstedt

Published in Cell Death and Differentiation, 29 November 2022
DOI: 10.1038/s41418-022-01096-8

Specific contributions:

- Analysis of RNA sequencing data of $KRAS^{WT}$ and $KRAS^{G12D}$-expressing cells
- Cell viability assays of $KRAS^{WT}$, $KRAS^{G12D}$ and $KRAS^{G12C}$-expressing cells
- Cell death assays of $KRAS^{WT}$ and $KRAS^{G12D}$-expressing cells, $KRAS^{WT}$ and $KRAS^{G12D}$ cells overexpressing empty Vector or FSP1 and siKEAP1 transfected clonal $KRAS^{WT}$ cells
- Live cell imaging of bulk-sorted MEFs expressing $KRAS^{WT}$ and $KRAS^{G12D}$
- IncuCyte quantification of $KRAS^{WT}$ or $KRAS^{G12D}$-expressing cells
- Evaluation of NADPH assay of $KRAS^{WT}$ and $KRAS^{G12D}$-expressing cells
- Quantification and validation of quantitative PCR analysis of $KRAS^{WT}$ and $KRAS^{G12D}$-expressing cells and stable FSP1 knockdown cells
- Quantification of lipid ROS and general ROS in $KRAS^{WT}$ and $KRAS^{G12D}$-expressing cells
- Western blot analysis of $KRAS^{WT}$ and $KRAS^{G12D}$-expressing cells, $KRAS^{WT}$ and $KRAS^{G12D}$ cells overexpressing empty Vector or FSP1 and siFSP1 transfected cells
- Quantification and validation of spheroid assays of $KRAS^{WT}$ and $KRAS^{G12D}$ cells overexpressing empty Vector or FSP1 and adenocarcinoma human alveolar basal epithelial cells (A549) cells
- Generation and validation of $KRAS^{WT}$ and $KRAS^{G12D}$ cells overexpressing empty Vector or FSP1 and stable FSP1 knockdown cells
- Generation of siRNA transfection of $KRAS^{WT}$ and $KRAS^{G12D}$-expressing cells

- Inhibitor treatment of $KRAS^{WT}$ and $KRAS^{G12D}$-expressing cells, $KRAS^{WT}$ and $KRAS^{G12D}$ cells overexpressing empty Vector or FSP1 and A549 cells
- Assistance in tumor xenograft experiments
- Assistance with isolation and treatment of murine pancreatic organoids
- Data evaluation
- Statistical analysis
- Manuscript reviewing and editing
- Figure design

CDDpress

www.nature.com/cdd

ARTICLE OPEN

Check for updates

Elevated FSP1 protects KRAS-mutated cells from ferroptosis during tumor initiation

Fabienne Müller[1,2], Jonathan K. M. Lim[3], Christina M. Bebber[1,2], Eric Seidel[1,2], Sofya Tishina[1,2], Alina Dahlhaus[1,2], Jenny Stroh[1,2], Julia Beck[1,2], Fatma Isil Yapici[1,2], Keiko Nakayama[4], Lucia Torres Fernández[1], Johannes Brägelmann[1,5,6], Gabriel Leprivier[3] and Silvia von Karstedt[1,2,5]✉

Oncogenic KRAS is the key driver oncogene for several of the most aggressive human cancers. One key feature of oncogenic KRAS expression is an early increase in cellular reactive oxygen species (ROS) which promotes cellular transformation if cells manage to escape cell death, mechanisms of which remain incompletely understood. Here, we identify that expression of oncogenic as compared to WT KRAS in isogenic cellular systems renders cells more resistant to ferroptosis, a recently described type of regulated necrosis. Mechanistically, we find that cells with mutant KRAS show a specific lack of ferroptosis-induced lipid peroxidation. Interestingly, KRAS-mutant cells upregulate expression of ferroptosis suppressor protein 1 (FSP1). Indeed, elevated levels of FSP1 in KRAS-mutant cells are responsible for mediating ferroptosis resistance and FSP1 is upregulated as a consequence of MAPK and NRF2 pathway activation downstream of KRAS. Strikingly, FSP1 activity promotes cellular transformation in soft agar and its overexpression is sufficient to promote spheroid growth in 3D in KRAS WT cells. Moreover, FSP1 expression and its activity in ferroptosis inhibition accelerates tumor onset of KRAS WT cells in the absence of oncogenic KRAS in vivo. Consequently, we find that pharmacological induction of ferroptosis in pancreatic organoids derived from the LsL-KRAS^{G12D} expressing mouse model is only effective in combination with FSP1 inhibition. Lastly, FSP1 is upregulated in non-small cell lung cancer (NSCLC), colorectal cancer (CRC) and pancreatic ductal adenocarcinoma (PDAC) as compared to the respective normal tissue of origin and correlates with NRF2 expression in PDAC patient datasets. Based on these data, we propose that KRAS-mutant cells must navigate a ferroptosis checkpoint by upregulating FSP1 during tumor establishment. Consequently, ferroptosis-inducing therapy should be combined with FSP1 inhibitors for efficient therapy of KRAS-mutant cancers.

Cell Death & Differentiation; https://doi.org/10.1038/s41418-022-01096-8

INTRODUCTION

The Ras proto-oncogenes (HRAS, NRAS and KRAS) are amongst the most frequently mutated genes across human cancers [1–3]. KRAS in particular is mutated in lung and pancreatic ductal adenocarcinoma (PDAC) as well as colorectal cancer. Point mutations within KRAS favor its active, GTP-bound state [2, 3]. Thereby, oncogenic forms of KRAS constitutively signal through the mitogen-activated protein (MAPK) pathway, PI3K and Rac1 signaling pathways endowing them with a variety of advantages including evasion of extrinsic apoptosis [4, 5]. It is established that KRAS-mediated cellular transformation requires the generation of reactive oxygen species (ROS) through elevated expression of NADPH oxidase 1 (Nox1) [6]. Yet, it is poorly understood how cells expressing mutated KRAS can mitigate the problem of ROS-induced cell death. We recently showed that cells expressing oncogenic KRAS upregulate the cystine/glutamate antiporter xCT (SLC7A11) upon hydrogen peroxide stimulation to promote cellular transformation [7]. Interestingly, xCT has been shown to protect cells from ferroptosis, an iron-dependent type of regulated necrosis executed by the accumulation of lipid ROS [8]. Cells are protected from ferroptosis by glutathione peroxidase 4 (GPX4) [9] which depends on glutathione (GSH) as an electron donor to reduce lipid hydroperoxides. GSH synthesis is coupled to the availability of intracellular cysteine which can be generated from cystine imported via xCT [10]. In addition, recent studies indicate that the Coenzyme Q10 (COQ10) oxidoreductase ferroptosis suppressor protein 1 (FSP1, formerly AIFM2) protects cells from ferroptosis through the generation of the lipid radical-trapping agent ubiquinol [11, 12]. Although ferroptosis has been suggested to represent a vulnerability in HRAS-mutant cells [13], GPX4 deletion in pancreatic intraepithelial neoplasia (PanINs) in genetically engineered mouse models driven by KRAS^{G12D} did not effectively kill PanINs [14] strongly suggesting KRAS^{G12D}-driven PanINs to be protected from ferroptosis through unknown mechanisms.

[1]University of Cologne, Faculty of Medicine and University Hospital Cologne, Department of Translational Genomics, Cologne, Germany. [2]CECAD Cluster of Excellence, University of Cologne, Cologne, Germany. [3]Heinrich Heine University, Medical Faculty and University Hospital Düsseldorf, Institute of Neuropathology, Düsseldorf, Germany. [4]Division of Cell Proliferation, ART, Graduate School of Medicine, Tohoku University, Sendai, Japan. [5]University of Cologne, Faculty of Medicine and University Hospital Cologne, Center for Molecular Medicine Cologne, Cologne, Germany. [6]Mildred Scheel School of Oncology Cologne, Faculty of Medicine and University Hospital Cologne, University of Cologne, Cologne, Germany. ✉email: s.vonkarstedt@uni-koeln.de

Edited by G. Melino

Received: 21 April 2022 Revised: 3 November 2022 Accepted: 14 November 2022
Published online: 29 November 2022

Here, through the use of various independent isogenic cellular models expressing near-endogenous levels of oncogenic or wild type (WT) KRAS, we demonstrate that oncogenic forms of KRAS render cells more resistant to ferroptosis through NRF2-mediated FSP1 upregulation in vitro and during tumor initiation in vivo.

MATERIALS AND METHODS

Cell lines

The panel of "Rasless" mouse embryonic fibroblasts (MEFs) reconstituted with various oncogenic KRAS mutations (RPZ26216, RPZ25854, RPZ26198, RPZ26186, RPZ26425, RPZ26299, RPZ26295) was generated and kindly provided by the RAS Initiative at the Frederick National Laboratory for Cancer Research (FNLCR), US. Independently, Rasless MEFs were also obtained from M. Barbacid to generate KRAS point mutants from bulk sorting without deletion of the endogenous floxed KRAS allele. All MEFs were grown in Dulbecco's modified Eagle's (DMEM) + GlutaMAX™ medium (Gibco) with 4 µg/ml of blasticidin. NIH-3T3 cells expressing $KRAS^{G12V}$ were generated and described previously [7]. NIH-3T3 stably expressing 4OHT-inducible $HRAS^{G12V}$ and freshly isolated $KRAS^{G12D}$-inducible mouse embryonic fibroblasts (MEFs) were cultured in DMEM (Gibco) supplied with 1% L-Glutamine (Sigma) and 1% Sodium Pyruvate (Sigma). Human pancreatic duct epithelial cells (HPDE) were kindly provided by A. Trauzold (University of Kiel) and cultured in 75% RPMI 1640/ medium in presence of 25% keratinocyte growth medium 2 (PromoCell). The human non-small cell lung cancer (NSCLC) cell line A549 and mouse Lewis lung carcinoma cell line (3LL) were kindly provided by Prof. Julian Downward and cultured in RPMI 1640 medium (Gibco). HEK-293T cells were cultured in DMEM medium (Gibco). All media were supplemented with 10% fetal calf serum (FCS) (Sigma Aldrich) and 1000 U/mL of both penicillin and streptomycin (Pen/Strep) (Sigma Aldrich). All cells were kept at 37 °C with 5% CO_2 and tested for mycoplasma at regular intervals (mycoplasma barcodes, Eurofins Genomics).

Reagents

Blasticidin (AppliChem GmbH), RSL3 (Selleckchem), ML210 (Tocris), ML162 (Caymann), Erastin (Biomol), Sulfasalazine (SAS) (MedChemExpress), Imidazole Ketone Erastin (IKE) (Sellekchem), Ferrostatin-1 (Sigma Aldrich), Liproxstatin-1 (Biozol), Necrostatin-1s (Abcam), zVAD (ENZO), iFSP1 (Cayman Chemicals), Tert-butylhydroquinone (TBHQ) (Sellekchem), AMG510 (MedChemExpress), ARS1620 (Chemgood), PD184352 (Sigma Aldrich), MK2206 (Sellekchem), DRAQ7 (Biolegend), BODIPY C11 (Invitrogen), H2DCFDA (Invitrogen), Dharmafect I (Dharmacon), Puromycin (Sigma), Doxycycline hydrochloride (Alfa Aesar), 4-hydroxy-tamoxifen (4OHT) (Sigma), Polybrene (Merck), CaCl2 (Sigma Aldrich), HBS (Sigma Aldrich), propidium iodide (Sigma).

Antibodies

Ras (clone RAS10, #05-516; Millipore, 1:1000), GPX4 (Abcam, ab41787, 1:2,000), xCT (Abcam, ab37185, 1:2000), ß-Actin (Sigma, A1978, 1:10,000), GAPDH (Cell Signaling, #97166, 1:2000), FSP1 (previously described [11], kindly provided by M. Conrad, undiluted hybridoma supernatant), p44/42 MAPK (Erk1/2) (Cell Signaling, #9102 1:1000), phospho-p44/42 MAPK (Erk1/2) (Thr202/Tyr204) (Cell Signaling, #4370, 1:1000), HRP-conjugated secondary antibodies: goat-anti-mouse-HRP (Linaris GmBH, 20400-1 mg, 1:10,000), goat-anti-rabbit-HRP (Linaris GmBH, 20402-1 mg, 1:10,000), goat-anti-rat-HRP (Sigma, A9037-1 ml, 1:10,000).

Plasmids

The packaging plasmids pCMV-VSV-G (#8454), pCMV-VSV-G (#8454), pMDLg/pRRE (#12251) were obtained from Addgene, P442-empty vector and P442-PLI-AIFM2-WT was kindly provided by J. P. Friedmann-Angeli, pLKO.1-empty vector and pLKO.1-shFSP1 were purchased from Merck (NM_153779/TRCN0000112139/pLKO.1). pCW-Puro-$KRAS^{G12D}$ to generate doxycycline $KRAS^{G12D}$-inducible HPDE cells was cloned from pCW (addgene #50661 [15]) by replacing the existing Cas9 gene by human $KRAS^{G12D}$ cDNA.

siRNA transfections

Two hundred microliters Opti-MEM (Gibco) and 1.5 µL Dharmafect Reagent I (Dharmacon) were mixed and incubated for 5–10 min at room temperature. 2.2 µL of siRNA (Stock 20 mM) (Dharmacon) were added to the mixture and incubated for another 30 min at room temperature. After incubation, 200 µL of the mixture was added to each well (6-well) plate and cells were plated on top. Knockdowns were incubated for 48–72 h, as indicated.

Cell viability assays

For this assay, 5000 or 10,000 (for iFSP1 ± RSL3 viability assays) cells were plated per 96-well plate 24 h before treatment. Cell viability was determined by Cell Titer Blue assay according to the manufacturer's instructions (Promega).

Cell death assays (flow cytometry)

One day before treatment 45,000 cells (clonal and bulk-sorted MEFs), 55,000 cells (cells expressing either P442-empty vector or P442-PLI-AIFM2-WT) or 50,000 cells (3LLs) were plated in each well of a 24-well plate. For FSP1 siRNA knockdown, 40,000 cells were seeded 48 h before treatment. To determine cell death, adherent and detached cells were harvested and stained with propidium iodide (PI) (1 µg/ml) (Sigma Aldrich) in PBS (Thermo Fisher) supplemented with 2% FBS. PI-positive cells were quantified by flow cytometry using an LSR-FACS Fortessa (BD Bioscience) and FlowJo software (BD Bioscience).

Live cell imaging (IncuCyte)

Five thousand, 7500 or 10,000 cells per 96-well plate, 55,000 cells per 24-well plate or 300,000 cells per 6-well plate were seeded 24 h in advance, respectively. For KEAP1 siRNA knockdown, 20,000 cells were seeded in a 24-well plate on top of the transfection mix and incubated for 48 h followed by treatments for 24 h. Upon treatment, (Ferrostatin-1 [1 or 5 µM], RSL3 [0.1 µM or 1 µM], iFSP1 [10 µM], Erastin [0.37 µM], Sulfasalazine (SAS) [0.17 mM], Imidazole Ketone Erastin (IKE) [1.11 µM], ML210 [0.37 µM], ML162 [1.11 µM], TBHQ [25 nM]) cells were imaged using the 10× objective within the IncuCyte live cell imager (Sartorius). For dead cell quantification, 100 nM DRAQ7 (Thermofisher) were added to each well. For lipid ROS determination, cells were stained with 5 µM BODIPY C11. Cells were imaged for indicated timepoints every 2 h. Analysis for confluence, DRAQ7-positive (dead) or BODIPY C11-positive cells was performed using the Software IncuCyte 2021A (Sartorius).

Quantitative PCR

For $KRAS^{WT}$ and $KRAS^{G12D}$ comparison, 300,000 cells were seeded per well in a 6-well plate and RNA was extracted 24 h later. For MEK and AKT inhibition treatment experiments 200,000 cells were seeded in a 6-well plate one day in advance followed by treatments for 48 h. For TBHQ treatment experiments, 150,000 of $KRAS^{WT}$ cells were seeded in a 6-well plate a day in advance followed by treatment for 24 h. For KEAP1 knockdowns, 200,000 of $KRAS^{WT}$ cells were seeded in a 6-well plate on top of the transfection mix and incubated for 72 h. For LsL-$KRAS^{G12D}$-inducible MEFs, 200,000 cells were seeded in 1 µg/ml 4OHT in a 6-well plate and incubated for 4 or 5 days. For doxycycline-inducible $KRAS^{G12D}$ HPDE cells, 450,000 cells were seeded in 0.5 µg/mL doxycycline in a 6-well plate and incubated for 72 h. For 4OHT-inducible $HRAS^{G12V}$ NIH-3T3 cell, 35,000 cells were seeded for 72 h in a 6-well plate and 100 nM 4OHT was added and incubated for another 48 h.

For total RNA isolation, the NucleoSpin RNA kit (740955.5, Macherey-Nagel) was used according to the manufacturer's instructions. Next, isolated RNA was reverse transcribed into cDNA using the LunaScript RT SuperMix Kit (E3010L, NEB). For quantitative PCR, 5 µl of Power SYBR GREEN PCR Master Mix (4368702, Thermo Fisher) was mixed with 2 µl of nuclease-free water (NEB), 1 µl (10 µM) of primer mix (forward and reverse primers) (see Supplementary Table 1 for primers used) and 2 µl of cDNA (5 µg/µl). Real-time qPCR was performed in triplicate or in quadruplicate on the Quant Studio5 qRT PCR cycler and results were normalized to the expression of the house-keeping gene indicated. Actin, Rplp0, Rpl13a or 18S were used as house-keeping gene controls as indicated.

Lipid ROS quantification (flow cytometry)

Thirty-five thousand cells per well were plated in a 24-well plate 24 h before treatment. Lipid ROS levels were quantified by BODIPY C11 (Invitrogen) staining. To this end, cells were stained using 5 µM BODIPY C11 during the last 30 min of treatment incubation. Mean fluorescence intensity (MFI) was determined by flow cytometry using an LSR-FACS

Fortessa (BD Bioscience) and FlowJo software (BD Bioscience). Flow cytometry data were collected from at least 5000 cells.

General ROS quantification (flow cytometry)

Fifty-five thousand cells per well were plated in a 24-well plate 24 h before treatment. Cells were incubated with 20 µM H2DCFDF (Invitrogen) per well to stain cellular ROS. Mean fluorescence intensity (MFI) was determined by flow cytometry using an LSR-FACS Fortessa (BD Bioscience) and FlowJo software (BD Bioscience). Flow cytometry data were collected from at least 5000 cells.

NADPH Assay

Twenty thousand cells per 96-well plate were seeded in advance. NADP/NADPH was determined by NADP/NADPH-Glo™ Detection Reagent assay according to the manufacturer's instructions (Promega).

Lipidomics to determine oxidized lipids and levels of total phospholipids

Mass spectrometry experiments to determine total phospholipids and oxidized lipids were performed as described previously [16]. In brief, levels of oxidized phosphatidylcholine (PC) and phosphatidylethanolamine (PE) species were determined by Liquid Chromatography coupled to Electrospray Ionization Tandem Mass Spectrometry (LC-ESI-MS/MS). Oxidized PC and PE species were quantified by normalizing their peak areas to those of the internal standards. Glycerophospholipids (PC and PE, including ether-linked species) in cells were analyzed by Nano-Electrospray Ionization Tandem Mass Spectrometry (Nano-ESI-MS/MS) with direct infusion of the lipid extract (Shotgun Lipidomics). The protein content of the homogenate was routinely determined using bicinchoninic acid. Endogenous glycerophospholipids were quantified by referring their peak areas to those of the internal standards. The calculated glycerophospholipid amounts were normalized to the protein content of the cell homogenate.

Western blotting

For $KRAS^{WT}$ and $KRAS^{G12D}$ 300,000 cells were seeded one day in advance in a 6-well plate before cells were treated for another 5 h with or without RSL3. For FSP1 knockdowns, 75,000 cells were seeded in a 6-well plate on top of the transfection mix and incubated for 72 h. For $KRAS^{WT}$ and $KRAS^{G12D}$ cells expressing either empty Vector or FSP1-WT 300,000 cells were seeded in a 6-well plate for 24 h. For LsL-$KRAS^{G12D}$-inducible MEFs, cells were incubated for 72 h with or without 1 µg/ml 4OHT before 250,000 cells were seeded into a 6-well plate for indicted timepoints. For MEKi and AKTi treatment experiments 150,000 cells were seeded one day in advance in a 6-well plate before cells were treated for 72 h. Cell lysates were prepared in lysis buffer (30 mM Tris-HCl [pH 7.4], 120 mM NaCl, 2 mM EDTA, 2 mM KCl, 1% Triton X-100, 1× COMPLETE protease-inhibitor and phosphatase- inhibitor cocktail). Lysate concentrations were adjusted to equal protein concentrations using the bicinchoninic acid (BCA) protein assay (Biorad). Equal amounts of protein were mixed with a final concentration of 1× reducing sample buffer (Invitrogen) and 200 mM DTT (VWR). Samples were heated to 95 °C for 10 min, separated via gel electrophoresis and transferred to nitrocellulose membranes (Biorad). Membranes were blocked in PBS with 0.1% Tween 20 (PBST) (VWR) with 5% (w/v) dried milk powder (AppliChem) for at least 30 min and incubated with primary antibodies over night. After washing with PBST, membranes were incubated with horse radish peroxidase (HRP)-coupled secondary antibodies (Biotium) diluted 1:10,000 for at least 1 h at room temperature. After another washing step, bound antibodies were detected using chemiluminescent Amersham ECL Prime Western Blotting Detection Reagent (Cytiva) or SuperSignal™ West Femto Maximum Sensitivity Substrate (Thermo Fisher). X-ray films CL-XPosure™ (Thermo Fisher) or the FUSION Solo S system and software (Vilber) were used to develop the membranes.

RNA sequencing

For RNA sequencing, 70,000 cells per well (6-well plate) of either $KRAS^{WT}$ or $KRAS^{G12D}$ were seeded 24 h in advance. The next day, cells were washed with PBS and RNA was isolated using the NucleoSpin RNA kit (740955.5, Macherey-Nagel) according to the manufacturer's instructions. cDNA libraries amplified from the 3′ UTR were generated from total RNA using the Lexogen QuantSeq kit (Lexogen, Austria) according to the standard protocol and sequenced with a 50-bp single-end protocol on Illumina HiSeq4000 sequencer (Illumina, USA). The raw-sequencing data was aligned to the respective mouse reference genomes and quantified prior to differential expression analyses. Raw FPKM values of each transcript were transformed by $\log_2$ (FPKM + 0.01). Data processing and statistical analyses were performed using Microsoft Excel (Microsoft, USA) and Instant Clue software [17] which performed a hierarchical clustering to classify the experiments and generate a heatmap for the visualization of different RNA expression.

Generation of FSP1-overexpressing cells

To generate stable cells overexpressing FSP1, viral particles were produced in HEK-293T cells. HEK-293T cells were plated in a 6-well plate the day before transfection. For 6 × 6 wells of a 6-well plate 5 µg of each packaging plasmid and 10 µg of transfer vector plasmid were mixed together. Fifty microliters of 250 mM $CaCl_2$ and 444 µl H_2O were added to the plasmid mixture and mixed well by pipetting. For the formation of calcium-phosphate-DNA co-precipitate, the plasmid transfection mix (~500 µl) was carefully dropped into 500 µl of 2× HBS buffer under constant vortexing. The precipitate was incubated for 20 min at room temperature and added dropwise into freshly replaced media without Pen/Strep. After 6–8 h of transfection medium was aspirated, and fresh normal medium was added. The following two days, virus-containing supernatant was harvested and filtered with 0.45 µm sterile syringe filter. Fresh medium was always added again on the cells. Virus harvest was centrifuged, and supernatant was collected and stored at −80 °C. For transduction of the $KRAS^{WT}$ and $KRAS^{G12D}$ cells viral supernatant was added to wells containing cells with 6 µg/ml polybrene and centrifuged for 45 min at 2500 rpm at 30 °C. Cells were incubated afterwards at 37 °C and 5% CO_2 until they were confluent and selected for positively-transfected cells using Puromycin ($KRAS^{WT}$ 1 µg/ml and $KRAS^{G12D}$ 2.5 µg/ml) for 7 days.

Generation of stable FSP1 knockdown cells

For stable transduction of FSP1 knockdown cells, lentiviral supernatant with an shFSP1 transfer plasmid was produced as described above and $KRAS^{G12D}$ cells were transduced with the virus. After selection with Puromycin (2.5 µg/ml) for 7 days, knockdown was validated using qPCR.

Generation of LsL-$KRAS^{G12D}$-inducible MEFs

Mouse embryonic fibroblasts (MEFs) were generated from E13.5 mouse embryos by standard Jacks lab procedure (https://jacks-lab.mit.edu/protocols/making_mefs). MEFs with positive genotypes for 4-hydroxytamoxifen (4OHT)-inducible Cre (primer: #1 GCG GTC TGG CAG TAA AAA CTA TC, #2 GTG AAA CAG CAT TGC TGT CAC TT) and LsL-$KRas^{G12D}$ (primer: #1 gtc ttt ccc cag cac agt gc, #2 ctc ttg cct acg cca cca gct c; #3 agc tag cca cca tgg ctt gag taa gtc tgc a) were used for the experiments. To obtain Cre expression cells were treated with 1 µg/ml 4OHT.

Generation of $HRAS^{G12V}$-inducible NIH-3T3

NIH-3T3 stably expressing 4OHT-inducible $HRAS^{G12V}$generated as previously described [18]. Activation of Ras was induced by exposure of cells to 100 nM 4OHT, with 4OHT-supplemented medium being refreshed every two days.

Generation of $KRAS^{G12D}$- inducible human pancreatic duct epithelial cells (HPDE)

Lentiviral particles were produced in HEK-293T cells transfected with packaging plasmids pCMV-VSV-6, pMDLg and pRSV-Rev as well as 10 µg pCW-Puro-$KRAS^{G12D}$ (a newly cloned pCW (addgene #50661 [15]) backbone replacing the existing Cas9 by human $KRAS^{G12D}$ cDNA) using a 1:1 mixture of 2× HBS and 250 mM CaCl2 in DMEM F12 medium with 10% FCS, 1% Pen/Strep and 1% Glutamine. After overnight incubation, medium was replaced for HPDE medium (see above), and medium containing viral particles was subsequently harvested after 48 h. HPDE cells were infected in a 6-well plate at 30% confluency by replacing the medium by viral supernatant after adding polybrene at a final concentration of 8 µg/mL. After 3 days, medium was replaced by selection medium containing 0.5 µg/mL puromycin. For $KRAS^{G12D}$ induction, HPDE cells were treated with 0.5 µg/ml doxycycline for 72 h.

Spheroid assays

To generate spheroid cultures, 5000 cells per 96-well were plated in a 96 ultra-low attachment multi-well plate (Corning) in 100 µl media containing

4 % Matrigel (Corning). After 24 h 2× iFSP1 [10 µM or 20 µM], 2× Fer1 [2.5 µM] or 2× Liproxstatin-1 [0.3 µM] treatment in 100 µl media was added to the cells and incubated for 9 (A549) or 14 days (MEFs). Pictures of the spheroids were taken with the BZ-X800E microscope (Keyence). Spheroid assay and organoid assay colony area and brightness were analyzed using the BZ-H4M/Measurement Application Software (Keyence).

Soft agar colony formation assays

Cells were plated in 6-well plates at 8000 cells per well. Equal volumes of culturing medium and agarose were used such that the final concentrations were DMEM, 10% bovine serum (for 3T3 KRAS) or RPMI, 10% fetal bovine serum (for A549) and 0.25% agarose for the top layer or 0.4% agarose for the bottom layer, respectively. Where indicated, DMSO, iFSP1 (10 or 20 µM) or Fer1 [5 µM] was added to the top agar layer. Cells were fed

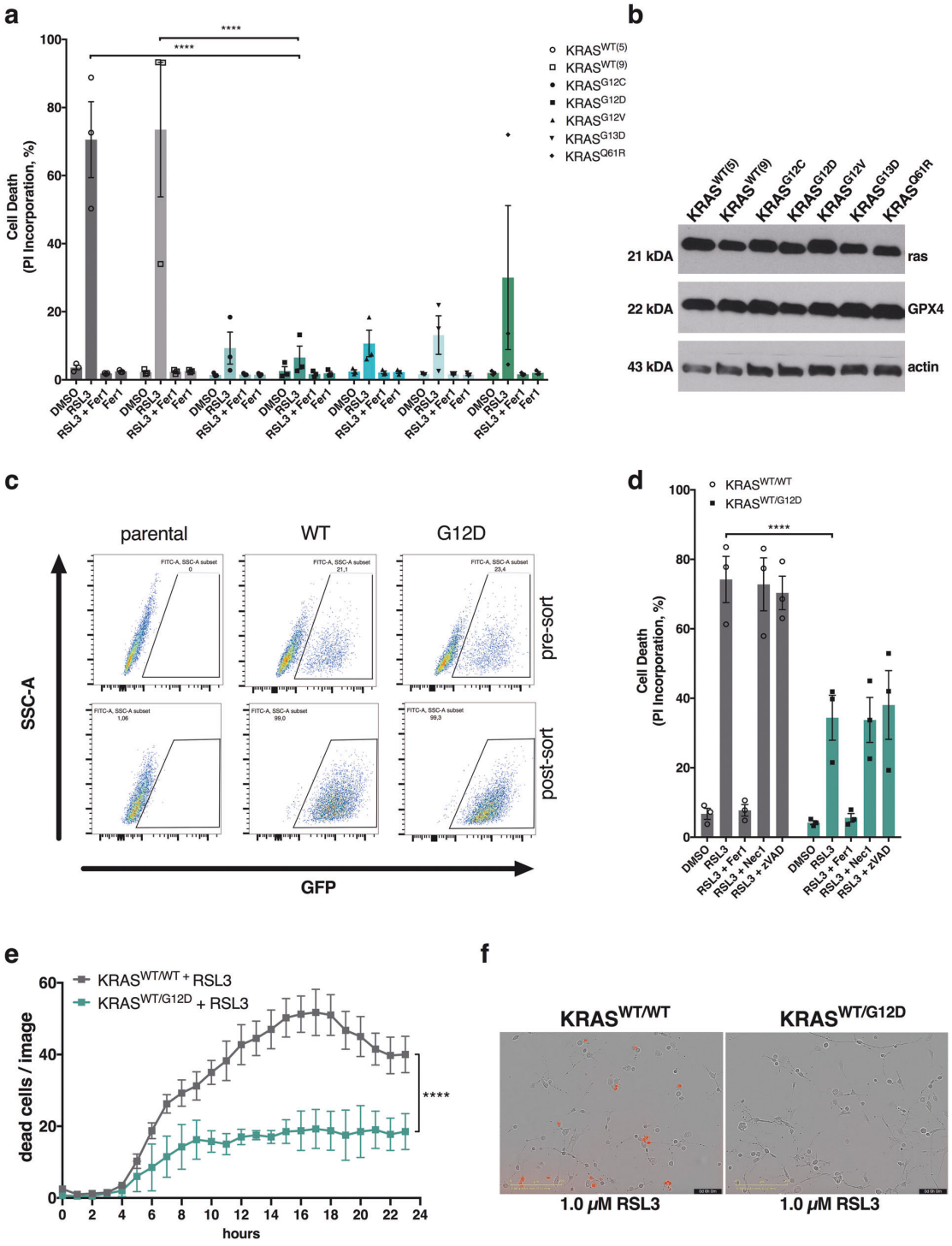

Fig. 1 Expression of oncogenic KRAS renders cells resistant to ferroptotic cell death. a Rasless MEFs expressing the indicated variants of either KRAS WT or mutants were treated either with DMSO, RSL3 [100 nM] alone or in combination with Ferrostatin-1 (Fer-1) [5 µM] for 24 h. Cell death was determined by propidium iodide (PI) uptake and flow cytometry. 0 % PI-Incorporation is gated to control untreated. **b** Protein extracts were obtained from cells as in (**a**) and expression of the indicated proteins was detected by Western blotting. **c** Parental Rasless MEFs were infected with viral supernatants containing the indicated stable expression plasmids. FACS dot plots before and after sorting for GFP + cells are shown. **d** Bulk-sorted cells as in (**c**) were treated as in (**a**) but including Necrostatin-1s (Nec1) [10 µM] and zVAD [20 µM]. 0 % PI-Incorporation is gated to untreated control. **e** Cells as in (**c**) were treated with RSL3 [1 µM] and DRAQ7 [100 nM] was added to all wells to visualize dead cells. Images were acquired at ×10 magnification every 2 h using the IncuCyte S3 bioimaging platform. **f** Representative phase contrast overlays are shown from cells treated as in (**e**). Data are means ± SEM of three independent experiments in each individual cell line or representative images were applicable. Two-way ANOVA + Tukey's multiple comparison test (**a, d**), two-tailed *t*-test at end timepoint (**e**), $^{****}p < 0.0001$. Uncropped blots are provided as Original Data file.

twice a week with 1 mL of corresponding DMSO or iFSP1 treated medium onto the top layer. Colonies were allowed to form over the course of 18 to 30 days, following which they were imaged and quantified using ImageJ.

Tumor xenograft studies

Mice were maintained on a 12-h light/dark cycle with water and food *ad libitum* throughout the duration of the project. Mouse embryonic fibroblast (MEF) cell lines (5×10^5 cells either $KRAS^{WT}$ e.V., $KRAS^{WT}$ FSP1-WT, $KRAS^{G12D}$ e.V. or $KRAS^{G12D}$ shFSP1) were injected in 200 µl PBS into both flanks of 8–10 weeks old male NMRI-Foxn1 nu/nu mice (Janvier). Mice were not randomized. A group size of at least 10 tumors per condition was assumed to achieve significantly different results ($p = 0.05$) with a power of 80%. For that, cells were harvested from plates using trypsin and washed five times with PBS to remove residual FCS. Mice injected with $KRAS^{WT}$ e.V. or $KRAS^{WT}$ FSP1-WT were assigned to either vehicle or Liproxstatin-1 treatment groups once tumors reached a minimum size of 2.5 × 2.5 mm. For two consecutive weeks, mice were injected 5 × per week either with vehicle (PBS with 1% DMSO) or Liproxstatin-1 (10 mg/kg). Tumor size was tracked by caliper measurements and volume was calculated as (length × width × width)/2. People performing tumor measurements and calculating tumor volume were blinded to the group allocation. Mice were sacrificed at the end of the treatment and fresh-frozen tumor tissue was used for further analysis.

Protein extraction from fresh-frozen tumors

For protein isolation, 20–30 mg of fresh-frozen tumor tissue were mixed in a peqlab vial with the adequate number of ceramic beads and 500 µl IP-lysis buffer (30 mM Tris-HCl, 120 mM NaCl, 2 mM EDTA, 2 mM KCl, 1% Triton-X-100, pH 7.4, Protease and Phosphatase inhibitor (Roche)). For lysis, samples were homogenized for 2 × 30 s using the Precellys 24-dual homogenisator (Peqlab). Samples were centrifuged at 14,000 RPM for 20 min at 4 °C and then further used for western blotting.

Isolation and treatment of murine pancreatic organoids

The pancreas was isolated from PDX1-Cre $KRAS^{G12D}$ mice, washed with cold mouse wash medium (DMEM high glucose + Pen/Strep + 1% FCS) and cut into 1–2 mm pieces using scalpels. Pancreatic pieces were transferred into 50 ml falcons containing 10 ml of mouse digestion medium (200 ml Mouse wash medium + 25 mg Collagenase P; Sigma-Aldrich #C9407 + 25 mg Dispase II; Thermo Fisher #17105041) and shaken at 130 rpm at 37 °C for 20 min. The supernatant was transferred to a Petri dish containing 10 ml of mouse washing medium to obtain the first wash fraction. Ten milliliters of mouse digestion medium were added to the remaining pancreatic pieces. Cycles of shaking at 130 rpm at 37 °C for 10 min were repeated until wash fractions with mainly pancreatic ducts and almost no acinar cells were observed. Wash fractions enriched with ducts were combined and spun down at 1200 rpm for 5 min. The obtained duct pellet was resuspended in 200 µl of ice-cold Matrigel (Growth Factor Reduced, Phenol Red Free; Corning #356231) and a 30 µl dome was seeded into the middle of a well in a prewarmed 24-well plate. Ducts were consecutively diluted in Matrigel to obtain a cellular density with the most favorable conditions for organoids growth. The plate containing domes was placed into the cell culture incubator for 10–15 min for the Matrigel to set before 500 µl of PancreaCult™ Organoid Growth Medium (Mouse) (Stemcell #06040) was added. The organoids were maintained in cell culture with splitting once a week and twice-weekly medium change. For organoids treatments, single cells from 5 days old PDX1-Cre $KRAS^{G12D}$ organoids were isolated according to Boj et al. [19] and Huch et al. [20] and seeded at 200 cells in 100 µl medium/well in a 96-well plate covered in Matrigel:DPBS (1:1). Organoids from single cells were left to grow for 6 days, then treated with 50 µl of PancreaCult medium containing the indicated treatments for 2 days before microscopic pictures were taken using the BZ-X800E microscope (Keyence).

Analysis software and bioinformatic analysis

Heatmaps visualizing ferroptosis and KEGG pathway component expression were generated using Instant Clue software [17]. FACS data were analyzed and quantified using the FlowJo 10.4.2 software. Cell Titer Blue viability assays and qPCR results were analyzed using Excel. Lipidomics measurements were analyzed by MultiQuant 3.0.2 software (SCIEX). IncuCyte experiments were analyzed by using the Software IncuCyte 2021A. Soft Agar colonies were imaged and quantified using ImageJ. Spheroid assay and organoid assay colony area and brightness were analyzed using the BZ-H4M/Measurement Application Software (Keyence). Figures were assembled and data plotted and analyzed using GraphPad Prism 7 for Mac OS X.

Quantification, statistical analysis and reproducibility

GraphPad Prism 7 software (GraphPad Software Inc.) was used for Mac OS X to execute statistical analysis. For comparison between two conditions two-tailed *t*-tests were performed and for comparison between multiple samples two-way ANOVA and Tukey's post test for multiple comparisons were used. All data are presented as mean ± SEM of at least three independent biological replicates. From at least three independent experiments all means are calculated and plotted. Biological replicates gave comparable results, and no technical or biological replicates were excluded. In the respective figure legends statistical tests are declared. The following *p* value cut-offs were used for all tests: $^{****}p < 0.0001$, $^{***}p < 0.001$, $^{**}p < 0.01$, $^{*}p < 0.05$, $^{ns}p > 0.05$. Representative western blots are shown.

RESULTS

Endogenous-level expression of oncogenic KRAS protects from ferroptosis

In order to interrogate the influence of oncogenic KRAS expression in genetically defined isogenic cellular systems, we made use of N- and HRAS-deficient mouse embryonic fibroblasts (MEFs) containing a LoxP-flanked KRAS gene as well as tamoxifen-inducible Cre recombinase. After induction of Cre recombinase-which renders these cells "Rasless" [21]- cells were reconstituted with comparable expression levels of either wild type KRAS 4B or commonly mutated forms of KRAS 4B (hereafter referred to as KRAS; cell line panel available from the Ras initiative at the NIH national cancer institute, US). Strikingly, when treating this cell line panel with the GPX4 small molecule inhibitor RSL3, both WT KRAS-expressing clones were killed within 24 h of treatment whilst all cells expressing oncogenic variants of KRAS were more resistant (Fig. 1a). Moreover, co-treatment with the ferroptosis-selective antioxidant ferrostatin-1 (Fer-1) [8], blocked cell death induced in KRAS WT cells confirming the induction of ferroptosis (Fig. 1a). Importantly, this phenotype was not caused by varying levels in KRAS or expression of GPX4, as all cell lines expressed comparable levels of both proteins (Fig. 1b). Moreover, treatment with other class II ferroptosis-inducing compounds (FINs) which directly inhibit GPX4 equally led to a more drastic loss of viability in KRAS

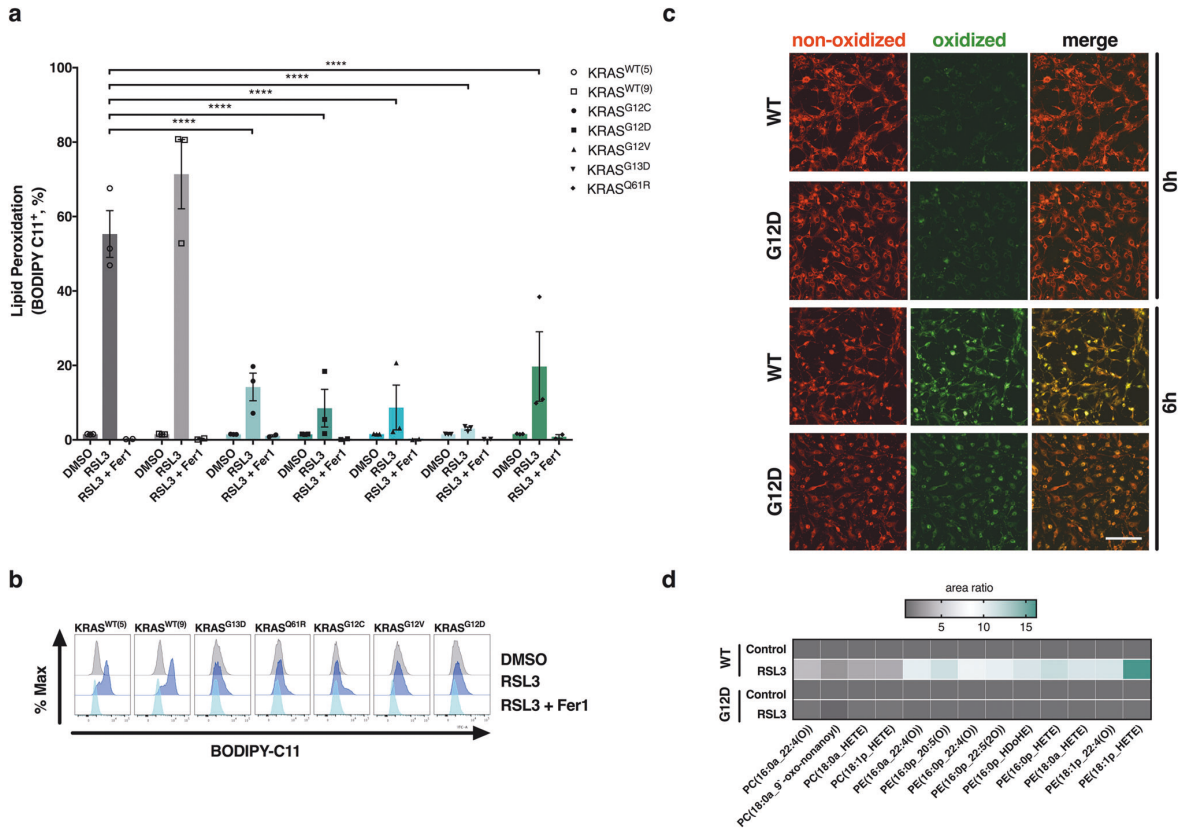

Fig. 2 Expression of oncogenic KRAS protects cells from ferroptosis-associated lipid ROS accumulation. a Rasless MEFs expressing the indicated variant of KRAS were treated either with DMSO, RSL3 [100 nM] alone or in combination with Ferrostatin-1 (Fer-1) [5 μM] for 5 h and stained for lipid ROS accumulation using BODIPY C11. Cells were analyzed by flow cytometry. Negative gates were placed based on DMSO controls. **b** Representative histograms from cells in (**a**) are shown. **c** Rasless MEFs expressing WT or $KRAS^{G12D}$ were treated with RSL3 [100 nM] and stained using BODIPY C11. Images were acquired every 2 h using the IncuCyte S3 bioimaging platform. Representative red, green and overlay fluorescent images (100×) are shown at 0 h and 6 h after treatment. **d** Heatmap showing the representation of mono-oxidized phospholipid species (PE phosphatidylethanolamine; PC phosphatidylcholine) in KRAS WT as compared to $KRAS^{G12D}$-expressing cells treated with either DMSO or RSL3 [100 nM] for 5 h and then subjected to lipidomics. Samples for each condition ($n = 5$) were averaged and normalized to the cell number (2.5×10^6). Each lipid species was normalized to levels detected in the respective DMSO control. Data are means ± SEM of three independent experiments in each individual cell line or representative images or histograms were applicable. Two-way ANOVA + Tukey's multiple comparison test (**a**), $^{****}p < 0.0001$.

WT cells as compared to oncogenic KRAS while for class I FINs no significant difference could be observed (Supplementary Fig. 1a). In addition, loss of cell confluence induced by RSL3 as well as cell death was consistently less pronounced over time also in live cell imaging kinetic experiments in a representative $KRAS^{G12D}$-mutated MEF line (Supplementary Fig. 1b, c). As these MEFs are generated from single cellular clones, we independently generated Rasless MEFs from bulk-sorted populations to exclude clonal effects. These express near endogenous levels of FLAG-tagged KRAS behind GFP and an internal ribosomal entry site (IRES) and were enriched via bulk sorting of GFP^+ cells (Fig. 1c). Importantly, expression of oncogenic $KRAS^{G12D}$ but not KRAS WT equally rendered cells more resistant to ferroptotic cell death in bulk-sorted MEFs (Fig. 1d). Of note, ferrostatin-1 but not the caspase inhibitor zVAD or the RIPK1 inhibitor nec-1s could block cell death induced by RSL3 indicating ferroptotic cell death. Moreover, WT KRAS-expressing cells also died more rapidly upon RSL3 treatment than KRAS-mutant cells (Fig. 1e, f). In order to determine whether direct signaling from oncogenic KRAS is responsible for increased ferroptosis resistance we made use of the fact that effective small molecule inhibitors against $KRAS^{G12C}$ have recently been developed [22–25]. Indeed, treating either $KRAS^{G12C}$-expressing MEFs or the established Lewis lung carcinoma cell line (3LL) - in which NRAS was knocked out (deltaNRAS86) leaving them only with an activating point mutation in $KRAS^{G12C}$ [26] - with the $KRAS^{G12C}$ inhibitor AMG510 sensitized these cells to ferroptosis (Supplementary Fig. 1d, e). Taken together, we find that expression of near-endogenous levels of oncogenic KRAS renders cells more resistant to ferroptotic cell death in various isogenic cellular and experimental setting.

KRAS-mutated cells are protected from ferroptosis-induced lipid peroxidation

A major hallmark of ferroptosis is a lipid ROS-dependent lipid peroxidation chain reaction [27] which oxidizes phosphatidylethanolamine (PE) and phosphatidylcholine (PC) species containing arachidonic (AA) and adrenic acid (AdA) [28, 29]. Since we observed that cells expressing various forms of mutated KRAS were more resistant to ferroptosis than KRAS WT cells, we next determined the extent of lipid ROS accumulation. Indeed, both WT KRAS clones readily accumulated lipid ROS 5 h after stimulation with RSL3 while all KRAS mutants tested did not show lipid ROS accumulation at this time (Fig. 2a, b). Bulk-sorted MEFs expressing flag-tagged mutant $KRAS^{G12D}$ but not WT KRAS, similarly

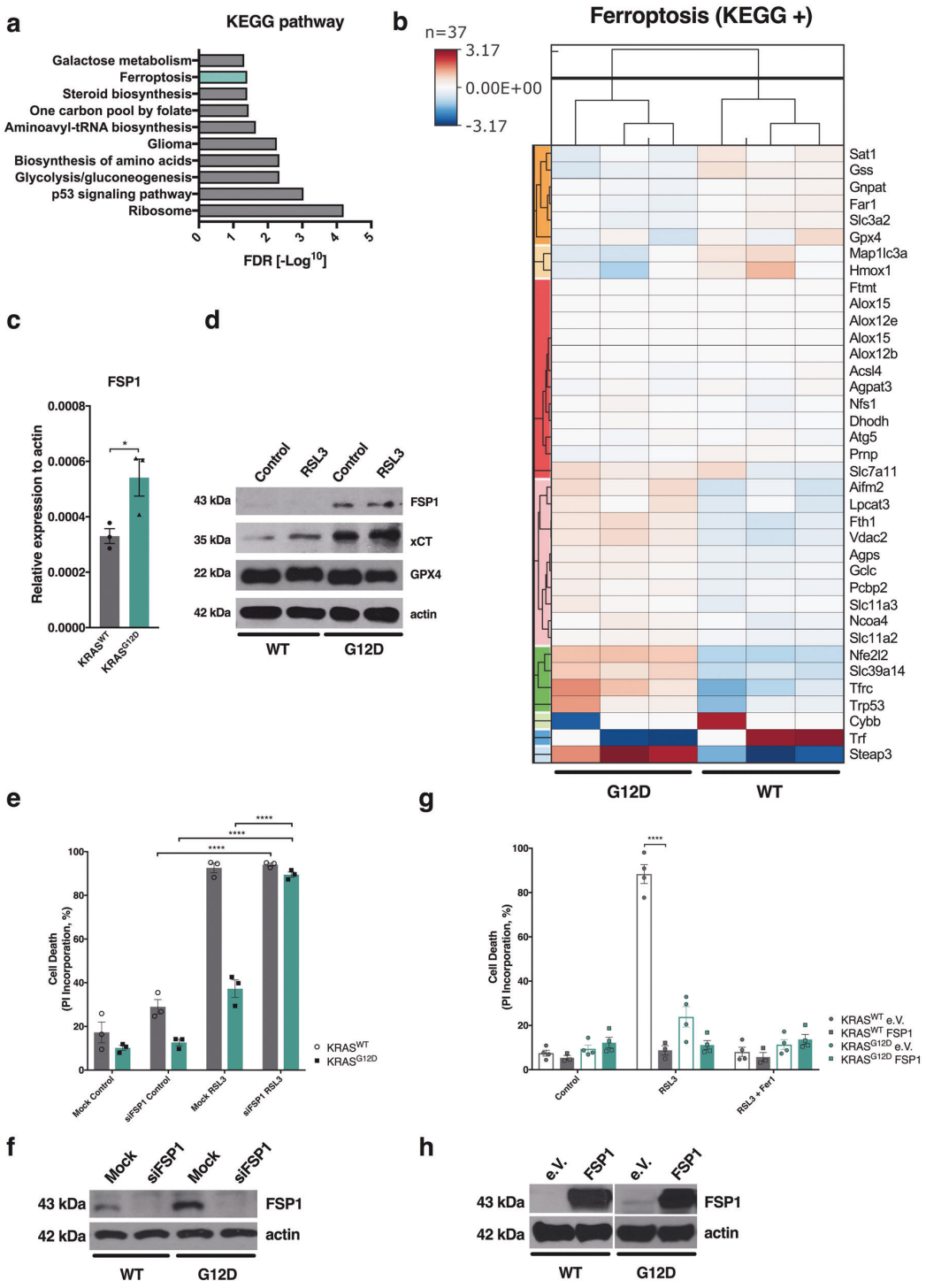

presented with decreased lipid ROS accumulation upon inhibition of GPX4 (Supplementary Fig. 2a). Moreover, KRAS-mutated cells also showed a decrease in the accumulation of oxidized BODIPY C11 indicative of the presence of lipid ROS in time-lapse imaging (Fig. 2c). These data suggested that oncogenic KRAS limits the propagation of lipid ROS and thereby acute lipid peroxidation upon induction of ferroptosis. As the extent of lipid peroxidation during ferroptosis is coupled to cellular amounts of AA-containing polyunsaturated fatty acid (PUFA) PE and PC species including ether-linked PUFAs [30], we first measured basal levels of

Fig. 3 FSP1 is upregulated in KRAS^{G12D}-expressing cells and mediates ferroptosis resistance. a KRAS WT or KRAS^{G12D}-expressing cells were subjected to RNA-sequencing. False discovery rate (FDR) [−Log^{10}] is shown for KEGG pathways significantly enriched within the top 1000 genes upregulated in KRAS^{G12D} cells. **b** Hierarchical clustering of fold change (FPKM + 0.01) of ferroptosis KEGG + genes in KRAS WT and KRAS^{G12D}-expressing cells. **c** Levels of FSP1 mRNA were quantified by qPCR in Rasless MEFs expressing WT or KRAS^{G12D} **d** Indicated cells were treated with RSL3 [100 nM] for 5 h and subjected to Western blotting. **e, f** The indicated cells were subjected to FSP1 or control knockdowns for 48 h and subsequently treated with RSL3 [100 nM] for 24 h. Cell death was determined by flow cytometry and propidium iodide (PI) incorporation. 0 % PI-Incorporation is gated to untreated control. Western blots of representative control lysates are shown. **g, h** WT and KRAS^{G12D} cells stably overexpressing FSP1 were generated and cells were treated with RSL3 [100 nM] alone or in combination with Ferrostatin-1 (Fer-1) [5 μM] for 24 h. Cell death was determined by propidium iodide (PI) uptake and flow cytometry. 0 % PI-Incorporation is gated to control untreated. Western blots of representative control lysates are shown. Data are means ± SEM of three independent experiments in each individual cell line or representative images or histograms were applicable. Two-tailed t-test (**c**), Two-way ANOVA + Tukey's multiple comparison test (**e, g**), ****$p < 0.0001$, *$p < 0.05$. Uncropped blots are provided as Original Data file.

diacylglycerol (DAG) and ether-linked PE and PC PUFAs in KRAS WT as compared to mutant cells using mass spectrometry. While levels of most PUFA species were comparable, a few PC species were elevated in KRAS WT cells (Supplementary Fig. 2b–e). Next, we determined the levels of phospholipid oxidation upon ferroptosis induction in Rasless MEFs expressing either KRAS WT or KRAS^{G12D} by mass spectrometry. Although we observed elevated basal lipid ROS in KRAS-mutated cells (Supplementary Fig. 2f) -likely as a result of elevated basal levels of total ROS due to oncogene expression (Supplementary Fig. 2g) - specific induction of lipid peroxidation upon GPX4 inhibition was absent in KRAS-mutated cells (Fig. 2d). Interestingly, total ROS was nevertheless readily induced in KRAS-mutated cells by GPX4 inhibition (Supplementary Fig. 2g) suggesting the protection from ROS to be specific towards lipid ROS. Together, these data establish that mutant KRAS endows cells with superior capacity to protect cells from a ferroptosis-specific increase in lipid peroxidation.

Elevated levels of FSP1 protect KRAS-mutated cells from ferroptosis

In order to determine the mechanism by which KRAS-mutated cells might buffer acute lipid peroxidation, we performed comparative 3′ RNA sequencing of KRAS WT and KRAS^{G12D}-mutated MEFs. Interestingly, when analyzing the top 1000 upregulated genes in KRAS-mutated cells for functional association networks using STRING, we obtained a significant enrichment of the ferroptosis pathway along with several other metabolic pathways (Fig. 3a). As the list of genes annotated in the KEGG ferroptosis pathway does not contain more recently discovered regulators of ferroptosis, we manually extended this list (KEGG+) and analyzed expression of these genes in our comparative dataset. Strikingly, AIFM2 mRNA, recently renamed as ferroptosis suppressor protein 1 (FSP1) due to its ferroptosis protective activity [11, 12], was upregulated in KRAS-mutated cells within a cluster of genes (Fig. 3b). Within several ferroptosis regulatory genes of the dataset, FSP1 was upregulated significantly (Supplementary Fig. 3a). Moreover, FSP1 mRNA upregulation in KRAS-mutated cells could also be confirmed by quantitative real-time PCR (qPCR) (Fig. 3c). Importantly, FSP1 was basally upregulated also on protein level in KRAS-mutated cells and, unlike xCT, a recently identified target gene further upregulated upon H2O2 [7], was not further increased upon stimulation with RSL3 (Fig. 3d). As FSP1 has been shown to render cells more resistant to ferroptosis, we next tested whether its elevated expression in KRAS-mutated cells was responsible for mediating increased ferroptosis resistance of KRAS-mutated cells. Indeed, FSP1 suppression was sufficient to sensitize KRAS-mutated cells to ferroptosis (Fig. 3e, f). Vice versa, overexpression of FSP1 was sufficient to render KRAS WT cells as resistant to ferroptosis as KRAS-mutated control cells (Fig. 3g, h). As FSP1 is an NADH ubiquinone oxidoreductase, FSP1 activity requires NADPH as an electron source [11, 12]. Therefore, we also tested whether basal levels of the FSP1 cofactor NADPH would differ in KRAS-mutated as compared to WT cells and thereby contribute to differential activity, yet this was not the case (Supplementary Fig. 3b). To next determine whether FSP1 activity may also protect KRAS-mutated cells from ferroptosis, we employed a recently developed small molecule inhibitor against FSP1 [11]. Strikingly, co-incubation with this inhibitor (iFSP1) reverted ferroptosis resistance endowed by oncogenic KRAS expression (Supplementary Fig. 3c, d). Of note, iFSP1 also slightly sensitized KRAS WT cells, yet due to the fact WT cells were already very sensitive, the relative sensitization observed was much stronger for KRAS-mutated cells. Thus, KRAS-mutated cells display increased ferroptosis resistance due to elevated levels of FSP1.

Oncogenic KRAS upregulates FSP1 via NRF2 and the MAPK pathway

To thoroughly test a direct mechanistic link of oncogenic KRAS and FSP1 induction, we generated primary MEFs with inducible expression of KRAS^{G12D} from its endogenous locus similar to an established approach [31] (LsL-KRAS^{G12D}-inducible MEFs). As expected, induction of KRAS^{G12D} by 4-hydroxytamoxifen (4OHT) treatment led to enhanced basal phosphorylation of ERK which was further increased upon refeeding with FCS (Fig. 4a). Moreover, KRAS^{G12D} induction readily elevated expression of the established MAPK target gene dual specificity phosphatase 6 (DUSP6) along with the antioxidant transcription factor nuclear factor erythroid 2-related factor 2 (NRF2) and its bona fide target genes glutamate-cysteine ligase catalytic subunit (GCLC) and heme oxigenase-1 (HO-1) (Fig. 4b). Strikingly, induction of KRAS^{G12D} was indeed sufficient to also directly induce FSP1 expression (Fig. 4b). In order to validate direct induction of FSP1 by oncogenic RAS, we validated this finding in human pancreatic duct epithelial cells (HPDE) with doxycycline-inducible expression of KRAS^{G12D} and HRAS^{G12V}-inducible NIH-3T3 cells (Supplementary Fig. 4a, b). Given that oncogenic KRAS is known to induce NRF2 [31] and FSP1 was very recently shown to be a direct transcriptional target of NRF2 [32] in NSCLC mutated in the NRF2 inhibitor kelch-like ECH-associated protein 1 (KEAP1), we next tested whether activating endogenous NRF2 would be sufficient in our cells to induce FSP1. Strikingly, silencing of KEAP1 readily induced FSP1 along with NRF2 target genes (Fig. 4c). Moreover, KEAP1 knockdown rendered KRAS WT cells resistant to ferroptosis, which could partially be reverted by iFSP1 treatment (Fig. 4d).

Furthermore, treatment with the chemical NRF2 activator tert-butylhydrochinone (TBHQ) equally induced NRF2 target genes along with FSP1 (Fig. 4e). While silencing of NRF2 was toxic to MEFs (a toxicity blockable by Fer-1), we mined publicly available datasets from the KRAS-mutated NSCLC cell line A549 in which NRF2 was knocked down (Fig. 4f) [33]. Indeed, upon NRF2 silencing, FSP1 expression was also significantly decreased (Fig. 4g) confirming NRF2-mediated FSP1 regulation to be present in KRAS-mutated cells. These data suggest that oncogenic KRAS-induced NRF2 directly leads to elevated transcription of FSP1 thereby protecting them from ferroptosis. To also determine which other major KRAS effector pathway may upregulate FSP1, KRAS-mutated

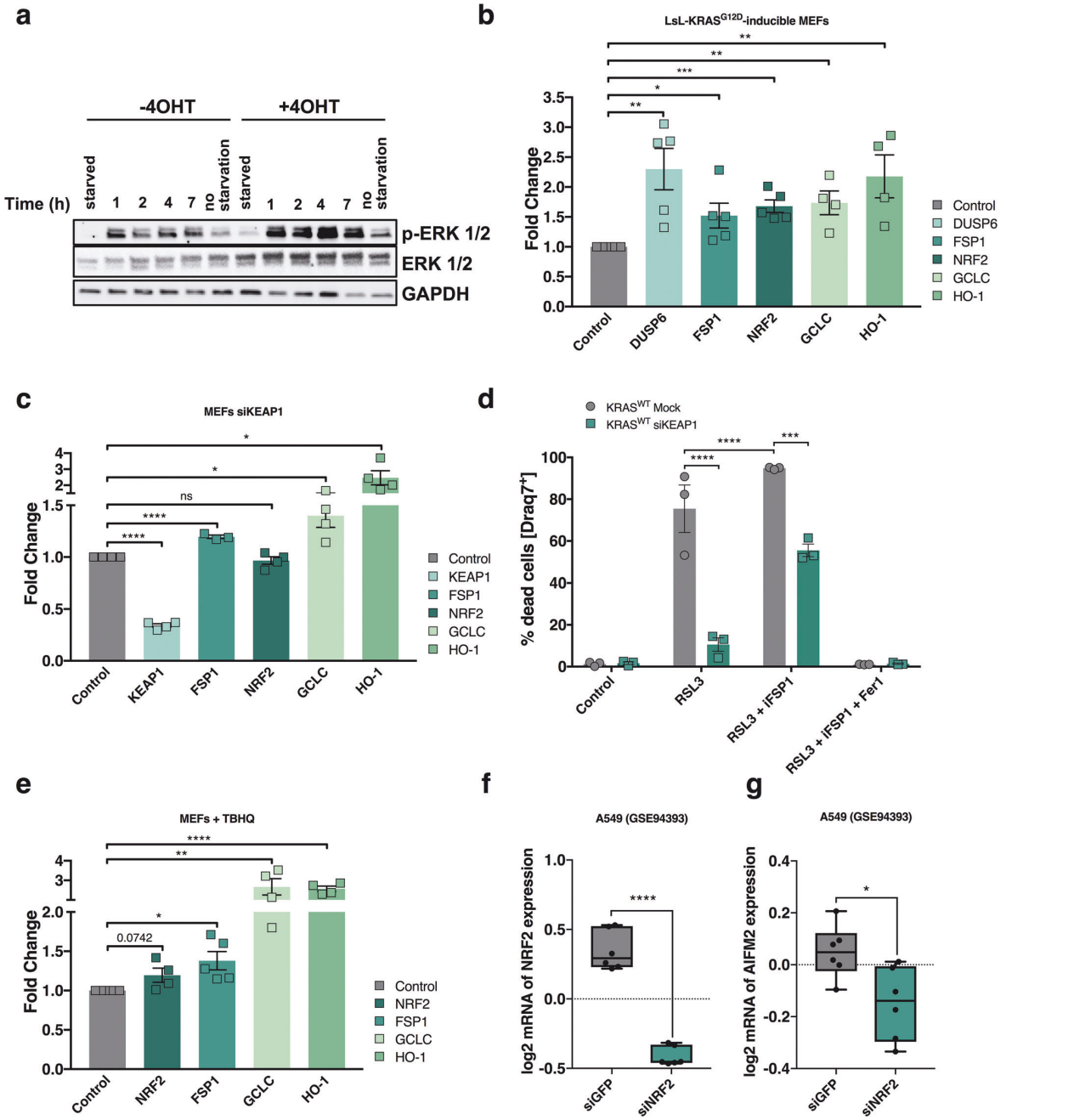

Fig. 4 FSP1 is upregulated in KRAS^{G12D}-expressing cells in an NRF2-dependent manner. a LsL-KRAS^{G12D}-inducible MEFs were treated for 72 h with or without tamoxifen (4OHT) [1 µg/ml] in 2% FCS before cells were starved overnight in 0.1% FCS and then refed with 2% FCS for the indicated timepoints. Cells were lyzed and subjected to protein analysis by Western blotting. **b** Levels of DUSP6, FSP1, NRF2, GCLC and HO-1 cDNA were quantified by qPCR in LsL-KRAS^{G12D}-inducible MEFs after 96 h or 120 h of tamoxifen (4OHT) treatment. Fold change relative to controls is shown. Means from MEF lines from 4–5 different embryos are shown. **c** Levels of KEAP1, FSP1, NRF2, GCLC and HO-1 cDNA were quantified by qPCR in Rasless MEFs expressing KRAS WT ± KEAP1 knockdowns for 72 h. Fold change relative to controls is shown. **d** siKEAP1 KRAS WT cells were treated after 48 h knockdown with DMSO, RSL3 [100 nM], ±iFSP1 [10 µM], ±Fer-1 [1 µM] for another 24 h. DRAQ7 [100 nM] was added to all wells to visualize dead cells. Images were acquired at ×10 magnification every 2 h using the IncuCyte S3 bioimaging platform. **e** Levels of NRF2, FSP1, GCLC and HO-1 cDNA were quantified by qPCR in Rasless MEFs expressing KRAS WT after cells were treated for 24 h with TBHQ [25 nM]. Fold change relative to controls is shown. **f** log2 mRNA expression data of A549 cells transfected with either siRNAs targeting NRF2 or GFP [33]. NRF2 mRNA expression is shown. **g** data as in f were analyzed for FSP1 (AIFM2) mRNA expression. Data are means ± SEM of three independent experiments in each individual cell line or representative images were applicable. Two-tailed *t*-test (**b, c, e, f, g**), Two-way ANOVA + Tukey's multiple comparison test (**d**), ****$p < 0.0001$, ***$p < 0.001$, **$p < 0.01$, *$p < 0.05$. Uncropped blots are provided as Original Data file.

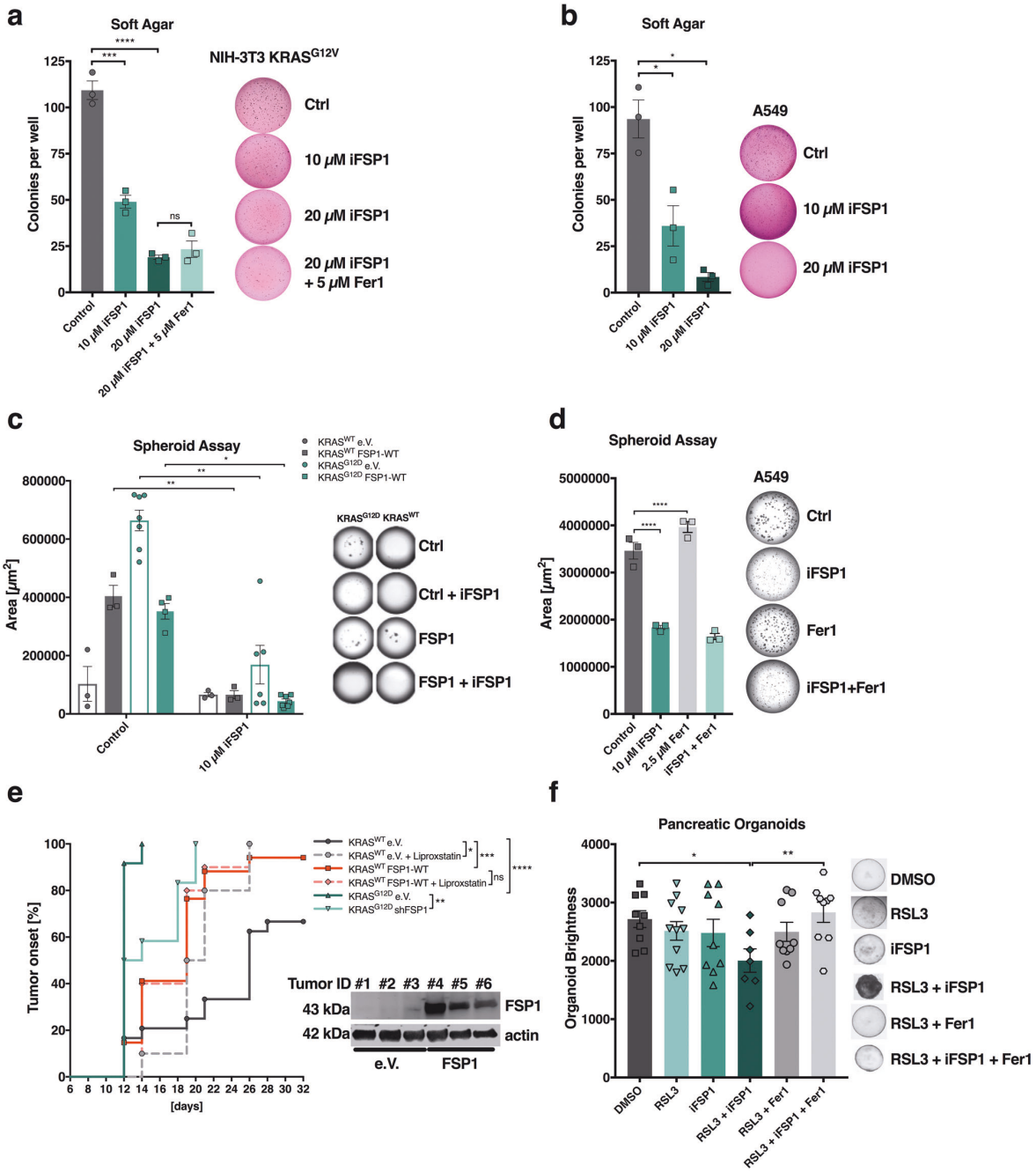

cells were treated with the MEK inhibitor PD184352 to block the MAPK arm downstream of KRAS as well as the AKT inhibitor MK2206. Interestingly, FSP1 mRNA was reduced only under MEK but not AKT inhibition indicating that MAPK pathway activation is responsible for elevated FSP1 levels in KRAS-mutated cells (Supplementary Fig. 4c). Of note, MEK inhibition in WT cells did not significantly regulate FSP1 mRNA despite effectively blunting expression of the established MAPK pathway target gene DUSP6 indicating preferential regulation in KRAS-mutated cells (Supplementary Fig. 4d). In support of this, MEK inhibition resulted in dose-dependent reduction in FSP1 protein levels along with decreased phosphorylation of ERK (Supplementary Fig. 4e). Furthermore, gene-set enrichment analysis of genes co-expressed with FSP1 in the lung adenocarcinoma (LUAD) TCGA dataset were significantly enriched for the MAPK pathway as indicated by enrichment of the RAF and MEK pathways (Supplementary Fig. 4f). Of note, NRF2 has been reported to be phosphorylated and activated by MAPK signaling [34]. Therefore, we also measured expression of the NRF2 target gene GCLC under MEK as compared to AKT inhibition. Indeed, GCLC was reduced by

Fig. 5 FSP1 aids cellular transformation and promotes tumor onset in vivo. a NIH-3T3 KRAS^{G12V} cells were treated either with DMSO, iFSP1 [10 µM, 20 µM], Fer-1 [5 µM] or both and subjected to soft agar assays for 18 days. Colony images were quantified using ImageJ. **b** The human NSCLC cell line A549 was treated as indicated and subjected to growth in soft agar for 30 days. Image analysis was done as in (**a**). **c** Indicated cells were grown in Matrigel for spheroid formation under the indicated treatment for 14 days. Images were quantified using the BZ-H4M/Measurement Application Software (Keyence). **d** A549 cells were subjected to spheroid assay growth for 9 days and treated either with DMSO, iFSP1 [10 µM], Fer-1 [2,5 µM] or both. Images were quantified using the BZ-H4M/Measurement Application Software (Keyence). **e** 8-weeks old male nude mice were injected with 5×10^5 cells of the indicated cell lines (G12D e.V. (empty Vector) $n = 11$; G12D shFSP1 $n = 12$; WT e.V. $n = 24$ + Vehicle; WT e.V. + Liproxstatin-1 n = 10; WT FSP1 $n = 24$ + Vehicle; WT FSP1 + Liproxstatin-1 $n = 10$) into both flanks. Mice were injected 5× per week either with vehicle (PBS with 1% DMSO) or Liproxstatin-1 (10 mg/kg). Time until palpable tumors (min. 2 × 2 mm) were detected is depicted (tumor onset). Representative ex vivo tumors were analyzed for FSP1 expression. **f** Pancreatic organoids were treated with DMSO, RSL3 [100 nM] or iFSP1 [10 µM] alone or in combination with Ferrostatin-1 (Fer-1) [5 µM] for 48 h. Images were quantified using the BZ-H4M/Measurement Application Software (Keyence). Data are means ± SEM of at least three independent experiments in each individual cell line or representative images were applicable. Two-way ANOVA (**a**, **b**, **c**, **d**), log-rank test (**e**), two-tailed *t*-test (**f**), ****$p < 0.0001$, ***$p < 0.001$, **$p < 0.01$, *$p < 0.05$.

inhibition of MEK but not AKT (Supplementary Fig. 4g). Taken together, our data propose that FSP1 is upregulated in KRAS-mutated cells as a direct result of MAPK and NRF2 pathway activation.

FSP1 aids KRAS-mediated cellular transformation and promotes tumor onset in vivo

One hallmark of oncogenic KRAS is its capacity to mediate cellular transformation. Therefore, we hypothesized that FSP1 activity may aid cellular transformation capacity of KRAS-mutated cells. Indeed, 3T3 cells transformed by KRAS^{G12V} expression presented with decreased colony formation in soft agar in the presence of iFSP1. Yet, this activity of FSP1 was not due to ferroptosis protection as co-treatment with Fer-1 did not rescue decreased colony formation (Fig. 5a). Moreover, human KRAS-mutated A549 cells equally showed decreased soft agar colony formation in the presence of iFSP1 (Fig. 5b) suggesting that elevated FSP1 expression additionally may promote cellular transformation of KRAS-mutated cells independently of ferroptosis protection. Recently, in 3D Matrigel-based spheroid assays, ferroptosis was shown to occur in spheroid centers thereby limiting their growth [35]. Therefore, we next tested the extent of spheroid formation in KRAS-mutated as compared to WT cells in this experimental system. As expected, KRAS-mutated cells formed spheroids much more efficiently than KRAS WT cells although a few colonies could be detected likely due to some extent of spontaneous transformation enabling continuous proliferation of KRAS WT MEFs (Fig. 5c). Here, overexpression of FSP1 was sufficient to allow for spheroid growth in KRAS WT cells to a similar extent as KRAS-mutant cells. While FSP1 overexpression in KRAS-mutant cells led to a slight decrease in colony formation, importantly, iFSP1 incubation readily reverted spheroid formation enabled by FSP1 overexpression in both cases (Fig. 5c). Moreover, iFSP1 also significantly impacted spheroid formation of human A549 cells yet again, this activity was not caused by protecting from ferroptosis (Fig. 5d, Supplementary Fig. 5a). Thereby, our data support the concept that cellular transformation endowed by KRAS may at least in part depend upon FSP1 expression and activity, yet this activity is independent of its role in ferroptosis protection. Next, we aimed to test whether FSP1 expression was sufficient to impact tumor initiation. To this end, we transplanted mice with KRAS WT cells with either control or FSP1 overexpression in comparison to KRAS-mutant control and cells with short hairpin RNA (shRNA)-mediated FSP1 silencing (Supplementary Fig. 5b). As expected, KRAS-mutated cells presented with earlier tumor onset than KRAS WT cells. Yet strikingly, FSP1 expression was sufficient in KRAS WT cells to significantly accelerate tumor onset and increase tumor incidence closer to the rates of KRAS-mutant tumors (Fig. 5e). Moreover, treatment of mice bearing KRAS WT tumors with the ferroptosis-selective inhibitor Liproxstatin-1 accelerated tumor onset to similar levels as FSP1 overexpression suggesting ferroptosis to be indeed responsible for suppression of tumor initiation capacity of WT cells in vivo. Importantly, Liproxstatin-1 treatment of FSP1-overexpressing WT tumors did not result in additional promotion of tumor onset indicating FSP1 to promote KRAS WT tumor initiation by protecting from ferroptosis. Interestingly, and, similar to our findings in spheroid assays, tumor volumes of tumors arising also increased when expressing exogenous FSP1, yet this increase was independent of ferroptosis protection as Liproxstatin-1 treatment did not affect tumor volumes (Supplementary Fig. 5c). Vice versa, FSP1 silencing in KRAS-mutated tumors delayed tumor onset albeit not to the levels of KRAS WT tumors. Therefore, oncogenic KRAS partially promotes its early tumor onset through FSP1-mediated ferroptosis protection. Moreover, FSP1 expression alone is sufficient to promote tumor initiation in the absence of oncogenic KRAS by suppressing ferroptosis in vivo.

Oncogenic mutations in KRAS are most frequently observed in patients with pancreatic ductal adenocarcinoma (PDAC). Yet, most small molecules inducing ferroptosis do not display pharmacokinetics and solubilities suitable for in vivo use yet. Therefore, we next generated organoids from mice developing pancreatic intraepithelial neoplasia (PanINs) as a result of KRAS^{G12D} expression from the endogenous promotor [36] and treated them either with RSL3 alone or in combination with iFSP1. Strikingly, RSL3 treatment alone was insufficient to induce ferroptosis in pancreatic organoids but the combination with iFSP1 led to effective killing of pancreatic organoids expressing KRAS^{G12D} (Fig. 5f). Based on these data, we propose that breaking ferroptosis resistance through the use of FSP1 inhibitors might be a particularly potent treatment strategy against KRAS-driven cancers.

FSP1 expression is upregulated in KRAS-mutated cancers and correlates with poor outcome in PDAC patients

In order to test whether FSP1 expression may be upregulated in KRAS-driven cancer, we probed publicly available tumor (TCGA) and normal (GTEX) datasets for FSP1 expression in colorectal cancer, lung adenocarcinoma and pancreatic adenocarcinoma in comparison to their respective normal tissue of origin using Gene Expression Profiling Interactive Analysis (GEPIA). Interestingly, FSP1 was significantly overexpressed in all three tumor types as compared to the respective normal tissues (Fig. 6a). While in pancreatic cancer the vast majority of patients present with activating KRAS mutations and a KRAS WT group is therefore difficult to obtain, in non-small cell lung cancer (NSCLC) about half of the patients are usually WT. Strikingly, when dividing an NSCLC dataset (GSE31852) by KRAS-mutation status, FSP1 expression was significantly upregulated in KRAS-mutated patient material (Fig. 6b). Moreover, in two independent PDAC datasets [37, 38] with included adjacent normal tissue, FSP1 expression was significantly upregulated in PDAC over normal pancreas and FSP1 mRNA correlated with NRF2 mRNA within these two datasets (Fig. 6c–f). Moreover, we

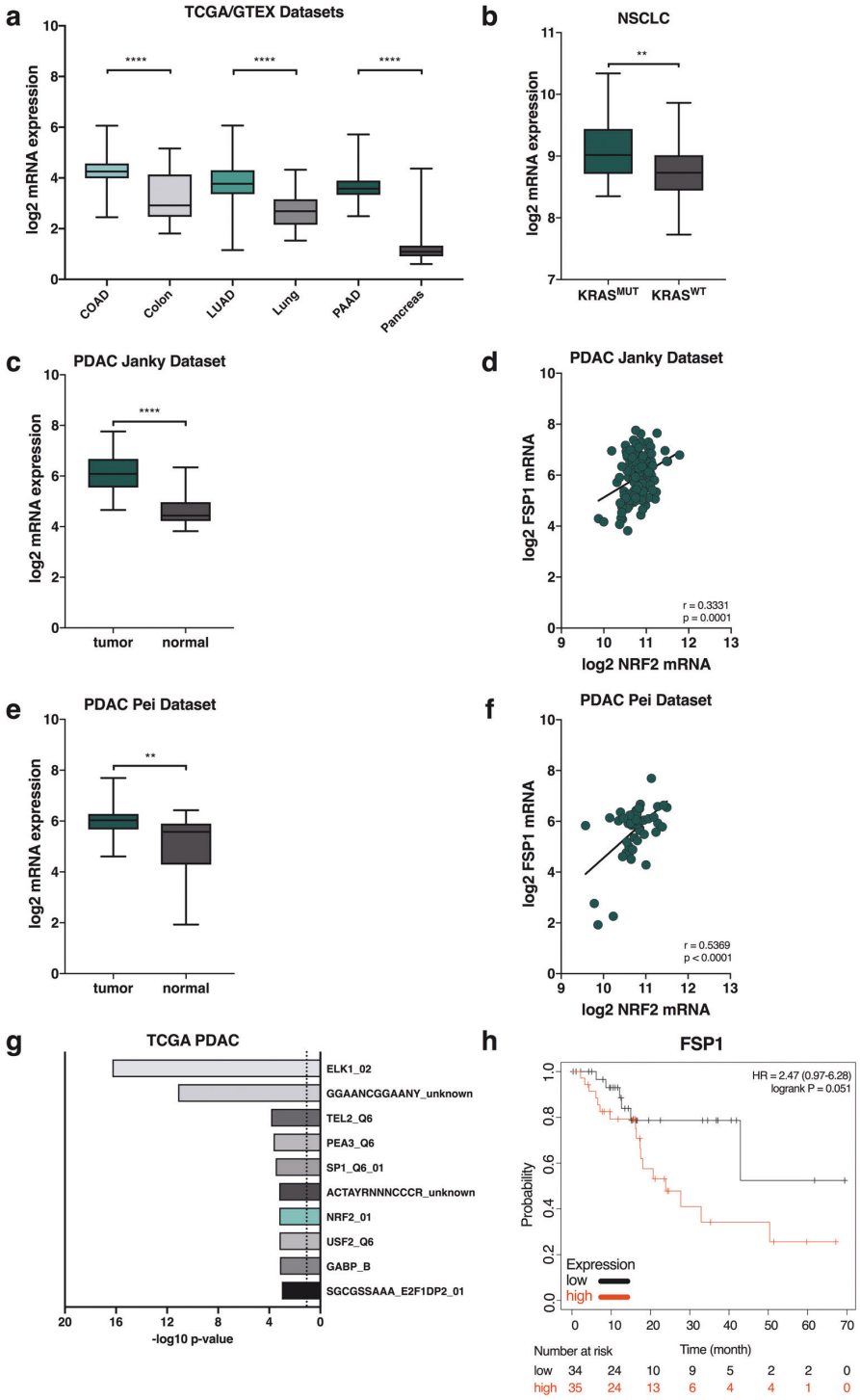

performed gene-set enrichment analysis (GSEA) on transcription factor motifs of genes co-expressed with FSP1 within the TCGA PDAC dataset. Strikingly, NRF2 was amongst the top 10 enriched motifs (Fig. 6g) suggesting FSP1 upregulation in PDAC patients to be a result of NRF2-mediated transcription. Lastly, high FSP1 expression in PDAC patients showed a strong trend towards drastically shortened relapse-free survival (Fig. 6h).

Taken together, our data establish that endogenous levels of oncogenic KRAS expression render cells more resistant to ferroptosis by upregulating FSP1 through the NRF2 and MAPK

Fig. 6 FSP1 is upregulated in KRAS-mutated cancers and correlates with poor relapse-free survival. a Log^2-transformed RPKM expression data for FSP1 (AIFM2) for the indicated TCGA tumor (COAD-colon adenocarcinoma; LUAD-lung adenocarcinoma; PAAD-pancreatic adenocarcinoma) or GTEX normal control datasets are plotted. **b** NSCLC expression data (GSE31852) were split into two groups by KRAS-mutation status (KRAS-mutated $n = 24$, KRAS WT $n = 100$) and analyzed for log^2 FSP1 expression. **c, d** PDAC expression data from Janky et al. [38] tumor n = 118, normal n = 13 were analyzed for log2 FSP1 expression in tumor as compared to adjacent normal as well as co-expression of FSP1 with NRF2 within tumor tissue. **e, f** PDAC expression data from Pei et al. [37] tumor $n = 36$, normal $n = 15$ were analyzed as in **c, d**. **g** Genes significantly co-expressed with FSP1 ($r \geq 0.3$, FDR < 0.01) within the PDAC TCGA dataset were analyzed for transcription factor binding motifs by gene-set enrichment (GSEA) and -log10-transformed false discovery rates (FDR) of significantly enriched motifs are plotted. **h** Kaplan Meier survival of relapse-free survival in PDAC patients $n = 69$ according to FSP1 expression high versus low split by median is shown. Data were analyzed by and downloaded from KM plotter [58]. Whiskers are shown from min to max. Two-tailed *t* test (**a, b, c, e**) and log-rank test (**h**), $^{****}p < 0.0001$, $^{**}p < 0.01$.

pathway allowing for a superior capacity to buffer acute lipid peroxidation during tumor initiation. Hence, only combined targeting of GPX4 and FSP1 is effective at killing KRAS-driven pancreatic organoids and FSP1 is upregulated in human KRAS-driven cancers. Based on these data, we propose that pro-ferroptotic therapy for KRAS-driven cancers should include inhibition of FSP1 in order to achieve efficient tumor cell killing.

DISCUSSION

In the present study, we identify that expression of near-endogenous levels of oncogenic KRAS renders cells more resistant to ferroptosis through elevated expression of FSP1. Of note, in earlier studies overexpression of oncogenic HRAS in fibroblasts as compared to cells expressing empty vector led to a sensitization to erastin-induced cell death [13, 39], later found to be ferroptotic due to erastin-mediated targeting of xCT [10]. What might seem as a discrepancy might in fact represent two distinct stages of cellular transformation. Upon acute overexpression of an oncogenic RAS variant, cellular levels of ROS are known to be upregulated due to NOX1 induction [6]. Moreover, in line with an earlier study by Yang et al. [40] we observed that a cluster of genes involved in iron uptake (TFRC, STEAP3) was in fact upregulated in KRAS-mutated cells (Fig. 3b), possibly to feed an increased requirement for iron in the mitochondrial respiratory chain. This may suggest that RAS expression would fuel lipid peroxidation due to elevated basal ROS which is also what was observed by Yang et al. 2008. Yet, chronic elevated levels of ROS are known to activate NRF2. In fact, endogenous expression levels as opposed to overexpression of oncogenic KRAS were shown to effectively induce NRF2 activation [31]. Along these lines, a recent study found that NRF1 and NRF2 protect cells from ferroptosis through distinct and independent mechanisms [41]. Moreover, NRF2 was recently shown to induce FSP1 transcription via NRF2 in KEAP1-mutant NSCLC [32]. In keeping with these results, we now find that cells expressing oncogenic KRAS directly induce FSP1 expression through MAPK-NRF2 pathway activation. Of note, class I FINs, which lead to GSH depletion, did not show a significant difference between KRAS-mutated and -WT cells. This observation may suggest that GSH depletion triggers general ROS accumulation which in turn activates NRF2 and via this route may upregulate FSP1 also in WT cells thereby neutralizing the difference in killing. Hence, we propose a model wherein effective activation of NRF2-mediated transcription might be decisive for whether oncogenic KRAS expression renders cells more or less sensitive to ferroptosis.

An interesting possibility is that the Nonsense-Mediated Decay (NMD) pathway might contribute to the regulation of FSP1 mRNA. NMD can regulate a number of perfectly functional transcripts many of which usually have an abnormally long 3′UTR. Indeed, FSP1 murine transcript variants contain several NMD-inducing features including an abnormally long 3′UTR in one of them. Interestingly, FSP1 mRNA was found to be upregulated in murine embryonic stem cells upon NMD inhibition [42], and oncogenic KRAS might inhibit NMD via several non-exclusive mechanisms. For instance, $KRAS^{G12D}$ is known to activate p38 MAPK [43–45] and p38 MAPK has been shown to inhibit NMD [46]. Additionally, ER stress is well-known to inhibit NMD [47] and has been observed in $KRAS^{G12D}$-expressing cells [48]. It is therefore tempting to speculate whether cells expressing oncogenic KRAS may inhibit NMD which in turn could result in FSP1 mRNA stabilization.

Expression of oncogenic KRAS creates selective metabolic addiction to nucleotide synthesis via the pentose phosphate pathway (PPP) [49]. Interestingly, high cellular levels of NADPH, the product of the PPP, were identified as markers of resistance to ferroptosis [50]. NADPH in turn is an important electron donor for a variety of cellular enzymes including FSP1. Consequently, high-level exogenous overexpression of FSP1, as obtained in our experiments, may impact cellular NADPH levels and, with that, be problematic for metabolic NADPH addiction of KRAS-mutant cells [49]. In line with this, FSP1 overexpression in KRAS-mutant cells decreased their capacity to form spheroids. Moreover, inhibition of the PPP was shown to reduce soft agar colony formation of transformed 3T3 MEFs [51]. In favor of another ferroptosis-independent function for FSP1 expression in cancer, we found that tumor volume growth in WT cells in vivo was promoted by FSP1 expression but not Liproxstatin-1 treatment. This growth promotion may be facilitated by FSP1- generated NAD+ which was shown to promote glycolysis [52], a mode of energy generation advantageous for hypoxic tumors.

Interestingly, two recent studies identified GTP cyclohydrolase-1 (GCH1) and its products tetrahydrobiopterin /dihydrobiopterin (BH_4/BH_2) to act as potent cellular antioxidants protecting from ferroptosis in the absence of GPX4 [53, 54]. Yet, cells not expressing GCH1 seem to solely depend upon FSP1 for the generation of endogenous radical-trapping agents, a fact used for screening for novel FSP1 inhibitors [55]. Of note, GCH1 mRNA expression was barely detectable in our cellular systems and also not influenced by KRAS-mutation status in contrast to FSP1 (data not shown).

In a genetically engineered mouse model of KRAS-driven PDAC, inducible whole-body deletion of xCT led to significant tumor regression [56]. However interestingly, cancer-associated fibroblast (CAF)-restricted deletion of xCT in the very same mouse model was sufficient to achieve a strong anti-tumor effect [57]. These data together with the fact that GPX4 deletion within PanINs was insufficient to trigger ferroptosis in pancreatic cancer [14], support the idea that KRAS-mutated cells have evolved an additional layer of protection against ferroptotic cell death. Our data propose that elevated FSP1 expression in KRAS-mutated cells is, at least in part, responsible for this protection. Based on these considerations, we propose that combined induction of ferroptosis and FSP1 inhibition should be considered for therapeutic strategies developed against KRAS-mutated cancers.

DATA AVAILABILITY

The data and material that support the findings of this study are available from the corresponding author upon reasonable request.

REFERENCES

1. Bos JL. ras oncogenes in human cancer: a review. 1989;49:4682–9.
2. Downward J. Targeting RAS signalling pathways in cancer therapy. Nat Rev Cancer. 2003;3:11–22.
3. Downward J. Targeting RAS and PI3K in lung cancer. Nat Med. 2008;14:1315–6.
4. Hoogwater FJH, Nijkamp MW, Smakman N, Steller EJA, Emmink BL, Westendorp BF, et al. Oncogenic K-Ras turns death receptors into metastasis-promoting receptors in human and mouse colorectal cancer cells. Gastroenterology. 2010;138:2357–67.
5. Karstedt S, von Conti A, Nobis M, Montinaro A, Hartwig T, Lemke J, et al. Cancer cell-autonomous TRAIL-R signaling promotes KRAS-driven cancer progression, invasion, and metastasis. Cancer Cell. 2015;27:561–73.
6. Mitsushita J, Lambeth JD, Kamata T. The superoxide-generating oxidase Nox1 is functionally required for Ras oncogene transformation. Cancer Res. 2004;64:3580–5.
7. Lim JKM, Delaidelli A, Minaker SW, Zhang H-F, Colovic M, Yang H, et al. Cystine/glutamate antiporter xCT (SLC7A11) facilitates oncogenic RAS transformation by preserving intracellular redox balance. Proc Natl Acad Sci USA 2019;1092:201821323.
8. Dixon SJ, Lemberg KM, Lamprecht MR, Skouta R, Zaitsev EM, Gleason CE, et al. Ferroptosis: an iron-dependent form of nonapoptotic cell death. Cell. 2012;149:1060–72.
9. Yang WS, SriRamaratnam R, Welsch ME, Shimada K, Skouta R, Viswanathan VS, et al. Regulation of ferroptotic cancer cell death by GPX4. Cell. 2014;156:317–31.
10. Dixon SJ, Patel DN, Welsch M, Skouta R, Lee ED, Hayano M, et al. Pharmacological inhibition of cystine-glutamate exchange induces endoplasmic reticulum stress and ferroptosis. eLife. 2014;3:e02523.
11. Doll S, Freitas FP, Shah R, Aldrovandi M, Silva MC da, Ingold I, et al. FSP1 is a glutathione-independent ferroptosis suppressor. Nature. 2019;149:1060–20.
12. Bersuker K, Hendricks J, Li Z, Magtanong L, Ford B, Tang PH, et al. The CoQ oxidoreductase FSP1 acts parallel to GPX4 to inhibit ferroptosis. Nature. 2019;575:688–92.
13. Yagoda N, Rechenberg M, von Zaganjor E, Bauer AJ, Yang WS, Fridman DJ, et al. RAS-RAF-MEK-dependent oxidative cell death involving voltage-dependent anion channels. Nature. 2007;447:864–8.
14. Dai E, Han L, Liu J, Xie Y, Zeh HJ, Kang R, et al. Ferroptotic damage promotes pancreatic tumorigenesis through a TMEM173/STING-dependent DNA sensor pathway. Nat Commun. 2020;11:6339–11.
15. Wang T, Wei JJ, Sabatini DM, Lander ES. Genetic screens in human cells using the CRISPR-Cas9 system. Science. 2014;343:80–84.
16. Bebber CM, Thomas ES, Stroh J, Chen Z, Androulidaki A, Schmitt A, et al. Ferroptosis response segregates small cell lung cancer (SCLC) neuroendocrine subtypes. Nat Commun. 2021;12:2048–19.
17. Nolte H, MacVicar TD, Tellkamp F, Krüger M. Instant clue: a software suite for interactive data visualization and analysis. Sci Rep. 2018;8:12648.
18. Hosogane M, Funayama R, Nishida Y, Nagashima T, Nakayama K. Ras-induced changes in H3K27me3 occur after those in transcriptional activity. PLoS Genet. 2013;9:e1003698.
19. Boj SF, Hwang C-I, Baker LA, Chio IIC, Engle DD, Corbo V, et al. Organoid models of human and mouse ductal pancreatic cancer. Cell. 2015;160:324–38.
20. Huch M, Bonfanti P, Boj SF, Sato T, Loomans CJM, Wetering Mvande, et al. Unlimited in vitro expansion of adult bi-potent pancreas progenitors through the Lgr5/R-spondin axis. Embo J. 2013;32:2708–21.
21. Drosten M, Dhawahir A, Sum EYM, Urosevic J, Lechuga CG, Esteban LM, et al. Genetic analysis of Ras signalling pathways in cell proliferation, migration and survival. EMBO J. 2010;29:1091–104.
22. Ostrem JM, Peters U, Sos ML, Wells JA, Shokat KM. K-Ras(G12C) inhibitors allosterically control GTP affinity and effector interactions. Nature. 2013;503:548–51.
23. Vasta JD, Peacock DM, Zheng Q, Walker JA, Zhang Z, Zimprich CA, et al. KRAS is vulnerable to reversible switch-II pocket engagement in cells. Nat Chem Biol. 2022;18:596–604.
24. Janes MR, Zhang J, Li L-S, Hansen R, Peters U, Guo X, et al. Targeting KRAS Mutant Cancers with a Covalent G12C-Specific Inhibitor. Cell. 2018;172:578–581.e17.
25. Canon J, Rex K, Saiki AY, Mohr C, Cooke K, Bagal D, et al. The clinical KRAS(G12C) inhibitor AMG 510 drives anti-tumour immunity. Nature. 2019;56:779–21.
26. Molina-Arcas M, Moore C, Rana S, Maldegem F van, Mugarza E, Romero-Clavijo P, et al. Development of combination therapies to maximize the impact of KRAS-G12C inhibitors in lung cancer. Sci. Transl. Med. 2019;11.
27. Angeli JPF, Krysko DV, Conrad M. Ferroptosis at the crossroads of cancer-acquired drug resistance and immune evasion. Nat Rev Cancer. 2019;15:348.
28. Kagan VE, Mao G, Qu F, Angeli JPF, Doll S, Croix CS, et al. Oxidized arachidonic and adrenic PEs navigate cells to ferroptosis. Nat Chem Biol. 2017;13:81–90.
29. Wiernicki B, Dubois H, Tyurina YY, Hassannia B, Bayir H, Kagan VE, et al. Excessive phospholipid peroxidation distinguishes ferroptosis from other cell death modes including pyroptosis. Cell Death Dis. 2020;11:922–11.
30. Zou Y, Henry WS, Ricq EL, Graham ET, Phadnis VV, Maretich P, et al. Plasticity of ether lipids promotes ferroptosis susceptibility and evasion. Nature. 2020;585:603–8.
31. DeNicola GM, Karreth FA, Humpton TJ, Gopinathan A, Wei C, Frese K, et al. Oncogene-induced Nrf2 transcription promotes ROS detoxification and tumorigenesis. Nature. 2011;475:106–9.
32. Koppula P, Lei G, Zhang Y, Yan Y, Mao C, Kondiparthi L, et al. A targetable CoQ-FSP1 axis drives ferroptosis- and radiation-resistance in KEAP1 inactive lung cancers. Nat Commun. 2022;13:2206.
33. Namani A, Cui QQ, Wu Y, Wang H, Wang XJ, Tang X. NRF2-regulated metabolic gene signature as a prognostic biomarker in non-small cell lung cancer. Oncotarget. 2017;8:69847–62.
34. Sun Z, Huang Z, Zhang DD. Phosphorylation of Nrf2 at multiple sites by MAP kinases has a limited contribution in modulating the Nrf2-dependent antioxidant response. PLoS ONE. 2009;4:e6588.
35. Takahashi N, Cho P, Selfors LM, Kuiken HJ, Kaul R, Fujiwara T, et al. 3D culture models with CRISPR screens reveal hyperactive NRF2 as a prerequisite for spheroid formation via regulation of proliferation and ferroptosis. Mol Cell. 2020;80:828–844.e6.
36. Hingorani SR, Petricoin EF, Maitra A, Rajapakse V, King C, Jacobetz MA, et al. Preinvasive and invasive ductal pancreatic cancer and its early detection in the mouse. Cancer Cell. 2003;4:437–50.
37. Pei H, Li L, Fridley BL, Jenkins GD, Kalari KR, Lingle W, et al. FKBP51 affects cancer cell response to chemotherapy by negatively regulating Akt. Cancer Cell. 2009;16:259–66.
38. Janky R, Binda MM, Allemeersch J, broeck AV den, Govaere O, Swinnen JV, et al. Prognostic relevance of molecular subtypes and master regulators in pancreatic ductal adenocarcinoma. Bmc Cancer. 2016;16:632.
39. Dolma S, Lessnick SL, Hahn WC, Stockwell BR. Identification of genotype-selective antitumor agents using synthetic lethal chemical screening in engineered human tumor cells. Cancer Cell. 2003;3:285–96.
40. Yang WS, Stockwell BR. Synthetic lethal screening identifies compounds activating iron-dependent, nonapoptotic cell death in oncogenic-RAS-harboring cancer cells. Chem Biol. 2008;15:234–45.
41. Forcina GC, Pope L, Murray M, Dong W, Abu-Remaileh M, Bertozzi CR, et al. Ferroptosis regulation by the NGLY1/NFE2L1 pathway. Proc Natl Acad Sci USA 2022;119:e2118646119.
42. Hurt JA, Robertson AD, Burge CB. Global analyses of UPF1 binding and function reveal expanded scope of nonsense-mediated mRNA decay. Genome Res. 2013;23:1636–50.
43. Munoz L, Yeung YT, Grewal T. Oncogenic Ras modulates p38 MAPK-mediated inflammatory cytokine production in glioblastoma cells. Cancer Biol Ther. 2016;17:355–63.
44. Houdt WJ van, Bruijn MT de, Emmink BL, Raats D, Hoogwater FJH, Rinkes IHMB, et al. Oncogenic K-ras activates p38 to maintain colorectal cancer cell proliferation during MEK inhibition. Cell Oncol. 2010;32:245–57.
45. Coelho MA, Tŕecesson S, de C, Rana S, Zecchin D, Moore C, et al. Oncogenic RAS signaling promotes tumor immunoresistance by stabilizing PD-L1 mRNA. Immunity. 2017;47:1083–1099.e6.
46. Nickless A, Cheruiyot A, Flanagan KC, Piwnica-Worms D, Stewart SA, You Z. p38 MAPK inhibits nonsense-mediated RNA decay in response to persistent DNA damage in noncycling cells. J Biol Chem. 2017;292:15266–76.
47. Li Z, Vuong JK, Zhang M, Stork C, Zheng S. Inhibition of nonsense-mediated RNA decay by ER stress. Rna. 2017;23:378–94.
48. Ramadori G, Konstantinidou G, Venkateswaran N, Biscotti T, Morlock L, Galié M, et al. Diet-induced unresolved ER stress hinders KRAS-driven lung tumorigenesis. Cell Metab. 2015;21:117–25.
49. Santana-Codina N, Roeth AA, Zhang Y, Yang A, Mashadova O, Asara JM, et al. Oncogenic KRAS supports pancreatic cancer through regulation of nucleotide synthesis. Nat Commun. 2018;9:4945–13.
50. Shimada K, Hayano M, Pagano NC, Stockwell BR. Cell-line selectivity improves the predictive power of pharmacogenomic analyses and helps identify NADPH as biomarker for ferroptosis sensitivity. Cell Chem Biol. 2016;23:225–35.
51. Kuo W, Lin J, Tang TK. Human glucose-6-phosphate dehydrogenase (G6PD) gene transforms NIH 3T3 cells and induces tumors in nude mice. Int J Cancer. 2000;85:857–64.
52. Nguyen HP, Yi D, Lin F, Viscarra JA, Tabuchi C, Ngo K, et al. Aifm2, a NADH oxidase, supports robust glycolysis and is required for cold- and diet-induced thermogenesis. Mol Cell. 2020;77:600–617.e4.
53. Kraft VAN, Bezjian CT, Pfeiffer S, Ringelstetter L, Müller C, Zandkarimi F, et al. GTP cyclohydrolase 1/Tetrahydrobiopterin counteract ferroptosis through lipid remodeling. Acs Cent Sci. 2020;6:41–53.
54. Soula M, Weber RA, Zilka O, Alwaseem H, La K, Yen F, et al. Metabolic determinants of cancer cell sensitivity to canonical ferroptosis inducers. Nat Chem Biol. 2020;16:1351–60.

55. Yoshioka H, Kawamura T, Muroi M, Kondoh Y, Honda K, Kawatani M, et al. Identification of a small molecule that enhances ferroptosis via inhibition of ferroptosis suppressor protein 1 (FSP1). Acs Chem Biol. 2022;17:483–91.
56. Badgley MA, Kremer DM, Maurer HC, DelGiorno KE, Lee H-J, Purohit V, et al. Cysteine depletion induces pancreatic tumor ferroptosis in mice. Science. 2020;368:85–89.
57. Sharbeen G, McCarroll JA, Akerman A, Kopecky C, Youkhana J, Kokkinos J, et al. Cancer-associated fibroblasts in pancreatic ductal adenocarcinoma determine response to SLC7A11 inhibition. Cancer Res. 2021;81:3461–79.
58. Lánczky A, Győrffy B. Web-based survival analysis tool tailored for medical research (KMplot): development and implementation. J Med Internet Res. 2021;23:e27633.

ACKNOWLEDGEMENTS

Susanne Brodesser for advice on lipidomics, M. Conrad for providing the FSP1 antibody, J.P. Friedmann-Angeli for providing FSP1 plasmids and advice on Liproxstatin-1 in vivo usage, Dennis Plencker for advice on pancreatic organoid cultures, A. Trauzold and J. Downward for providing cells (HPDE, A549, respectively), Nina Wobst for additional validation in human cell lines, and Karin Schlegelmilch for solving cloning problems.

AUTHOR CONTRIBUTIONS

Conceptualization: SvK; visualization, FM; methodology: FM, JKML, CMB, ES, ST, AD, JS, JuBe, FIY, KN, JB, SvK; investigation: FM, JKML, CMB, ES, ST, AD, JS, JuBe, FIY, JB, SvK; formal analysis: FM, JKML, GL and SvK; writing-original draft: SvK; writing-review and editing: FM, JKML, ES, ST, FIY, SvK, LTF, GL, JB; funding acquisition; SvK; project administration: SvK; supervision: SvK, GL.

FUNDING

Work in the von Karstedt lab was funded through a Max Eder junior research group grant (701125509) by the German cancer aid, a project grant (A06) by the center for molecular medicine cologne (CMMC), an eMed consortium grant by the BMBF (InCa-01ZX1901A) and a collaborative research center grant on cell death (CRC1403, project ID 414786233) and predictability in evolution (CRC1310, project ID 325931972) funded by the Deutsche Forschungsgemeinschaft (DFG). JB was funded through a Mildred Scheel Junior Research Group Grant (ID 70113307) by the German cancer aid, JKML was funded by the Volkswagen foundation (Experiment!; A131649-97391) and by the German research foundation (Walter Benjamin Program; LI3844/1-1). Work in the Leprivier lab was funded by the German research foundation (LE 3751/2-1), the German Cancer Aid (70112624), and the Dr. Rolf M. Schwiete Stiftung (2020-018). Open Access funding enabled and organized by Projekt DEAL.

COMPETING INTERESTS

The authors declare no competing interests.

ETHICS APPROVAL

Our study makes use of publicly available RNA-sequencing datasets as cited in the results section. As such, prior ethics approval has been obtained for these studies and no additional approval is required. All mouse experiments were conducted in accordance with an Institutional Animal Care and Use Committee (IACUC). All people involved in animal experiments received prior training and have passed the additionally required personal licensing course (FELASA B). All animal experiments were approved by the local authorities (LANUV, North-Rhine-Westphalia, Germany) and performed under license number 81-02.04.2017.A477.

ADDITIONAL INFORMATION

Supplementary information The online version contains supplementary material available at https://doi.org/10.1038/s41418-022-01096-8.

Correspondence and requests for materials should be addressed to Silvia von Karstedt.

Reprints and permission information is available at http://www.nature.com/reprints

Publisher's note Springer Nature remains neutral with regard to jurisdictional claims in published maps and institutional affiliations.

2.2 SUPPLEMENTARY INFORMATION

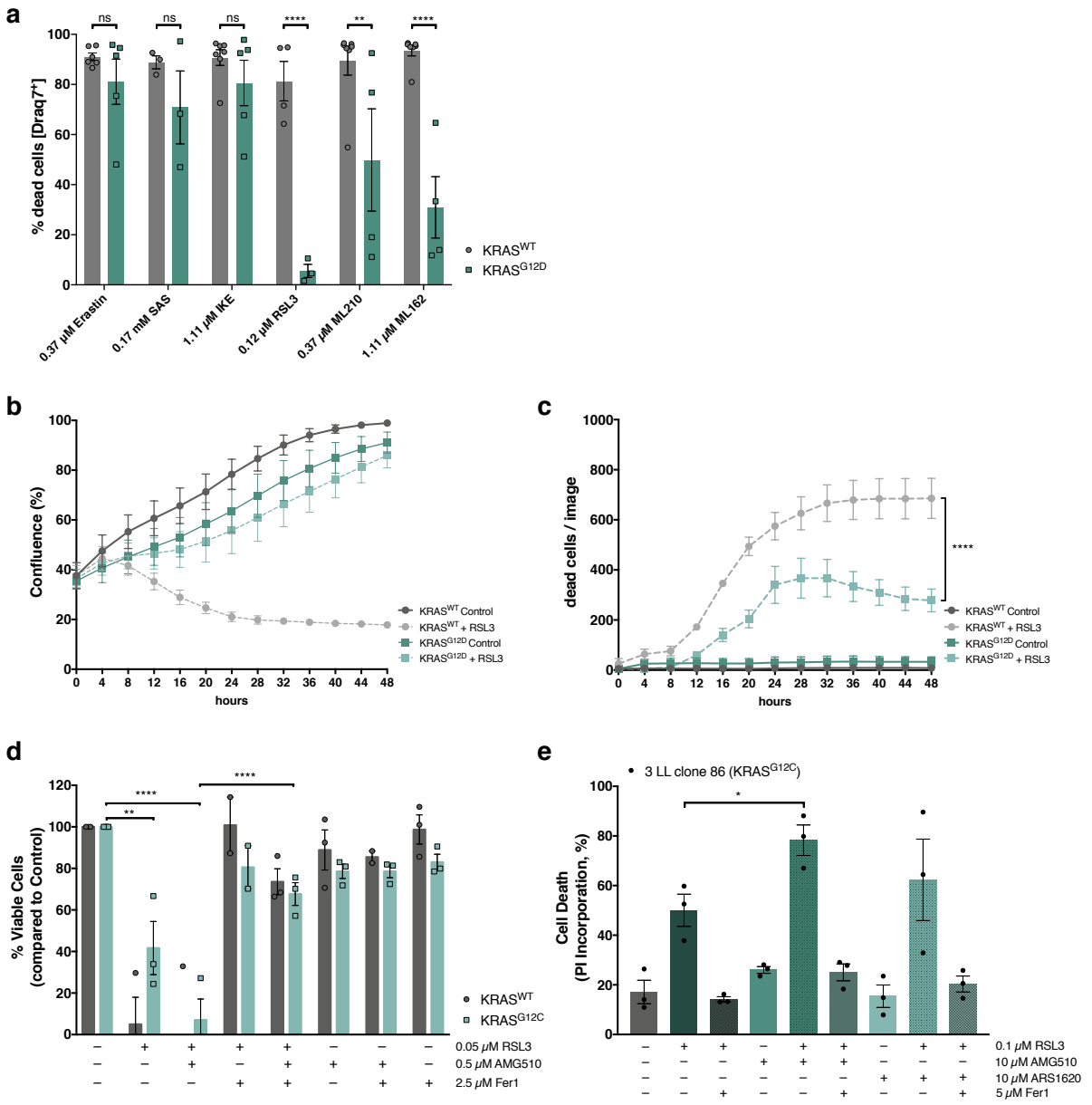

Supplementary Fig. 1: Oncogenic KRAS activity renders cells resistant to ferroptosis. a KRAS WT or KRAS^{G12D}-expressing MEFs were treated with either erastin [0.37 μM], SAS [0.17 mM], IKE [1.11 μM], RSL3 [120 nM], ML210 [0.37 μM] or ML162 [1.11 μM] for 24 h. DRAQ7 [100 nM] was added to visualize dead cells. Dead cells were analyzed by using the IncuCyte quantification software. Images were acquired at 10x magnification every 2 h using the IncuCyte S3 bioimaging platform. **b, c** KRAS WT or KRAS^{G12D}-expressing MEFs were treated with or without RSL3 [100 nM] for 48 h and confluence was determined by analyzing phase contrast using the IncuCyte quantification software or DRAQ7 [100 nM] (**c**) was added to wells to visualize dead cells. Images were acquired at 10x magnification every 4 h using the IncuCyte S3 bioimaging platform. **d** KRAS WT or KRAS^{G12C}-expressing MEFs were treated with RSL3 [50 nM], AMG510 [500 nM] and Fer1 [2.5 μM] alone or in combination for 24 h. Cell viability was determined by Cell Titer blue. % viability is calculated relative to untreated KRAS WT MEFs (100%). **e** 3LL cells were treated with RSL3 [100 nM], AMG510 [10 μM], ARS1620 [10 μM] and Fer1 [5 μM] alone or in combination for 24 h. Cell death was determined by propidium iodide (PI) uptake and flow cytometry. Gates are set on PI+ cells in control untreated

cells. Data are means +/- SEM of three independent experiments in each individual cell line. Two-way ANOVA + Tukey's multiple comparison test (**a, d, e**), two-tailed t-test of end timepoint (**c**), **** p<0.0001, ** p<0.01, * p<0.05.

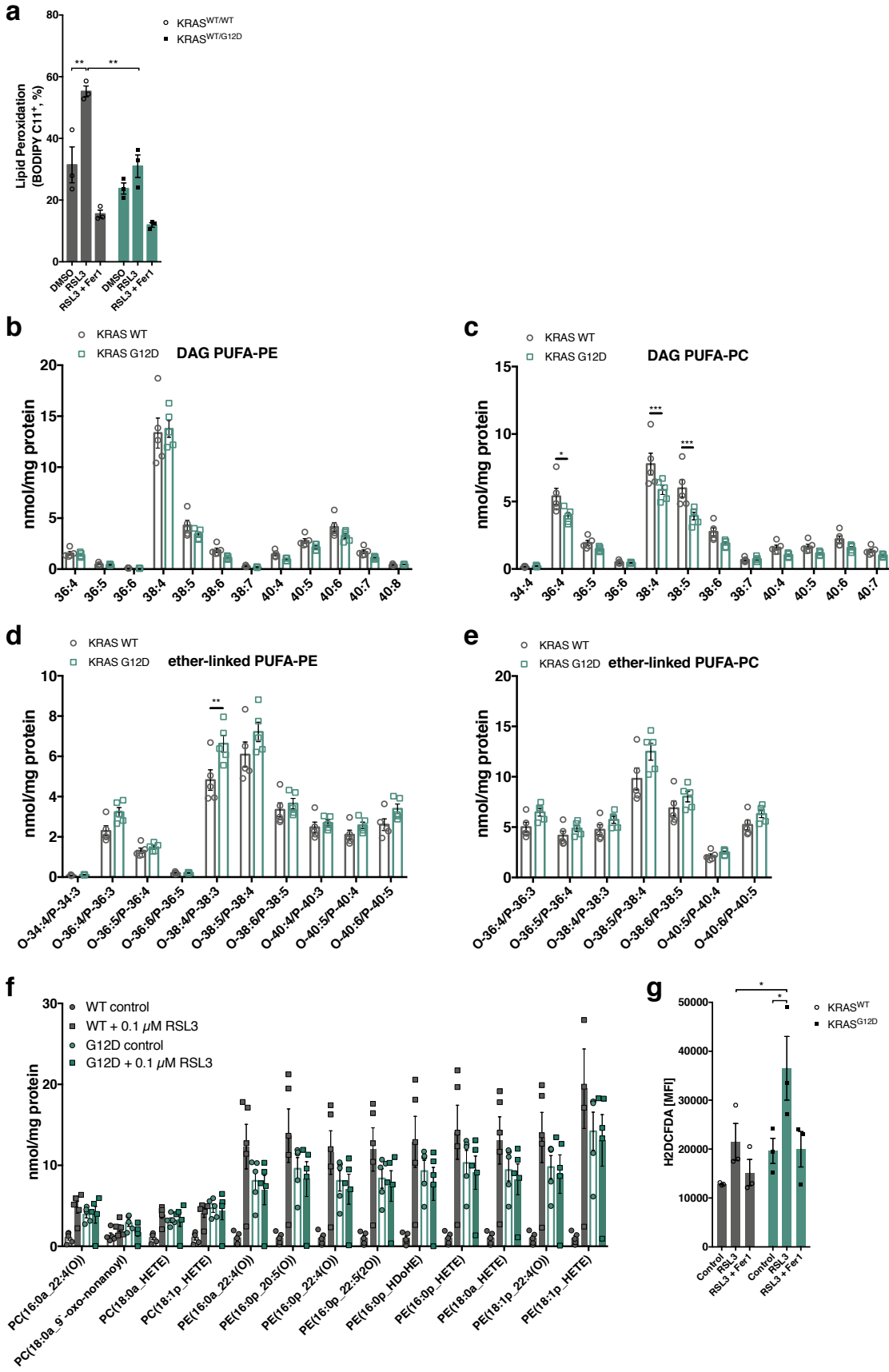

Supplementary Fig. 2: Comparative lipidomics in KRAS WT and KRAS^{G12D}-expressing cells. a Bulk-sorted MEFs expressing KRAS^{WT} or KRAS^{G12D} were treated either with DMSO, RSL3 [100 nM] alone or in combination with Ferrostatin-1 (Fer-1) [5 μM] for 5 h and stained for lipid ROS accumulation using BODIPY C11. Cells were analyzed by flow cytometry. Negative gates were placed based on DMSO controls. **b - e** KRAS^{WT}-expressing cells (n = 5 samples) as compared to KRAS^{G12D}-expressing cells (n = 5 samples) were analyzed for basal diacylglycerol (DAG) and ether-linked lipids by mass spectrometry. Lipid content was normalized to infused protein for each condition and replicate. Individual PUFAs (4 double bonds or more) are plotted. **f** Data showing the representation of mono-oxidized phospholipid species (PE phosphatidylethanolamine; PC phosphatidylcholine) in KRAS wild type as compared to KRAS^{G12D}-expressing cells treated with either DMSO or RSL3 [100 nM] for 5 h and then subjected to lipidomics. Samples for each condition (n=5) were averaged and normalized to the cell number ($2.5x10^6$). nmoles lipid/mg protein lysate is shown. **g** Rasless MEFs expressing KRAS wild type or KRAS^{G12D} were treated either with DMSO, RSL3 [100 nM] alone or in combination with Ferrostatin-1 (Fer-1) [5 μM] for 5 h and stained for ROS accumulation using H2DCFDA. Cells were analyzed by flow cytometry. Negative gates were placed based on DMSO controls. Data are means +/- SEM of three independent experiments in each individual cell line. Two-way ANOVA + Tukey's multiple comparison test, *** p<0.001, ** p<0.01, * p<0.05.

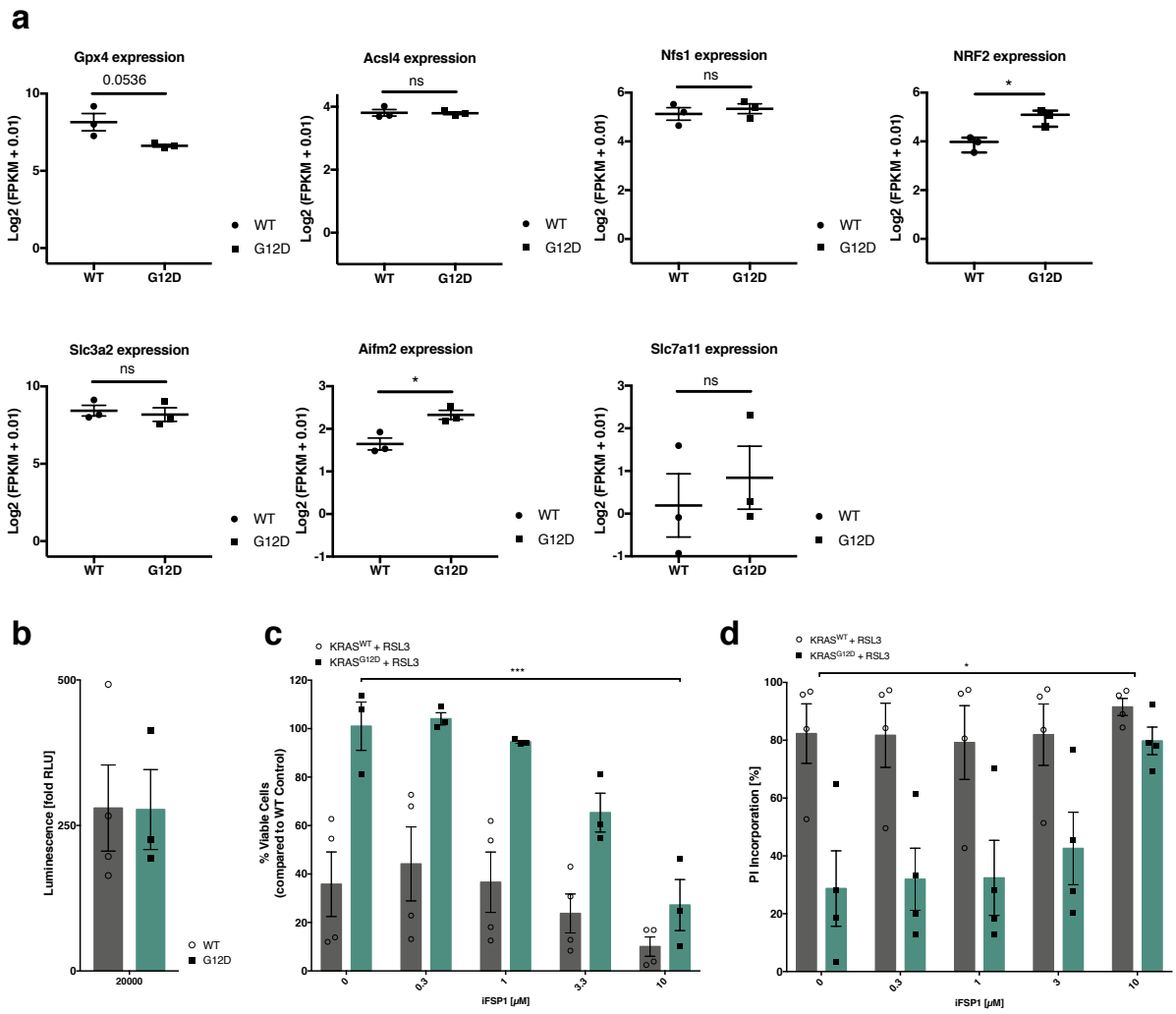

Supplementary Fig. 3: RNA expression of ferroptosis regulators. a RNA-seq expression data in FPKM (fragments per kilobase of exon model per million reads mapped) from KRAS WT and KRAS^{G12D}-expressing cells were log2 transformed (+0.01) and plotted for relative

expression of genes involved in ferroptosis. **b** Ratio of total oxidized and reduced nicotinamide adenine dinucleotide phosphates (NADP+ and NADPH, respectively) was measured in lysates from 20,000 cells of either KRAS WT or $KRAS^{G12D}$-expressing cells using the NADP/NADPH-Glo™ kit (Promega). **c** KRAS WT or $KRAS^{G12D}$-expressing cells were treated with RSL3 [100 nM] alone or in combination with rising concentrations of iFSP1. Cell viability was determined by Cell Titer blue. % viability is calculated relative to untreated KRAS WT MEFs (100%). **d** Cell death of cells treated as in (**c**) was determined by flow cytometry and propidium iodide (PI) incorporation. Gates are set on PI+ cells in control untreated cells. Data are means +/- SEM of three independent experiments in each individual cell line. Two-tailed t-tests (**a**), Two-way ANOVA + Tukey's multiple comparison test (**c, d**), **** $p<0.0001$, * $p<0.05$.

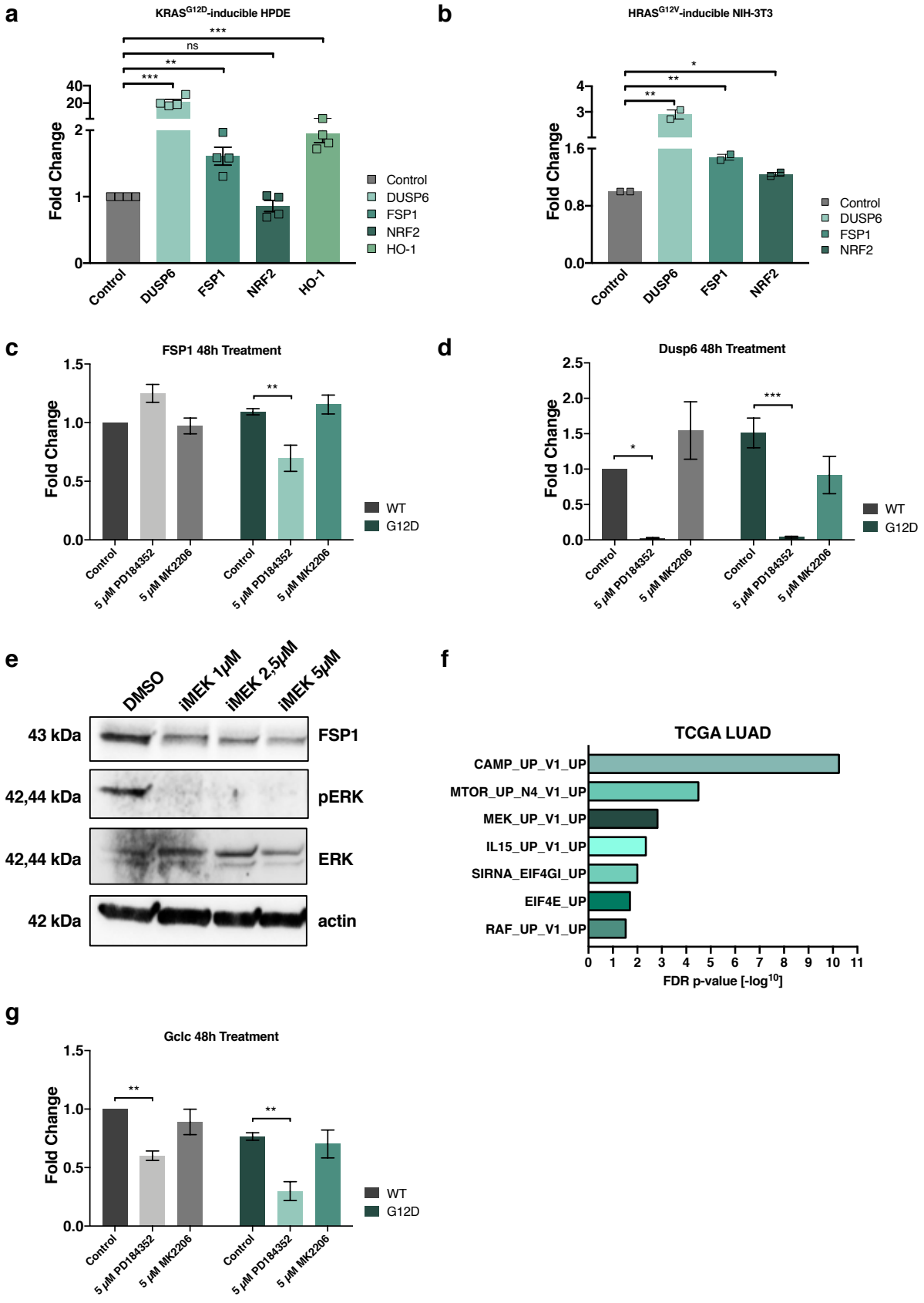

Supplementary Fig. 4:MEK activity elevates FSP1 mRNA levels. a Levels of the indicated cDNAs were quantified by qPCR in KRAS^{G12D}-inducible HPDE cells after 72 h of doxycycline [0.5 µg/ml] treatment. Fold change relative to controls is shown. **b** Levels of the indicated cDNAs were quantified by qPCR in HRAS^{G12V}-inducible NIH-3T3 cells after 48 h of tamoxifen

(4OHT) treatment [100 nM]. Fold change relative to controls is shown. **c** Levels of FSP1 cDNA were quantified by qPCR in Rasless MEFs expressing WT or $KRAS^{G12D}$ treated with either DMSO, iMEK (PD184352) [5 μM] or iAKT (MK2206) [5 μM] for 48 h. Fold change relative to DMSO KRAS WT controls is shown. **d** Levels of DUSP6 cDNA were determined in cells treated as in (**c**). **e** $KRAS^{G12D}$-expressing cells were treated with the indicated concentrations of iMEK (PD184352) for 72 h, lyzed and subjected to protein analysis by Western blotting. **f** Genes significantly co-expressed with FSP1 within the LUAD TCGA dataset were analyzed by gene-set enrichment (GSEA) and $-\log^{10}$-transformed false discovery rates (FDR) of significantly enriched gene sets are plotted. **g** Levels of GCLC cDNA were determined in cells treated as in (**c**). Data are means +/- SEM of at least two independent experiments in each individual cell line. Two-tailed t-test, *** p<0.001, ** p<0.01, * p<0.05.

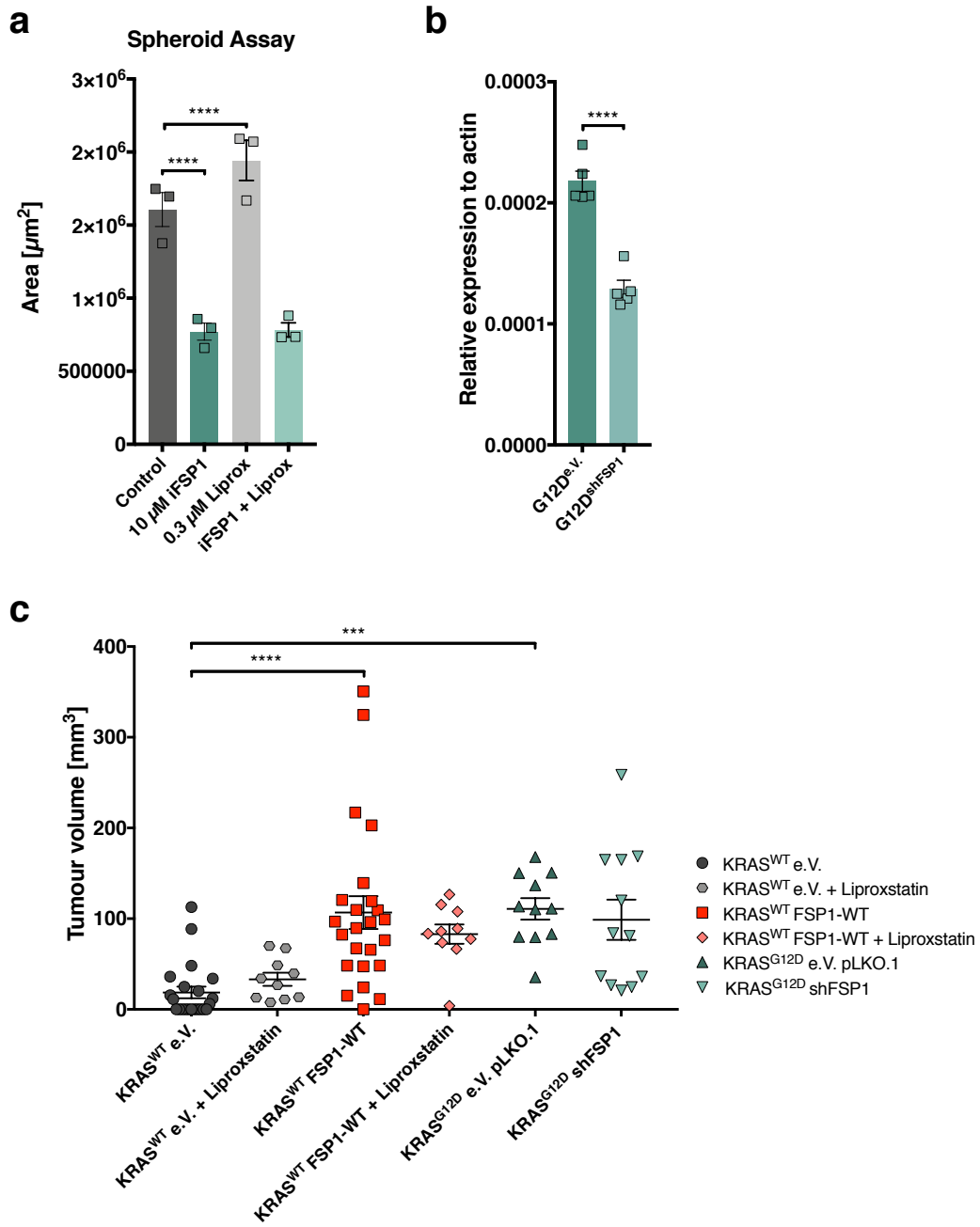

Supplementary Fig. 5: **Spheroid growth and FSP1 silencing controls. a** A549 cells were subjected to spheroid assay growth for 4 days and treated as indicated. Images were quantified using the BZ-H4M/Measurement Application Software (Keyence). **b** Levels of FSP1 cDNA

were quantified by qPCR in Rasless MEFs expressing either $KRAS^{G12D}$ pLKO.1 empty Vector or $KRAS^{G12D}$ pLKO.1 shFSP1 stable expression plasmids. **c** 8-weeks old male nude mice were injected with 5 x 10^5 cells of the indicated cell lines (G12D e.V. (empty Vector) n=11; G12D shFSP1 n=12; WT e.V. n=24 + Vehicle; WT e.V. + Liproxstatin-1 n=10; WT FSP1 n=24 + Vehicle; WT FSP1 + Liproxstatin-1 n=10) into both flanks. Mice were injected 5x per week either with vehicle [PBS with 1% DMSO] or Liproxstatin-1 [10 mg/kg]. Tumor length and width were measured by caliper at day 26 and volume was calculated as (length x width x width)/2. Data are means +/- SEM of three independent experiments in each individual cell line. Two-way ANOVA + Tukey's multiple comparison test (**a, c**), two-tailed t-test (**b**), **** p<0.0001, *** p<0.001.

Supplementary Table 1: qPCR mouse primers

Primer mouse	Sequence
mouse FSP1 FWD	TGCCTCGCAATGAGTATCGG
mouse FSP1 REV	GCCAGCCTACTCTCTGCAAAT
mouse DUSP6 FWD	ATAGATACGCTCAGACCCGTG
mouse DUSP6 REV	ATCAGCAGAAGCCGTTCGTT
mouse NRF2 FWD	GCTGCTCGGACTAGCCATTG
mouse NRF2 REV	TCAAATCCATGTCCTGCTGGG
mouse GCLC FWD	GGACAAACCCCAACCATCC
mouse GCLC REV	GTTGAACTCAGACATCGTTCCT
mouse HO-1 FWD	GCCGAGAATGCTGAGTTCATG
mouse HO-1 REV	TGGTACAAGGAAGCCATCACC
mouse Rpl13a FWD	AGCCTACCAGAAAGTTTGCTTAC
mouse Rpl13a REV	GCTTCTTCTTCCGATAGTGCATC
mouse Rplp0 FWD	TAAAGACTGGAGACAAGGTG
mouse Rplp0 REV	GTGTACTCAGTCTCCACAGA
mouse Actin FWD	GGCTGTATTCCCCTCCATCG
mouse Actin REV	CCAGTTGGTAACAATGCCATGT

Supplementary Table 2: qPCR human primers

Primer human	Sequence
human FSP1 FWD	GACTCCTTCCACCACAATGTGG
human FSP1 REV	CAGCACCATCTGGTTCTTCAGG
human DUSP6 FWD	GCAATACTTTGGGTTGGTTTC
human DUSP6 REV	AACTCTCCCTTCTTCACAATC
human NRF2 FWD	CCAACTACTCCCAGGTTGCC

human NRF2 REV	AGTGACTGAAACGTAGCCGAA
human HO-1 FWD	ACCTTCCCCAACATTGCCAG
human HO-1 REV	CAACTCCTCAAAGAGCTGGATG
human 18S FWD	GCAGAATCCACGCCAGTACAAG
human 18S REV	GCTTGTTGTCCAGACCATTGGC

3 RESULTS

To investigate ferroptosis resistance in another cellular system, bulk-sorted mouse embryonic fibroblasts (MEFs) expressing endogenous levels of KRAS wild type (WT) and additionally exogenous levels of different KRAS mutations ($KRAS^{WT/GFP}$, $KRAS^{WT/WT}$, $KRAS^{WT/G12A}$, $KRAS^{WT/G12C}$, $KRAS^{WT/G12D}$, $KRAS^{WT/G12R}$, $KRAS^{WT/G12S}$, $KRAS^{WT/G12V}$, $KRAS^{WT/G13C}$, $KRAS^{WT/G13D}$, $KRAS^{WT/Q61H}$ and $KRAS^{WT/Q61L}$) were treated with either 0.1 µM or 1 µM RSL3 and cell death was determined by propidium iodide (PI) uptake.

Only MEFs expressing $KRAS^{WT/G12D}$ were resistant to RSL3 treatment at a concentration of 0.1 µM (Figure 8a). At a higher concentration (1 µM RSL3) also $KRAS^{WT/G12D}$ mutant cells showed an increased sensitivity to ferroptosis. To further determine whether RSL3 treatment induces ferroptotic cell death and to exclude any other type of cell death such as apoptosis or necroptosis, bulk-sorted MEFs expressing different exogenous KRAS mutations were treated with 0.5 µM RSL3 in combination with either Ferrostatin-1 (Fer1), pan-caspase inhibitor (z-VAD) or RIPK1 inhibitor Necrostatin-1 (Nec1). Only Fer-1, which specifically inhibits ferroptosis, could rescue cell death which confirmed that RSL3 induces ferroptosis in bulk-sorted MEFs expressing exogenous levels of wild type or mutant KRAS (Figure 8b).

Moreover, GPX4, a key player to protect cells from ferroptosis, reduces lipid peroxidation by using GSH as a co-factor. When GPX4 is blocked by e.g. RSL3, it is unable to protect cells from ferroptotic cell death [29]. To study whether different GSH levels of different KRAS mutant cells were responsible for varying ferroptosis sensitivity, and to evaluate whether $KRAS^{WT/G12D}$ cells contain higher GSH levels and are therefore more resistant to ferroptosis, GSH levels were determined by using the fluorescent dye monochlorobimane (MCB) for FACS analysis. In contrast to this assumption, cells expressing oncogenic $KRAS^{G12D}$ showed lower GSH levels compared to cells expressing other oncogenic mutations, indicating that resistance of $KRAS^{WT/G12D}$ mutant cells to RSL3 induced ferroptosis cannot be caused by elevated levels of GSH (Figure 8c).

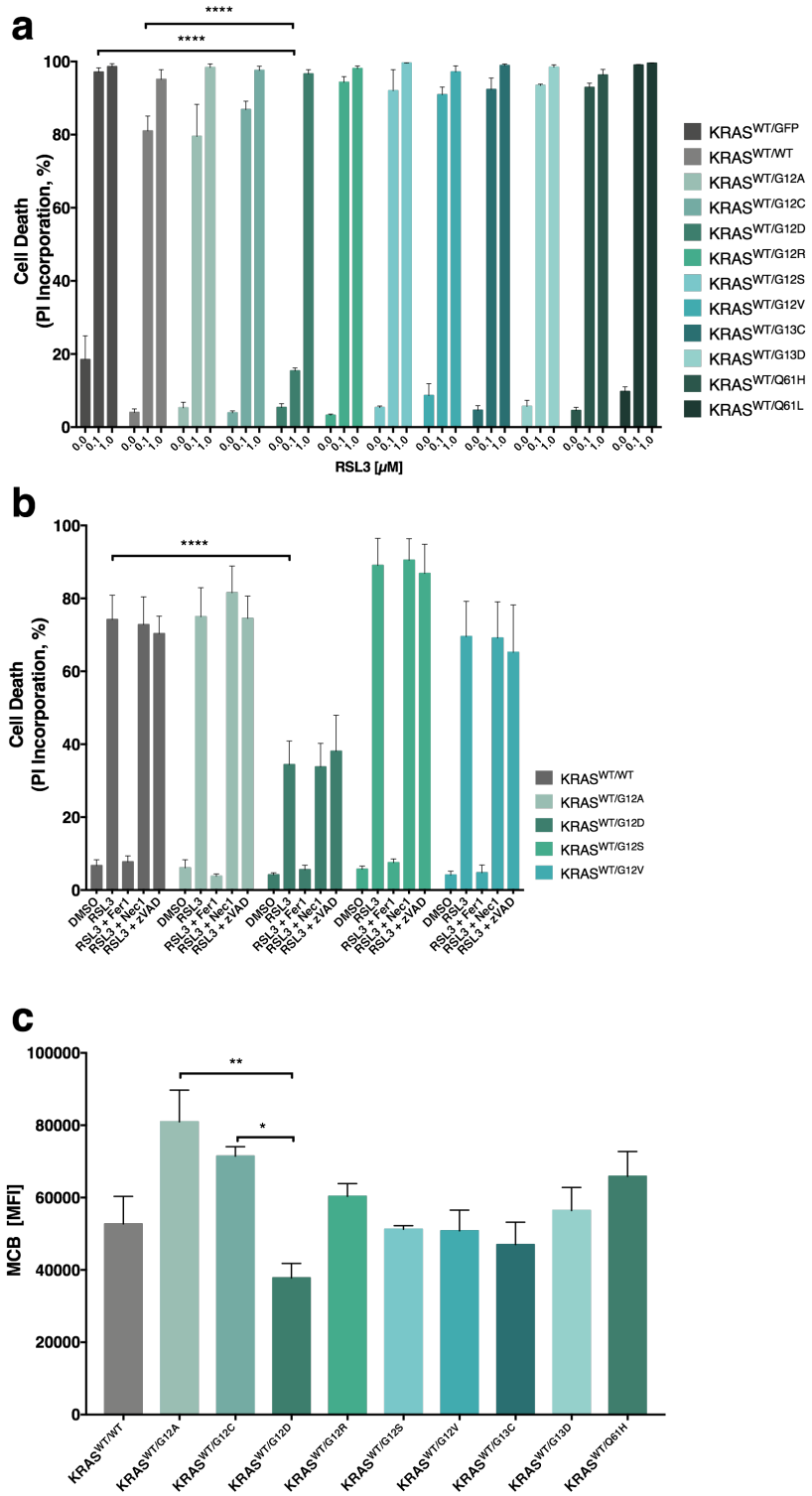

Figure 8: Cells expressing KRAS^{G12D} are the most resistant to ferroptosis induction
a Bulk-sorted MEFs expressing indicated variants of either KRAS WT or mutants were treated either with DMSO or RSL3 [0.1 μM or 1.0 μM] for 24 h. Cell death was determined by propidium iodide (PI) uptake and flow cytometry. 0% PI-Incorporation is gated to control untreated. **b** Bulk-sorted MEFs were treated either with DMSO, RSL3 [0.5 μM] alone or in combination with either Ferrostatin-1 (Fer1) [5 μM], Necrostatin-1s (Nec1) [10 μM] or zVAD [20 μM]. 0% PI-Incorporation is gated to untreated control. **c** Cellular GSH levels were determined by monochlorobimane (MCB) staining and flow cytometry (MFI- mean fluorescent intensity) in the indicated bulk-sorted MEFs expressing indicated variants of either KRAS WT or mutants upon

24 h. Data are means +/- SEM of three independent experiments in each individual cell line. Two-way ANOVA + Tukey's multiple comparison test, **** p<0.0001, ** p<0.01, * p<0.05.

To next resolve ferroptosis resistance of KRAS-mutated cells over time in cells expressing different oncogenic KRAS mutations, bulk-sorted MEFs were treated for 72 hours with 0.1 µM RSL3 and therefore seeded 24 hours before treatment in low density (10-20% confluence). As expected, untreated $KRAS^{WT/WT}$ cells showed significantly lower cell confluence after 72 hours compared to $KRAS^{WT/G12D}$-expressing cells suggestive of increased proliferation of KRAS-mutated cells (Figure 9c). These results should be considered in the following experiments since it is known that ferroptosis resistance is cell density dependent [125], [185]. However, upon 72 hours of 0.1 µM RSL3 treatment, $KRAS^{WT/G12D}$ cells showed 100% confluence whereas all other cell lines expressing different KRAS mutations were sensitive to ferroptosis induction and reached a lower cell confluence after treatment (Figure 9b, 9d). Therefore, our results confirm that cells expressing $KRAS^{WT/G12D}$ compared to cells expressing other KRAS mutations are the most resistant to ferroptosis induction. The experiments were analyzed using IncuCyte real-time live cell imaging.

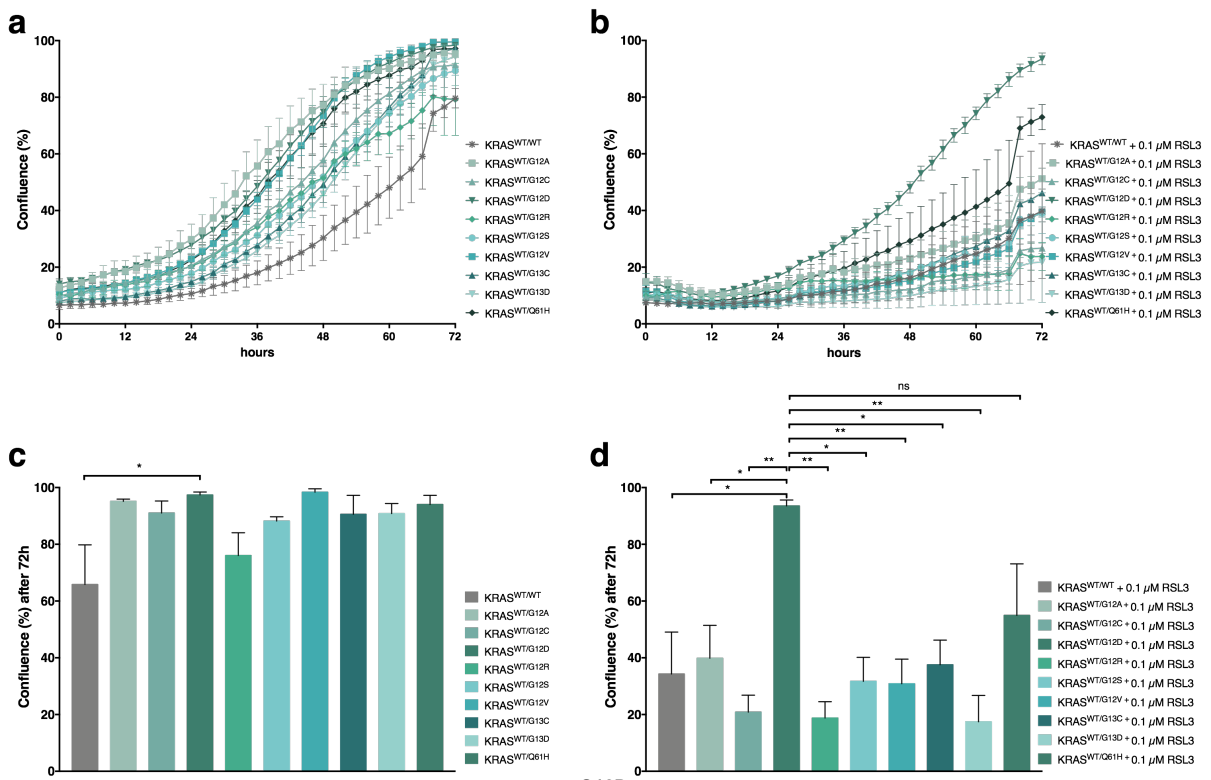

Figure 9: Expression of oncogenic KRAS^{G12D} protects cells from cell growth inhibition during ferroptosis induction

a, b Bulk-sorted MEFs expressing indicated variants of either KRAS WT or mutants were treated with or without RSL3 [0.1 μM] for 72 h and confluence was determined by analyzing phase contrast using the IncuCyte quantification software. Images were acquired at 10x magnification every 4 h using the IncuCyte S3 bioimaging platform. **c, d** Representative data of cells is in (**a, b**) at timepoint 72 h. Data are means +/- SEM of three independent experiments in each individual cell line. Two-way ANOVA + Tukey's multiple comparison test, ** p<0.01, * p<0.05.

To further validate ferroptosis resistance of KRAS-mutated cells in different cell lines, also human cancer cell lines expressing KRAS mutations were tested for ferroptosis response. To this end, the human pancreatic cancer cell lines BxPC3, which expresses KRAS WT, and L36pl, which harbors a KRAS^{G12D} mutation [186], were treated with either RSL3 or erastin. Indeed, L36pl cells, expressing an oncogenic KRAS mutation, were more resistant to ferroptosis induced by RSL3 or erastin treatment compared to the human pancreatic cancer cell line BxPC3, which lacks a KRAS mutation (Figure 10a, 10b). Although these two cell lines are from distinct origins and therefore comparative results have to be taken with a grain of salt, these results further support our findings made in isogenic cellular systems (Müller et al. 2022) and therefore indicate that oncogenic KRAS^{G12D} renders cells more resistant to ferroptosis. Cell death was determined by PI uptake.

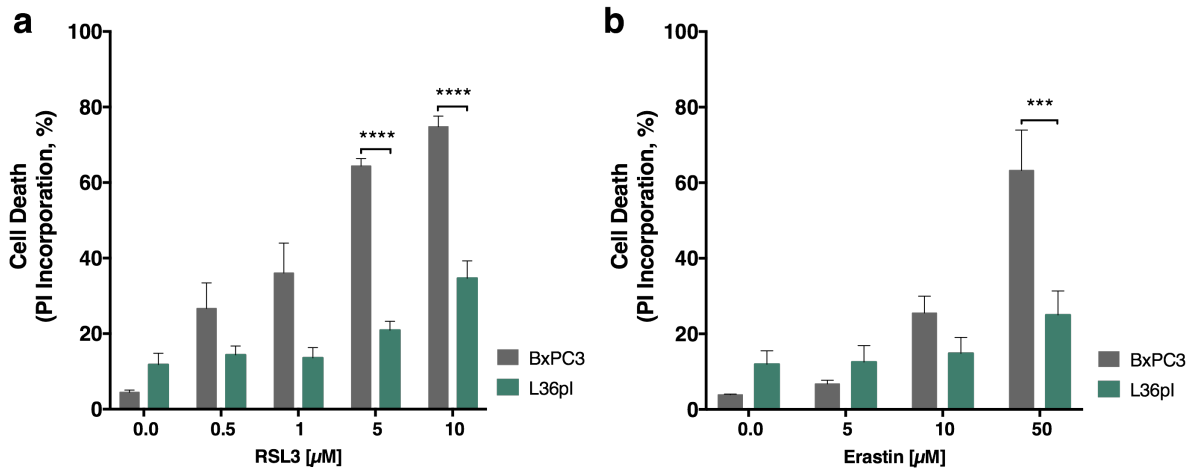

Figure 10: KRAS^{G12D}-mutated human pancreatic cancer cell lines are more resistant to ferroptosis induction

a, b BxPC3 and L36pl cells were treated with indicated concentrations of RSL3 (**a**) or erastin (**b**) for 24 h. Cell death was determined by propidium iodide (PI) uptake and flow cytometry. 0% PI-Incorporation is gated to control untreated. Data are means +/- SEM of three independent experiments in each individual cell line. Two-way ANOVA + Tukey's multiple comparison test, **** p<0.0001, *** p<0.001.

KRAS G12C inhibitors such as ARS1620 and AMG510 have been reported to selectively inactivate mutated KRAS^{G12C} [164]. In our published work we showed that KRAS^{G12C} inhibition renders cells more sensitive to ferroptosis induction (Müller et al. 2022 Supplementary Figure 1d, e). To further validate these data, "Rasless" MEFs expressing either KRAS^{WT} or KRAS^{G12C} were treated with ARS1620 and AMG510. Indeed, treatment with ARS1620 in combination with RSL3 also decreased cell viability in KRAS^{G12C}-expressing cells (Figure 11a). Furthermore, ferroptosis induction by RSL3 in combination with KRAS inhibition by AMG510 also rendered cells more sensitive to cell death (Figure 11b). These data reinforce the hypothesis, that constitutively active mutant KRAS leads to increased ferroptosis resistance. Based upon our own observations (Müller et al. 2022 Figure 1a; Supplementary Figure 3d) KRAS^{WT}-expressing cells die upon RSL3 induction by up to 75%-80%. Surprisingly, in Figure 11b cell death in KRAS^{WT} cells was less effective when treated with 0.1 µM RSL3 alone. Knowing that higher cell confluence leads to ferroptosis resistance [125], [187], we hypothesized that these data discrepancies might be explained by increased cell confluence of KRAS^{WT} cells upon RSL3 treatment.

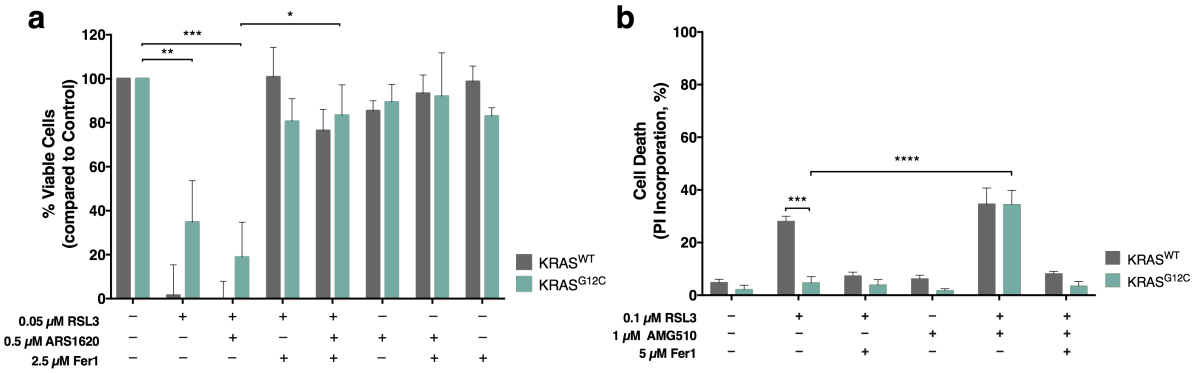

Figure 11: G12C-inhibition enhances sensitivity to ferroptosis induction
a $KRAS^{WT}$ or $KRAS^{G12C}$-expressing MEFs were treated with RSL3 [0.05 µM], ARS1620 [0.5 µM] and Fer1 [2.5 µM] alone or in combination for 24 h. Cell viability was determined by Cell Titer Blue. % viability is calculated relative to untreated $KRAS^{WT}$ MEFs (100%). **b** $KRAS^{WT}$ or $KRAS^{G12C}$-expressing MEFs were treated with RSL3 [0.1 µM], AMG510 [1 µM] and Fer1 [5 µM] alone or in combination for 24 h. Cell death was determined by propidium iodide (PI) uptake and flow cytometry. Gates are set on PI+ cells in control untreated cells. Data are means +/- SEM of three independent experiments in each individual cell line. Two-way ANOVA + Tukey's multiple comparison test, **** p<0.0001, *** p<0.001, ** p<0.01, * p<0.05.

It is known that ferroptosis is density dependent and that cells grown in high density are more resistant to ferroptosis than cells grown in low density [125], [187]. To test this hypothesis, cells were seeded in three different seeding densities (low 25,000, middle 55,000 and high 120,000/cells per 24-well) 24 hours before treatment with or without RSL3. Indeed, we could confirm that upon low density $KRAS^{G12D}$ cells became as sensitive to ferroptosis as $KRAS^{WT}$ cells, while cells seeded in high density resulted in less ferroptotic cell death upon ferroptosis induction also in $KRAS^{WT}$ cells (Figure 12). Interestingly, although confluence levels of $KRAS^{WT}$ and $KRAS^{G12D}$ cells seeded in middle density were comparable at timepoint 0 hours, $KRAS^{G12D}$-expressing cells did not die upon RSL3 induced ferroptosis whereas $KRAS^{WT}$-expressing cells in the same density were sensitive to ferroptosis (Figure 12a, c). Additionally, cell death was fully rescued in cells expressing $KRAS^{G12D}$ seeded in high density when treated with RSL3, while in cells expressing $KRAS^{WT}$ dead cells were detectable in every density upon RSL3 treatment (Figure 12b, d). These data suggest that cells expressing oncogenic $KRAS^{G12D}$ are protected from ferroptosis when seeded in middle densities through a ferroptosis defense mechanism that is regulated density independent while in addition, increasing density will render cells ferroptosis resistant. Cells were seeded one day prior treatment. The data was analyzed by using the IncuCyte real-time live cell imaging.

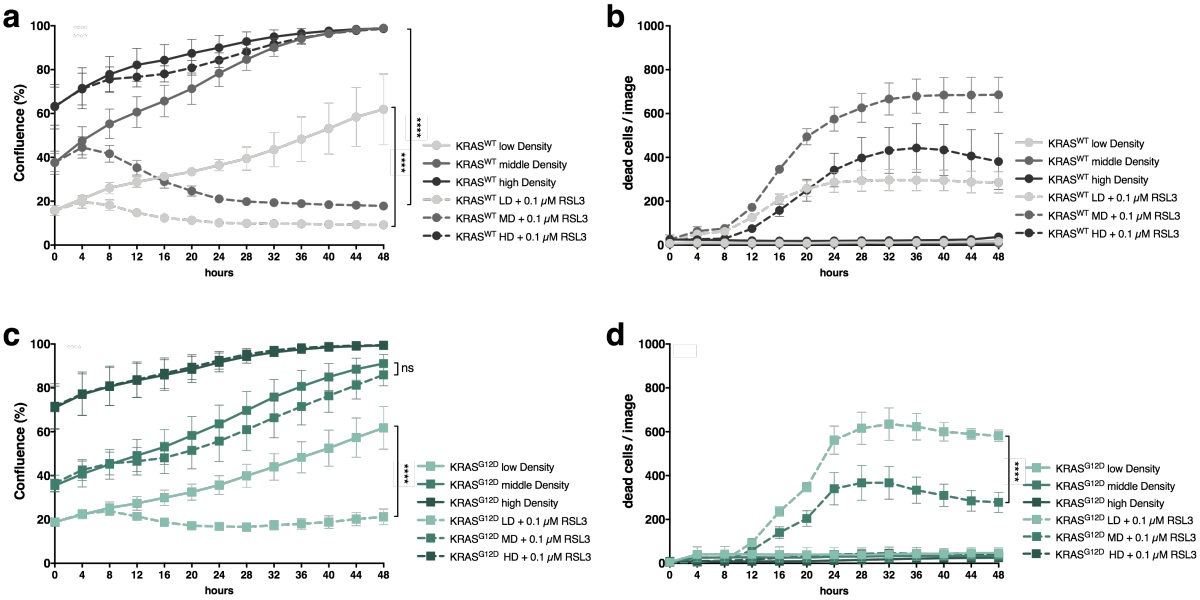

Figure 12: Ferroptosis resistance is density dependent
a, b KRAS^{WT}-expressing MEFs were treated with or without RSL3 [0.1 μM] in low, middle or high densities for 48 h. Confluence was determined by analyzing phase contrast using the IncuCyte quantification software or DRAQ7 [0.1 μM] was added to wells (**b**) to visualize dead cells. Images were acquired at 10x magnification every 4 h using the IncuCyte S3 bioimaging platform. **c, d** KRAS^{G12D}-expressing MEFs were treated as in (**a**) and (**b**). LD = low density, MD = middle density, HD = high density. Data are means +/- SEM of three independent experiments in each individual cell line. Two-way ANOVA + Tukey's multiple comparison test, **** p<0.0001.

Since in this study we could confirm that cell density influences ferroptosis sensitivity and resistance, it was important to determine at which cell confluence ferroptosis sensitivity was altered comparing KRAS WT and KRAS mutant cells. Therefore, KRAS^{WT} and KRAS^{G12D}-expressing cells were seeded the day before treatment in four different densities in the range of low (25,000 cells/24-well) to middle (55,000 cells/24-well) density from the previous experiments (Figure 12). Interestingly, we could determine the exact density in which KRAS^{G12D}-expressing cells turned from ferroptosis resistant to sensitive, which was at a cell confluence of 35,000 to 45,000 cells per 24-well plate (Figure 13d). Moreover, although KRAS^{WT} and KRAS^{G12D}-expressing cells showed similar levels of confluence over time (Figure 13a, c), KRAS^{WT} cells were sensitive to ferroptosis induction at any density while KRAS^{G12D} cells switched from ferroptosis resistant to sensitive at a density between 35,000 to 45,000 cells per 24-well (Figure 13b, d). However, in future studies it needs to be further investigated which cellular process exactly renders cells more resistant at a specific cell density and which metabolic switch KRAS^{G12D} mutant cells overcome to survive

ferroptotic cell death. The data was analyzed using the IncuCyte real-time live cell imaging.

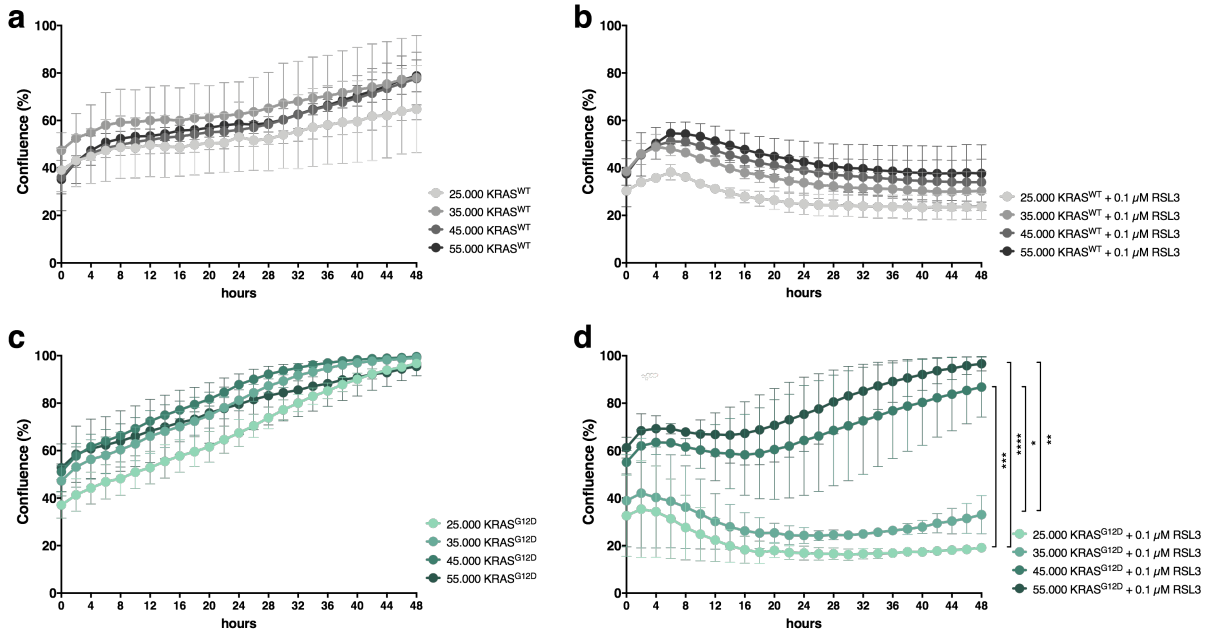

Figure 13: KRAS^{G12D} protects cells from ferroptosis in middle density
a, b KRAS^{WT}-expressing MEFs were untreated (**a**) or treated with (**b**) RSL3 [0.1 µM] in different densities for 48 h and confluence was determined by analyzing phase contrast using the IncuCyte quantification software. Images were acquired at 10x magnification every 4 h using the IncuCyte S3 bioimaging platform. **c, d** KRAS^{G12D}-expressing MEFs were treated as in (**a**) and (**b**). Data are means +/- SEM of three independent experiments in each individual cell line. Two-way ANOVA + Tukey's multiple comparison test, **** p<0.0001, *** p<0.001, ** p<0.01, * p<0.05.

To test whether the observed enhanced ferroptosis resistance upon increased cell density correlates with expression of FSP1, the molecular determinant of ferroptosis resistance of KRAS-mutated cells (Müller et al. 2022), FSP1 mRNA and protein levels were determined from cells seeded in different densities.

Strikingly, we found that KRAS^{WT} cells elevated FSP1 mRNA expression upon increased cell density, which could explain ferroptosis resistance of KRAS^{WT} cells when seeded and treated in high density (Figure 14a). Interestingly, we could observe that in KRAS^{G12D}-expressing cells already basal levels of FSP1 mRNA were elevated in comparison to KRAS^{WT}-expressing cells, explaining ferroptosis resistance in lower densities (Figure 14a). Moreover, on protein levels we could confirm that KRAS^{WT} cells increase FSP1 levels upon enhanced cell density, while KRAS^{G12D} cells already express high levels of FSP1 in lower densities (Figure 14c). These results reveal that FSP1 mRNA elevates upon enhanced density in KRAS WT cells offering a potential

explanation for increasing ferroptosis resistance in KRAS WT cells upon enhanced density.

In our published work, we could show that FSP1 expression is regulated by NRF2 activation (Müller et al. 2022 Figure 4c, d, e, f, g). NRF2 is a transcription factor which induces expression of the antioxidant molecular machinery. This includes antioxidant response element (ARE)-containing genes, which induce the expression of genes such as SLC7A11, GPX4, GCLC, GCLM, HO-1, NQO1 and also FSP1 [54], [58], [69], [188]. Therefore, to test whether the conditional density regulated FSP1 elevation is also NRF2-dependent, mRNA levels of NRF2 and its target genes Gclc and Ho-1 were measured in KRAS^{WT} cells grown in different densities. However, NRF2 mRNA levels were not upregulated in cells seeded for longer periods (72 h), which have an increased cell confluence, compared to cells seeded short-term (24 h) showing lower densities (Figure 14b). Although Ho-1, one target gene of NRF2, was upregulated over time, this could not be confirmed in Gclc, which is also a target gene of NRF2.

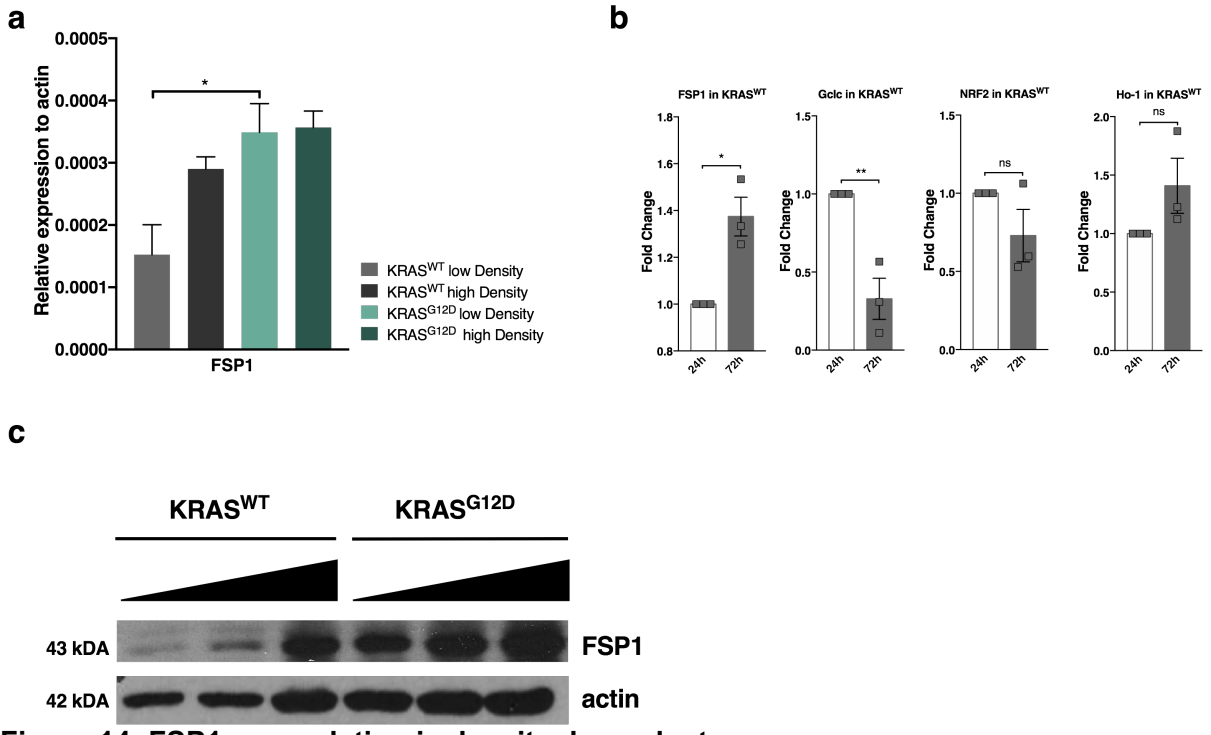

Figure 14: FSP1 upregulation is density dependent

a Levels of FSP1 cDNA were quantified after 24 h by qPCR in Rasless MEFs expressing KRAS^{WT} or KRAS^{G12D} seeded in low or high density. **b** Levels of FSP1, Gclc, NRF2 and Ho-1 cDNA were quantified after 24 h and 72 h by qPCR in Rasless MEFs expressing KRAS^{WT}. **c** Indicated cells were seeded for 24 h in three different densities. Cells were lyzed and subjected to protein analysis by Western blotting. Data are means +/- SEM of three independent experiments in each individual cell line. Western blots of representative control lysates are

shown. Two-way ANOVA + Tukey's multiple comparison test, two-tailed t-test, ** p<0.01, * p<0.05.

One metabolic characteristic effect of oncogenic RAS is the upregulation of general ROS [108], [109], [189], [190]. Moreover, ROS is a major activator of NRF2 activation. Therefore, we also tested whether cell density may influence cellular ROS levels. ROS levels were stained with the fluorescent dye H2DCFDA and cells were analyzed by flow cytometry. Indeed, we could confirm that cells expressing $KRAS^{G12D}$ accumulate higher ROS levels not only on basal levels but also upon ferroptosis induction (Figure 15a). Interestingly though, ROS levels decreased with increasing cell density in $KRAS^{WT}$ as well as in $KRAS^{G12D}$ cells. Based upon these data, we conclude that density-mediated regulation of FSP1 is NRF2-independent.

Taken together, our observations reveal FSP1 upregulation with increasing density. Therefore, in all subsequent experiments cell numbers were controlled and it was ensured that in experiments studying FSP1, FSP1 was not upregulated in $KRAS^{WT}$ or $KRAS^{G12D}$ cells due to increased confluence.

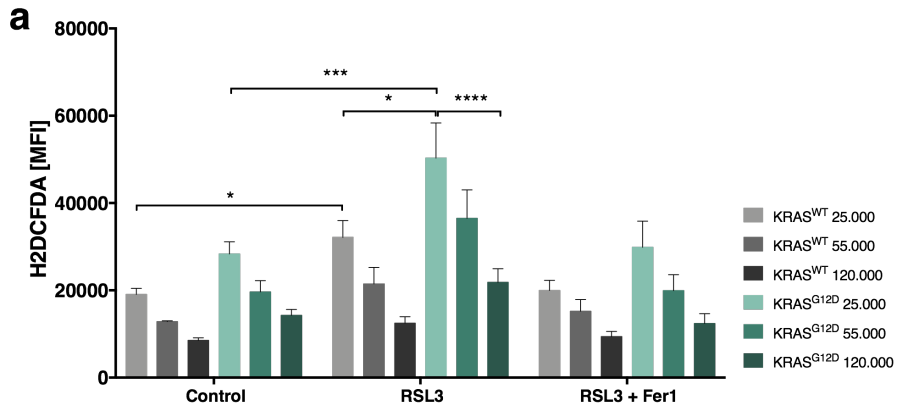

Figure 15: General ROS accumulation is density dependent
a Rasless MEFs expressing KRAS WT or $KRAS^{G12D}$ were seeded in different densities for 24 h, treated after either with DMSO, RSL3 [0.1 µM] alone or in combination with Ferrostatin-1 (Fer-1) [5 µM] for 5 h and stained for ROS accumulation using H2DCFDA. Cells were analyzed by flow cytometry. Negative gates were placed based on DMSO controls. Data are means +/- SEM of three independent experiments in each individual cell line. Two-way ANOVA + Tukey's multiple comparison test, **** p<0.0001, *** p<0.001, * p<0.05.

In our study the FSP1 inhibitor iFSP1 was first tested in different concentrations to exclude toxicity in cell death assays. We could observe that even in high concentrations iFSP1 did not induce cell death in $KRAS^{WT}$ and $KRAS^{G12D}$ cells (Figure 16a). FSP1 is an oxidoreductase reducing ubiquinone (CoQ10) to ubiquinol and

thereby protecting cells from lipid peroxidation [35], [36]. To determine whether its protective effect comes from the enzymatic activity of FSP1 or from its starting product ubiquinone (CoQ10), ferroptosis sensitivity was tested on cells by adding additional other analogues of CoQ10 such as mitochondrially-targeted MitoQ or chemical CoQ10 itself upon ferroptosis induction. Of note, MitoQ is a synthetic analogue of CoQ10 which has been developed to prevent cells from oxidative stress and lipid ROS and functions as a mitochondria-targeted antioxidant [191], [192].

$KRAS^{WT}$ and $KRAS^{G12D}$-expressing cells were treated with either MitoQ (Figure 16b) or CoQ10 (Figure 16c) in combination with or without RSL3 and iFSP1, to study ferroptosis resistance upon addition of CoQ10. We could observe that MitoQ rescued cell death completely in cells treated with either RSL3 alone or in combination with iFSP1, assuming that MitoQ treatment functions as an antioxidant, which protects cells from ferroptosis although FSP1 is inhibited using iFSP1 (Figure 16b). Moreover, CoQ10 treatment also slightly rescued ferroptotic cell death upon RSL3 induction in combination with iFSP1 in $KRAS^{G12D}$ cells (Figure 16c). In $KRAS^{WT}$ cells the strong protective effect from treatment with MitoQ upon ferroptosis induction and FSP1 inhibition could not be observed when cells were treated with CoQ10. However, these data show that the generation of ubiquinol by FSP1 is important to prevent cells from ferroptosis. Cell death was determined by PI uptake.

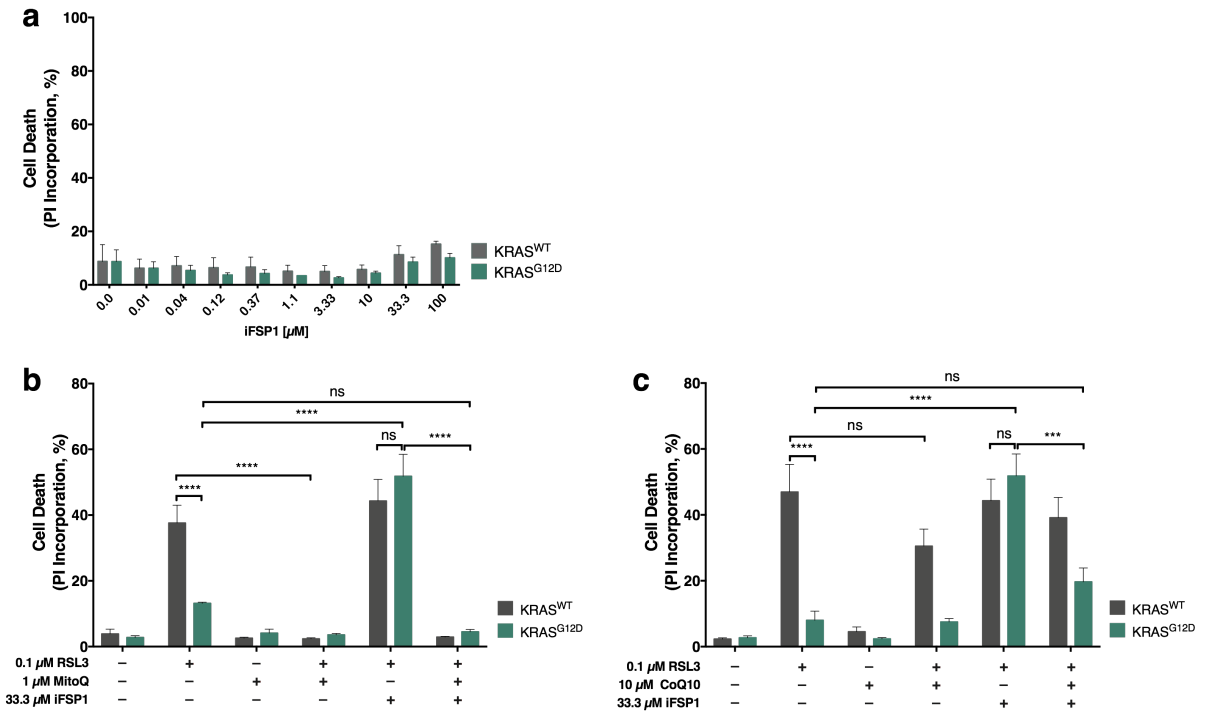

Figure 16: Analogues of CoQ10 protect cells from ferroptosis
a KRAS^{WT} or KRAS^{G12D}-expressing MEFs were treated with indicated concentrations of iFSP1. **b** KRAS^{WT} or KRAS^{G12D}-expressing MEFs were treated with RSL3 [0.1 μM], MitoQ [1 μM] and iFSP1 [33.3 μM] alone or in combination for 24 h. Cell death was determined by propidium iodide (PI) uptake and flow cytometry. Gates are set on PI+ cells in control untreated cells. **c** KRAS^{WT} or KRAS^{G12D}-expressing MEFs were treated with RSL3 [0.1 μM], CoQ10 [10 μM] and iFSP1 [33.3 μM] alone or in combination for 24 h. Cell death was determined by propidium iodide (PI) uptake and flow cytometry. Gates are set on PI+ cells in control untreated cells. Data are means +/- SEM of three independent experiments in each individual cell line. Two-way ANOVA + Tukey's multiple comparison test, **** p<0.0001, *** p<0.001.

We found that FSP1 expression is regulated by NRF2 activation (Müller et al. 2022 Figure 4c, d, e). Therefore, we investigated whether silencing of KEAP1, which under basal conditions facilitates NRF2 ubiquitination resulting in NRF2 degradation, is sufficient to protect cells from ferroptosis induction. Our data reveals that indeed, KEAP1 silencing renders KRAS^{WT} cells more resistant to ferroptosis as well as to ferroptosis induction combined with FSP1 inhibition (Figure 17a). Moreover, 24 hours pretreatment with the chemical NRF2 activator tert-butylhydrochinone (TBHQ) completely rescued cell death upon RSL3 induction in KRAS^{WT} cells (Figure 17b). These data confirm the hypothesis, that oncogenic KRAS upregulates FSP1 via the NRF2 pathway and thereby protecting cells from ferroptosis. The data was analyzed using the IncuCyte real-time live cell imaging.

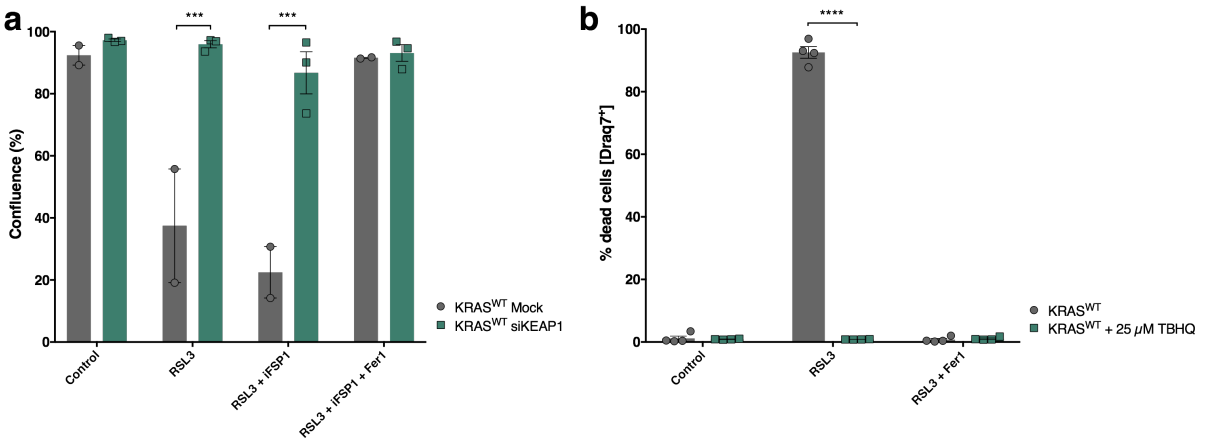

Figure 17: NRF2 upregulation via siKEAP1 knockdown or TBHQ treatment protects cells from ferroptosis

a siKEAP1 KRAS^{WT} cells were treated after 48 h knockdown with DMSO, RSL3 [0.1 µM], +/- iFSP1 [10 µM] and +/- Fer-1 [1 µM] for another 24 h. Confluence was determined by analyzing phase contrast using the IncuCyte quantification software. Images were acquired at 10x magnification every 2 h using the IncuCyte S3 bioimaging platform. **b** KRAS^{WT} cells were treated after 24 h incubation with or without TBHQ [25 µM] for another 24 h with DMSO, RSL3 [0.1 µM] and +/- Fer-1 [1 µM]. DRAQ7 [0.1 µM] was added to all wells to visualize dead cells. Images were acquired at 10x magnification every 2 h using the IncuCyte S3 bioimaging platform. Data are means +/- SEM of at least two independent experiments in each individual cell line. Two-way ANOVA + Tukey's multiple comparison test, **** p<0.0001, *** p<0.001.

Since in this study we showed that overexpression of FSP1 was sufficient to allow spheroid growth of KRAS^{WT} cells (Müller et al. 2022 Figure 5c), we further investigated how ferroptosis inhibition by using Fer1 affected spheroid growth. Surprisingly, spheroid growth was massively reduced in KRAS^{WT} and KRAS^{G12D} cells overexpressing FSP1 but not in KRAS^{G12D}-expressing cells, indicating that FSP1 expression affects spheroid growth independently of ferroptosis inhibition as also pointed out in our published work (Figure 18a). However, controversially to these results our study could show different effects of ferroptosis inhibition by using either Fer1 or the ferroptosis selective inhibitor Liproxstatin-1 on spheroids growing from A549 cells (Müller et al. 2022 Figure 5d; Supplementary Figure 5a). We could observe that ferroptosis inhibition did not decrease spheroid growth. Moreover, our study could reveal that ferroptosis inhibition *in vivo* by treating mice with Liproxstatin-1 accelerated tumor onset to a similar level as mice harboring FSP1 overexpressing WT tumors. Therefore, our results indicate that spheroid growth promoted by FSP1 overexpression is independent of ferroptosis protection and the effect of ferroptosis inhibition by Fer1 treatment in cells overexpressing FSP1 needs to be further investigated.

Since only in KRAS^{WT} and KRAS^{G12D} cells overexpressing FSP1 treatment of Fer1 decreased spheroid growth, these data suggest that KRAS mutant cells metabolically

change overtime and increase FSP1 levels, while overexpression of FSP1 for a short period could not adapt to this metabolic rewiring. Spheroid growth was quantified by using the BZ-H4M/Measurement Application Software (Keyence).

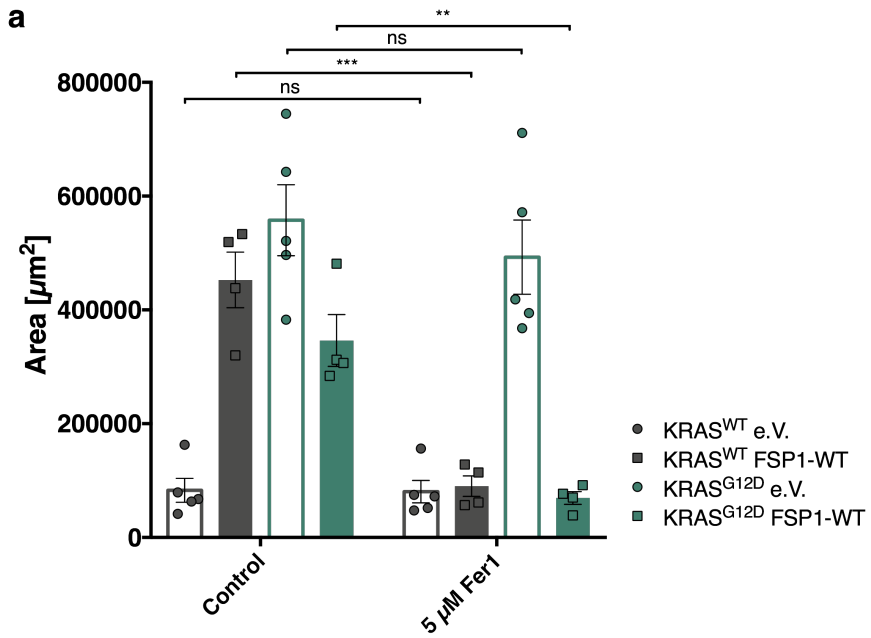

Figure 18: Ferroptosis inhibition suppresses spheroid growth
a Indicated cells were grown in Matrigel for spheroid formation under the indicated treatment for 14 days. Images were quantified using the BZ-H4M/Measurement Application Software (Keyence). Data are means +/- SEM of at least four independent experiments in each individual cell line. Two-way ANOVA + Tukey's multiple comparison test, *** $p<0.001$, ** $p<0.01$.

4 DISCUSSION

In this present study, we investigated how oncogenic KRAS protects cells from ferroptosis via upregulation of FSP1. Furthermore, we identified that KRAS-mutated cells limit the propagation of lipid ROS and thereby defend cells from acute lipid peroxidation upon ferroptosis induction. Importantly, we demonstrated that FSP1 expression is regulated by the MAPK-NRF2-pathway and increases upon activation in KRAS-mutated cells. Additionally, we showed that FSP1 overexpression in $KRAS^{WT}$ cells mediated cellular transformation *in vitro*. Interestingly, FSP1 overexpression promoted tumor onset in wild type mice *in vivo* suggesting FSP1 protects $KRAS^{WT}$ tumors from ferroptotic cell death. Moreover, only combined treatment of ferroptosis induction and FSP1 inhibition in pancreatic organoids expressing $KRAS^{G12D}$ could significantly induce organoid killing, indicating that ferroptosis resistance can be reversed by inducing ferroptosis in combination with inhibition of FSP1. Finally, we evaluated that FSP1 expression is upregulated in KRAS-driven cancers and correlates with poor outcome in pancreatic ductal adenocarcinoma (PDAC) patients. Lastly, in line with other studies, this work additionally validated that ferroptosis resistance *in vitro* is cell density dependent.

4.1 FERROPTOSIS RESISTANCE IN KRAS-MUTATED CELLS

RAS is the most common mutated oncogene worldwide, with KRAS being the most frequent RAS variant. RAS-GTPases regulate several cellular processes and its activation leads to downstream effector pathway stimulation resulting in proliferation, differentiation, angiogenesis, migration and survival [133].

Predominantly in pancreatic, lung and colon cancer RAS and especially KRAS mutations occur frequently and as of today, only very few anti-RAS therapies have reached the clinic to specifically target and inhibit mutated RAS to treat cancer patients [145]. Therefore, further investigation of specific vulnerabilities of tumors expressing oncogenic KRAS variants in order to induce cell death is warranted.

Ferroptosis is one type of regulated cell death and it is characterized by iron-dependent lipid peroxidation [11]. In this study, we investigated ferroptosis sensitivity of cells expressing oncogenic KRAS, since studies on this topic have been controversially discussed in the past. It has been shown that fibroblasts, which overexpress oncogenic

$HRAS^{G12V}$, show enhanced ferroptosis sensitivity upon erastin induction compared to control cells [12]. Additionally, ferroptosis induction via erastin treatment resulted in higher sensitivity of a lung carcinoma cell line (Calu-1) harboring a $KRAS^{G12C}$ mutation compared to cells expressing two different short hairpin RNAs (shRNAs) targeting KRAS [12], [13]. Controversially, in a study with 117 different cancer cell lines it has been demonstrated that ferroptosis sensitivity was RAS mutation independent [30]. Moreover, rhabdomyosarcoma cells (RMS13) expressing either $NRAS^{G12V}$, $HRAS^{G12V}$ or $KRAS^{G12V}$ treated with erastin or RSL3 showed ferroptosis resistance compared to control cells [118]. Another study recently reported that $KRAS^{G12V}$ cells upregulate xCT and are thereby protected from ferroptosis [119]. In this study, we could confirm that oncogenic KRAS renders cells more resistant to ferroptosis in cells which overexpress exogenous levels of KRAS mutations and endogenous KRAS wild type levels, as well as in cells which overexpress near endogenous levels of KRAS mutations (Müller et al. 2022 Figure 1a, d, c; Supplementary Figure 1b, c; Figure 8a, b). Furthermore, we showed that $KRAS^{G12D}$ protected human pancreatic cancer cells (L3.6pl $KRAS^{G12D}$) from ferroptosis induction compared to a pancreatic cancer cell line lacking a KRAS mutation (BxPC3 $KRAS^{WT}$) (Figure 10). Moreover, we validated that $KRAS^{G12D}$ is the most resistant type out of several different KRAS mutations occurring in the hotspot areas G12, G13 and Q61 (Figure 8a, b, Figure 9). As mentioned before the frequency of RAS gene mutations is different in every hotspot and also in each isoform. In KRAS, G12D is the most frequent substitution occurring in 41% of all cases [129]. However, there is evidence that each different RAS mutation has distinct effects on the cell. Why specifically $KRAS^{G12D}$ is the most frequent and most ferroptosis resistant mutation remains elusive.

4.2 ONCOGENIC KRAS-MEDIATED PROTECTION OF LIPID PEROXIDATION

It is known that expression of oncogenic RAS increases intracellular ROS levels through metabolic changes and modified cellular signaling. One strategy of RAS, specifically KRAS, to promote ROS production is via the upregulation of subunits of the NADPH oxidase complex (NOX1/4), which generate superoxide anions ($O2^{-\bullet}$) [108], [109], [189], [190]. Moderate ROS levels enhance tumor development and progression, but strongly increased ROS levels can result in senescence or cell death

[193]. Hence, oxidative stress either promotes or sensitizes RAS driven cancers to ferroptosis. Therefore, cells expressing oncogenic RAS, which leads to increased ROS accumulation, must have a ROS scavenging mechanism to protect and defend themselves from lipid peroxidation [194]. These studies offer an explanation why in our system KRAS-mutated cells revealed elevated basal levels of lipid and general ROS (Müller et al. 2022 Figure 2d; Supplementary Figure 2; Figure 15a). In our study we observed that cells expressing $KRAS^{G12D}$ mutation did not increase lipid ROS accumulation upon ferroptosis induction (Müller et al. 2022 Figure 2d; Supplementary Figure 2a, f), which suggests that oncogenic KRAS inhibits lipid ROS propagation through an antioxidant defense mechanism and thereby protect cells from ferroptosis explaining ferroptosis resistance of these cells.

4.3 FSP1 AS AN ANTIOXIDANT DEFENSE MECHANISM

In this study we identified FSP1 as the defense mechanism of cells expressing oncogenic KRAS to protect cells from lipid ROS and ferroptotic cell death. The elevated expression of FSP1 functions as an oxidoreductase to reduce ubiquinone to ubiquinol, which operates as a lipophilic RTA and captures lipid peroxyl radicals leading to lipid peroxidation [35], [36]. Of note, FSP1 needs NAD(P)H to mediate ubiquinone to ubiquinol reduction [40]. Other studies revealed that FSP1 expression correlates with ferroptosis resistance in different cancer cell lines [35], [36]. In line with these data, our study confirms that FSP1 expression renders KRAS mutant cells more resistant to ferroptosis induction (Müller et al. 2022 Figure 3 e, g). We showed that oncogenic KRAS leads to an upregulation of FSP1 which protects KRAS-mutated cells from ferroptosis (Figure 14).

It is known that oncogenic KRAS reprograms metabolic pathways and maintains nucleotide biosynthesis via the non-oxidative pentose phosphate pathway (PPP) [195]. Oncogenic KRAS controls these metabolic changes by activating the MAPK signaling pathway [195]. One product of the PPP is NAD(P)H [196]. Interestingly, high cellular levels of NAD(P)H result in ferroptosis resistance [197]. Additionally, as mentioned before, NAD(P)H is an important electron donor for FSP1 to reduce ubiquinol to ubiquinone. Therefore, it is possible that overexpression of FSP1, regulated by oncogenic KRAS, may influence NADPH/NADP+ levels and thereby influence the

KRAS-dependent metabolic NAD(P)H addiction. In our study we showed that FSP1 overexpression in KRAS-mutated cells decreased their spheroid growth even though FSP1 overexpression in $KRAS^{WT}$ cells resulted in increased spheroid formation (Müller et al. 2022 Figure 5c). One explanation could be that overexpression of FSP1 results in inhibition of the PPP and its NAD(P)H consumption could reduce the capacity to form spheroids. In line with this, it has been demonstrated that inhibition of the PPP reduces soft agar colony formation in NIH-3T3 cells [198].

Moreover, we demonstrated in our study that FSP1 overexpression in xenograft experiments increases tumor volume in $KRAS^{WT}$ cells *in vivo* (Müller et al. 2022 Figure 5e). Surprisingly, Liproxstatin-1 treatment, which also inhibits ferroptosis, did not enhance tumor volume (Müller et al. 2022 Supplementary Figure 5c). Therefore, these data indicate that FSP1 not only functions as a ferroptosis inhibitor but also has a ferroptosis-independent effect to induce cellular transformation and influence tumor onset. It has been shown that FSP1 regenerates NAD+ to support glycolysis [199]. Under hypoxic conditions, tumors use glycolysis as the predominant energy fuel [200], which could explain the ferroptosis-independent mechanism of FSP1 to promote tumor volume. Counter-intuitively, ferroptosis inhibition with Fer1 treatment significantly reduced spheroid formation in $KRAS^{WT}$ and $KRAS^{G12D}$ cells overexpressing FSP1 (Figure 18). These results need to be further validated, since we did not determine the same effects in spheroid assays from A549 cells treated with Fer1 or Liproxstatin-1 (Müller et al. 2022 Figure 5d; Supplementary Figure 5a). Indeed, treatment with ferroptosis inhibitors increased spheroid growth of A549 cells, but as mentioned before these effects could not be observed in our *in vivo* experiment.
However, these results further indicate that FSP1 can also function ferroptosis-independently. Another explanation could be that FSP1 rewires metabolic changes over time in KRAS-mutated cells and is not directly affecting $KRAS^{WT}$ cells which overexpress FSP1 short-term. In line with this, it is important to mention that KRAS-mutant cells are metabolically addicted to NAD(P) while $KRAS^{WT}$ cells are not [195]. As mentioned before, $KRAS^{G12D}$ cells which additionally overexpress FSP1 could struggle with the metabolic changes and therefore reduce spheroid growth even upon ferroptosis inhibition with Fer1. Nevertheless, these results need to be further studied and explained.

Since we observed FSP1 mRNA upregulation in our KRAS-mutated cells (Müller et al. 2022 Figure 3c; Figure 14), another possible regulation of FSP1 mRNA could be the Nonsense-Mediated Decay (NMD) pathway. This mRNA-controlled pathway is among others characterized by the regulation of transcripts which have an abnormally long 3' untranslated region (UTR) and transcripts which contain a premature termination codon (PTC), occurring in alternative upstream open reading frames (uORF) [201], [202]. We ascertained that FSP1 murine transcript variants reveal an abnormally long 3'UTR in one protein-coding variant and an uORF in three variants. Interestingly, in murine embryonic stem cells FSP1 mRNA was upregulated upon UPF1 knockdown mediated NMD inhibition [203]. Moreover, it has been investigated that p38 MAPK inhibits NMD [204] and it is known that $KRAS^{G12D}$ activates p38 MAPK [205]–[207]. Additionally, KRAS-driven lung tumors showed increased ER stress, which is also well known to inhibit NMD [208], [209]. Therefore, these studies could indicate that FSP1 mRNA stability and protein upregulation could be mediated via NMD inhibition in KRAS-mutated cells.

Of note, another mechanism to protect cells from ferroptosis independent of the GPX4/GSH system has been identified recently. The GCH1-BH4-phospholipid axis acts as a potent cellular antioxidant defense system by producing BH4 antioxidants and enhancing ubiquinol, thereby leading to ferroptosis resistance [83], [84]. Therefore, GCH1-missing cells are used for novel FSP1 inhibitor screenings to identify cells, which are dependent on FSP1 [210]. However, our RNA sequencing data showed that GCH1 mRNA expression was barely detectable and not increased in KRAS mutant cells (data not shown), indicating that FSP1 expression in our cellular system was not regulated or mediated by the GCH1-BH4-phospholipid axis.

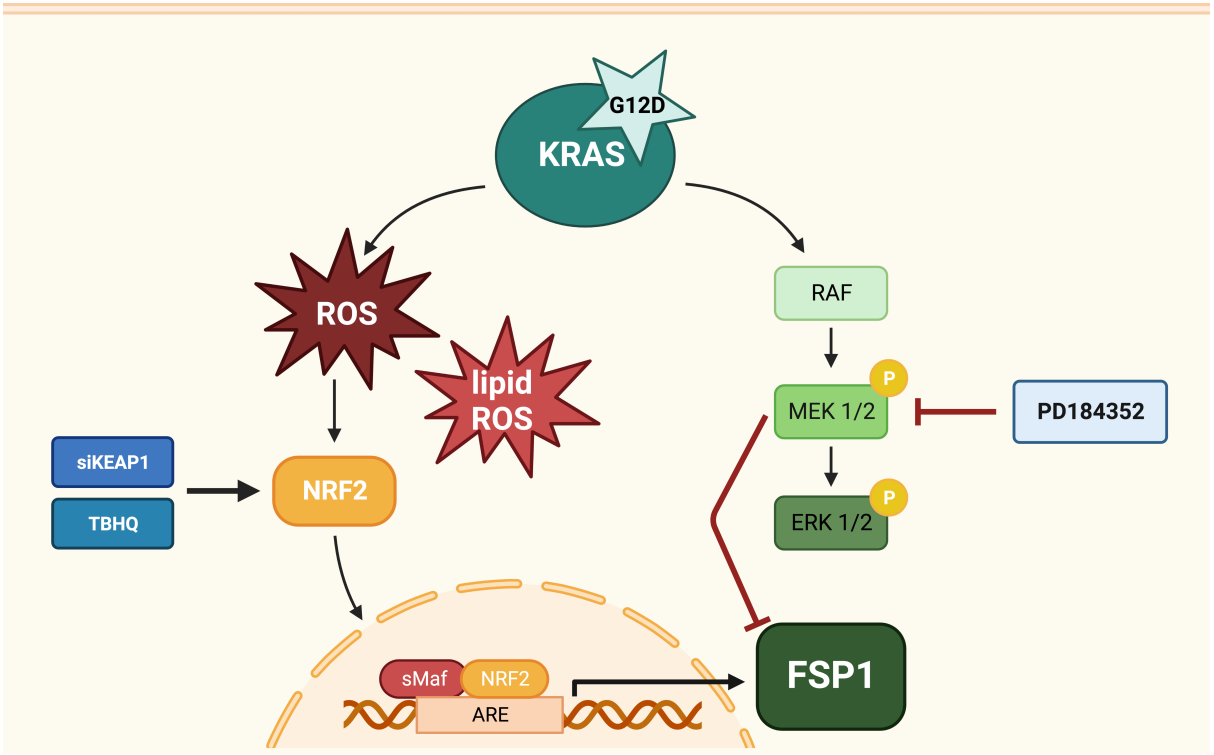

Figure 19: The KRAS-NRF2-FSP1-axis
Schematic illustration of the KRAS-NRF2-FSP1 axis. Cells expressing oncogenic $KRAS^{G12D}$ increase general ROS and lipid ROS levels and thereby activating the antioxidant machinery NRF2. Upon oxidative stress NRF2 shuttles into the nucleus and thereby activates an antioxidant defense program including anti-ferroptotic genes such as FSP1. Activation of NRF2 via the compound tert-butylhydroquinone (TBHQ) or silencing of KEAP1 with siRNA further increases FSP1 levels. Additionally, mutant KRAS activates continuously further downstream signaling pathways such as RAF, MEK1/2 and ERK1/2, which also enhance FSP1 levels. Therefore, inhibition of MEK by the inhibitor PD184352 decreases FSP1 levels. Scheme was drawn by using licensed biorender.com.

4.4 UPREGULATION OF FSP1 VIA NRF2 AND THE MAPK PATHWAY IN KRAS-MUTATED CELLS

Besides upregulated mRNA levels of FSP1 in cells expressing $KRAS^{G12D}$ we could also observe an upregulated cluster of genes involved in the iron metabolism network such as TRFC and STEAP3 (Müller et al. 2022 Figure 3b). In line with our data, Yang and Stockwell, discovered in 2008 that oncogenic RAS signaling affects iron metabolism by regulating expression levels of e.g. TRFC and thereby enhances the cellular iron pool [14]. Moreover, it was shown that oncogenic HRAS alters metabolic iron and increases the LIP [211]. Therefore, we suggest that in our oncogenic KRAS cell system upregulation of TRFC and STEAP3 influences iron metabolism and enhances LIP which increase basal ROS levels. As mentioned previously, it is known

that oncogenic RAS increases ROS levels and thereby inducing an antioxidant machinery such as NRF2 to protect cells from oxidative stress. Therefore, it was not surprising that NRF2 mRNA levels were also upregulated in our RNA sequencing data of $KRAS^{G12D}$-mutated cells (Müller et al. 2022 Figure 3b). In line with our data, DeNicola et al., published that oncogene expression such as $KRAS^{G12D}$ increases the transcription of NRF2 and thereby reduces intracellular ROS levels. They also showed that enhanced NRF2 activity promotes tumorigenesis [115]. Moreover, it has recently been shown that hyperactive NRF2 facilitates spheroid formation via regulation of proliferation and ferroptosis [212]. Of note, another study just recently revealed that nuclear factor erythroid-2–related factor 1, NRF1/NFE2L1, also regulates oxidative stress pathways and enhances ferroptosis resistance, independent of NRF2, through GPX4 expression [213]. More importantly for our study, it has recently been shown that ferroptosis resistance is mediated by FSP1 upregulation via NRF2 activation in KEAP1-mutant cancer cells [69]. In line with this, we could demonstrate that FSP1 upregulation in cells expressing oncogenic KRAS is NRF2 dependent by silencing of KEAP1 or NRF2 activation via TBHQ treatment (Müller et al. 2022 Figure 4c, e).
Furthermore, we could observe that FSP1 expression is mediated by the MAPK pathway, since inhibition of MEK resulted in reduced FSP1 mRNA levels (Müller et al. 2022 Supplementary Figure 4c). Of note, AKT pathway inhibition did not affect FSP1 mRNA or protein levels. Importantly, we intentionally used PD184352 to inhibit MEK, since it is known that the MEK inhibitor U0126 is a direct ROS scavenger and blocks ferroptotic cell death independently of MEK inhibition, which could have influenced our results [15], [214], [215]. Interestingly, our study revealed that MAPK pathway inhibition only reduced FSP1 mRNA levels in KRAS-mutated cells, but not in $KRAS^{WT}$ cells (Müller et al. 2022 Supplementary Figure 4c). Therefore, these results suggest that oncogenic KRAS constantly activates its effector pathway MAPK, which upregulates FSP1 via the NRF2 pathway, assuming that inhibition of MAPK, and thereby FSP1 downregulation, does only affect cells expressing oncogenic KRAS and not KRAS wild type cells.

Of note, it has been demonstrated that oncogenic RAS stabilizes PD-L1 mRNA via the MEK pathway. MEK signaling inhibits tristetraprolin (TTP), which negatively regulates PD-L1 expression through AU-rich elements in the 3’ UTR [205]. Since MAPK pathway

is involved in mRNA stability as well as in downstream effector signaling of RAS, it needs to be further investigated, how exactly FSP1 regulation is mediated.

4.5 FSP1 EXPRESSION IN KRAS-MUTATED CANCERS

Importantly, we could investigate that elevated FSP1 expression mediates cellular transformation in soft agar and spheroid assays *in vitro* (Müller et al. 2022 Figure 5c). Furthermore, we determined that FSP1 upregulation leads to the capacity to initiate tumors in MEF cells, resulting in an earlier tumor onset in $KRAS^{WT}$ cells in the absence of oncogenic KRAS *in vivo* (Müller et al. 2022 Figure 5e). Interestingly, Sharbeen et al., recently discovered that stable xCT knockdown reduces tumor growth and metastatic spread in PDAC cells and cancer-associated fibroblasts (CAFs). They also found that PDAC-derived CAFs are highly dependent on xCT, which regulates cystine uptake and GSH synthesis and inhibition of it results in increased sensitivity to oxidative stress [216]. However, xCT specific ablation in transgenic mouse PDAC tumors did not affect tumor growth, suggesting that KRAS-mutated cells develop a GSH synthesis independent regulation to protect cells from lipid peroxidation and ferroptosis [216]. Moreover, GPX4 deletion in PDAC cells did not induce ferroptosis, but promoted KRAS-driven pancreatic tumorigenesis [103]. These data support the idea that KRAS-mutated cells have evolved an additional layer of protection against ferroptotic cell death. Therefore, we hypothesize that FSP1 could be the other ferroptosis protection regulator.

Of note, in line with the data that xCT-inhibition in PDAC resulted in increased ferroptosis sensitivity, whereas GPX4-inhibition in PDAC led to ferroptosis resistance, we observed, that KRAS-mutated cells were more sensitive to treatment with class I FINs compared to class II FINs (Müller et al. 2022 Supplementary Figure 1a). Class I FINs inhibit GPX4 indirectly through GSH depletion, whereas class II FINs inactivate GPX4 directly. Treatments with these compounds inhibit the Xc-/GSH/GPX4 axis thereby resulting in ferroptosis [30]. One reason why KRAS-mutated cells were more sensitive to treatment with class I FINs could be that cells expressing oncogenic KRAS upregulate xCT [119]. Since class I FINs such as erastin or IKE target and inhibit xCT directly, treatment of these compounds could result in a more drastically GSH depletion leading to enhanced ferroptotic cell death. Alternatively, cell density could play a role in class I FIN sensitivity of $KRAS^{G12D}$-expressing cells in our cell system. Another

possible explanation could be that class I FINs also target FSP1, while class II FINs do not, which would explain the difference in sensitivity of the two different FIN classes. Therefore, it needs to be further evaluated why cells, which upregulate FSP1 through oncogenic KRAS, react differently to class I and class II FIN treatments.
Taken together, our data reveals that elevated FSP1 expression in KRAS-mutated cells protects cells from ferroptosis induction. Based on these results, we suggest that combination treatment of targeting ferroptosis and FSP1 could be a strategic opportunity for cancer patients harboring KRAS mutations.

Of note, Harris et al. 2015 showed in a mice model which exhibited mammary tumors, that BSO treatment influenced tumor onset of mammary tumors when treated prior cancer development. Interestingly, when mice were treated with BSO upon mammary tumor onset, tumor burden was unchanged [99]. While these data indicate that there must be an alternative antioxidant mechanism to protect malignant tumors from ROS levels due to the fact that BSO fails to impact tumor growth at later stages of tumor progression, we assume that FSP1 could be the main reason for these results.

4.6 FERROPTOSIS RESISTANCE IS DENSITY DEPENDENT

Moreover, it is important to mention that ferroptosis is known to be density dependent. We could demonstrate, that ferroptosis sensitivity in $KRAS^{G12D}$-expressing cells as well as ferroptosis resistance in $KRAS^{WT}$-expressing cells was influenced by cell density (Figure 12, Figure 13).
Already in 2013, without connecting it to ferroptosis, it has been shown that cell density regulates sensitivity to system Xc- inhibition [217]. Interestingly, GPX4-KO-MEFs seeded in 2D died after 48 hours whereas the same cells seeded in 3D (embedded in BD Matrigel) were able to form tumor spheroids [218]. Recently, certain papers have been published highlighting the Hippo-YAP pathway as the main player in the density-dependent resistance mechanism in ferroptosis [125], [185], [219], [220]. The role of the Hippo-YAP pathway in ferroptosis was discovered when cells grown in high density were more resistant to ferroptosis than cells grown in low density [125], [187]. In general, the Hippo-YAP pathway is involved in several biological functions such as cell proliferation, differentiation and organ size control [123], [124]. Mechanistically, this pathway is characterized by cell-cell contacts mediated by E-cadherin, activating the

Hippo phosphorylation signaling pathway [123]. When Hippo pathway is inactive due to low density, YAP shuttles into the nucleus and acts as an transcription co-regulator leading to upregulation of ACSL4 and TFRC resulting in ferroptosis sensitivity [125]. It is important to mention that the role of the Hippo-YAP pathway seems to only apply to adherent cells [221], [222]. However, in our study we only investigated adherent cells. Surprisingly, in our studies we could ascertain that FSP1 mRNA and protein levels increased upon higher cell confluence (Figure 14). Additionally, in another study it was recently shown that cell density plays a major role on ferroptosis resistance when FSP1 is inhibited [41].Therefore, it is indicated that FSP1 upregulation is another crucial mechanism for density dependent ferroptosis resistance in addition to the Hippo-YAP signaling pathway. How FSP1 is upregulated in the context of higher cell-cell-contact, whether YAP is also regulating FSP1 and which signaling pathway is necessary for the FSP1 enhancement needs to be further investigated.

5 CONCLUDING REMARKS AND FUTURE PERSPECTIVES

In conclusion, we could identify that cells expressing oncogenic KRAS are more resistant to ferroptosis compared to cells which express KRAS wild type. Moreover, we could validate that $KRAS^{G12D}$ is the most resistant clone to ferroptosis in our tested cell line panel with different oncogenic KRAS mutations occurring in the hotspot areas G12, G13 and Q61. Additionally, we could show that cells expressing $KRAS^{G12D}$ were more protected from lipid peroxidation and already revealed higher basal lipid ROS and general ROS levels. We could observe that FSP1 is upregulated in cells expressing $KRAS^{G12D}$ and thereby protecting cells from lipid peroxidation and ferroptosis. We could validate and confirm that upregulation of FSP1 is mediated by the NRF2 antioxidant machinery, which is enhanced in $KRAS^{G12D}$ mutant cells due to higher lipid ROS and general ROS levels. Moreover, in our study we could identify the MAPK pathway as another regulator of FSP1.

Strikingly, our study reveals for the first time that elevated FSP1 levels mediate cellular transformation and spheroid growth *in vitro*, independently from its ferroptosis protective regulation. Additionally, we could show that FSP1 overexpression in $KRAS^{WT}$ tumors resulted in an earlier tumor onset. Since ferroptosis inhibition with Liproxstatin-1 treatment did not affect tumor onset, we hypothesize that FSP1 acts independently of ferroptosis in tumorigenesis. How exactly FSP1 functions independently of ferroptosis needs to be further investigated in future studies.
Interestingly, our data indicates that in $KRAS^{G12D}$ expressing pancreatic organoids combination treatment of ferroptosis and FSP1 inhibition significantly induced organoids killing. Since different cancer cells expressing oncogenic RAS are resistant to ferroptosis, ferroptosis induction combined with FSP1 inhibition could circumvent ferroptosis resistance. Our data therefore proposes to consider ferroptosis induction in combination with FSP1 inhibition in clinical therapies, which could be a novel therapeutic vulnerability to target cancers in patients harboring RAS mutations.

Of note, our studies reinforce the impact of cell density on ferroptosis. We could show that dependent on cell density cells expressing $KRAS^{WT}$ increased resistance upon

higher density and cells expressing $KRAS^{G12D}$ decreased resistance upon lower density. Therefore, we recommend considering proper cell density validations for specific adherent cell lines when studying ferroptosis resistance.

6 REFERENCES

[1] D. R. Green and F. Llambi, ‘Cell Death Signaling’, *Cold Spring Harb Perspect Biol*, vol. 7, no. 12, p. a006080, Dec. 2015, doi: 10.1101/cshperspect.a006080.

[2] Y. Fuchs and H. Steller, ‘Programmed Cell Death in Animal Development and Disease’, *Cell*, vol. 147, no. 4, pp. 742–758, Nov. 2011, doi: 10.1016/j.cell.2011.10.033.

[3] D. E. Place and T.-D. Kanneganti, ‘The innate immune system and cell death in autoinflammatory and autoimmune disease’, *Current Opinion in Immunology*, vol. 67, pp. 95–105, Dec. 2020, doi: 10.1016/j.coi.2020.10.013.

[4] K. L. Double, S. Reyes, E. L. Werry, and G. M. Halliday, ‘Selective cell death in neurodegeneration: Why are some neurons spared in vulnerable regions?’, *Progress in Neurobiology*, vol. 92, no. 3, pp. 316–329, Nov. 2010, doi: 10.1016/j.pneurobio.2010.06.001.

[5] I. Jorgensen, M. Rayamajhi, and E. A. Miao, ‘Programmed cell death as a defence against infection’, *Nature Reviews Immunology*, vol. 17, no. 3, pp. 151–164, Mar. 2017, doi: 10.1038/nri.2016.147.

[6] L. Galluzzi *et al.*, ‘Molecular mechanisms of cell death: recommendations of the Nomenclature Committee on Cell Death 2018’, *Cell Death Differ*, vol. 25, no. 3, pp. 486–541, Mar. 2018, doi: 10.1038/s41418-017-0012-4.

[7] L. Galluzzi, J. M. Bravo-San Pedro, O. Kepp, and G. Kroemer, ‘Regulated cell death and adaptive stress responses’, *Cell. Mol. Life Sci.*, vol. 73, no. 11–12, pp. 2405–2410, Jun. 2016, doi: 10.1007/s00018-016-2209-y.

[8] L. Galluzzi *et al.*, ‘Cell death modalities: classification and pathophysiological implications’, *Cell Death Differ*, vol. 14, no. 7, pp. 1237–1243, Jul. 2007, doi: 10.1038/sj.cdd.4402148.

[9] G. Kroemer *et al.*, ‘Classification of cell death: recommendations of the Nomenclature Committee on Cell Death’, *Cell Death Differ*, vol. 12, no. S2, pp. 1463–1467, Nov. 2005, doi: 10.1038/sj.cdd.4401724.

[10] A. Ashkenazi and G. Salvesen, ‘Regulated Cell Death: Signaling and Mechanisms’, *Annu. Rev. Cell Dev. Biol.*, vol. 30, no. 1, pp. 337–356, Oct. 2014, doi: 10.1146/annurev-cellbio-100913-013226.

[11] S. J. Dixon *et al.*, ‘Ferroptosis: An Iron-Dependent Form of Nonapoptotic Cell Death’, *Cell*, vol. 149, no. 5, pp. 1060–1072, May 2012, doi: 10.1016/j.cell.2012.03.042.

[12] S. Dolma, S. L. Lessnick, W. C. Hahn, and B. R. Stockwell, ‘Identification of genotype-selective antitumor agents using synthetic lethal chemical screening in engineered human tumor cells’, *Cancer Cell*, vol. 3, no. 3, pp. 285–296, Mar. 2003, doi: 10.1016/S1535-6108(03)00050-3.

[13] N. Yagoda *et al.*, ‘RAS–RAF–MEK-dependent oxidative cell death involving voltage-dependent anion channels’, *Nature*, vol. 447, no. 7146, pp. 865–869, Jun. 2007, doi: 10.1038/nature05859.

[14] W. S. Yang and B. R. Stockwell, ‘Synthetic Lethal Screening Identifies Compounds Activating Iron-Dependent, Nonapoptotic Cell Death in Oncogenic-RAS-Harboring Cancer Cells’, *Chemistry & Biology*, vol. 15, no. 3, pp. 234–245, Mar. 2008, doi: 10.1016/j.chembiol.2008.02.010.

[15] M. Gao, P. Monian, N. Quadri, R. Ramasamy, and X. Jiang, ‘Glutaminolysis and Transferrin Regulate Ferroptosis’, *Molecular Cell*, vol. 59, no. 2, pp. 298–308, Jul. 2015, doi: 10.1016/j.molcel.2015.06.011.

[16] B. Zhou, J. Liu, R. Kang, D. J. Klionsky, G. Kroemer, and D. Tang, ‘Ferroptosis is a type of autophagy-dependent cell death’, *Seminars in Cancer Biology*, vol. 66, pp. 89–100, Nov. 2020, doi: 10.1016/j.semcancer.2019.03.002.

[17] H. Yu *et al.*, ‘Sulfasalazine-induced ferroptosis in breast cancer cells is reduced by the inhibitory effect of estrogen receptor on the transferrin receptor’, *Oncol Rep*, Jun. 2019, doi: 10.3892/or.2019.7189.

[18] Z. Cheng and Y. Li, ‘What Is Responsible for the Initiating Chemistry of Iron-Mediated Lipid Peroxidation: An Update’, *Chem. Rev.*, vol. 107, no. 3, pp. 748–766, Mar. 2007, doi: 10.1021/cr040077w.

[19] S. J. Dixon and B. R. Stockwell, ‘The role of iron and reactive oxygen species in cell death’, *Nat Chem Biol*, vol. 10, no. 1, pp. 9–17, Jan. 2014, doi: 10.1038/nchembio.1416.

[20] E. Agmon, J. Solon, P. Bassereau, and B. R. Stockwell, ‘Modeling the effects of lipid peroxidation during ferroptosis on membrane properties’, *Sci Rep*, vol. 8, no. 1, p. 5155, Dec. 2018, doi: 10.1038/s41598-018-23408-0.

[21] W. S. Yang, K. J. Kim, M. M. Gaschler, M. Patel, M. S. Shchepinov, and B. R. Stockwell, ‘Peroxidation of polyunsaturated fatty acids by lipoxygenases drives

ferroptosis', *Proc. Natl. Acad. Sci. U.S.A.*, vol. 113, no. 34, Aug. 2016, doi: 10.1073/pnas.1603244113.

[22] V. E. Kagan *et al.*, 'Oxidized arachidonic and adrenic PEs navigate cells to ferroptosis', *Nat Chem Biol*, vol. 13, no. 1, pp. 81–90, Jan. 2017, doi: 10.1038/nchembio.2238.

[23] S. Hao *et al.*, 'Metabolic networks in ferroptosis (Review)', *Oncol Lett*, Feb. 2018, doi: 10.3892/ol.2018.8066.

[24] C. C. Winterbourn, 'Toxicity of iron and hydrogen peroxide: the Fenton reaction', *Toxicology Letters*, vol. 82–83, pp. 969–974, Dec. 1995, doi: 10.1016/0378-4274(95)03532-X.

[25] P. Lei, T. Bai, and Y. Sun, 'Mechanisms of Ferroptosis and Relations With Regulated Cell Death: A Review', *Front. Physiol.*, vol. 10, p. 139, Feb. 2019, doi: 10.3389/fphys.2019.00139.

[26] S. Doll *et al.*, 'ACSL4 dictates ferroptosis sensitivity by shaping cellular lipid composition', *Nat Chem Biol*, vol. 13, no. 1, pp. 91–98, Jan. 2017, doi: 10.1038/nchembio.2239.

[27] H. Yuan, X. Li, X. Zhang, R. Kang, and D. Tang, 'Identification of ACSL4 as a biomarker and contributor of ferroptosis', *Biochemical and Biophysical Research Communications*, vol. 478, no. 3, pp. 1338–1343, Sep. 2016, doi: 10.1016/j.bbrc.2016.08.124.

[28] S. J. Dixon *et al.*, 'Human Haploid Cell Genetics Reveals Roles for Lipid Metabolism Genes in Nonapoptotic Cell Death', *ACS Chem. Biol.*, vol. 10, no. 7, pp. 1604–1609, Jul. 2015, doi: 10.1021/acschembio.5b00245.

[29] J. P. Friedmann Angeli *et al.*, 'Inactivation of the ferroptosis regulator Gpx4 triggers acute renal failure in mice', *Nat Cell Biol*, vol. 16, no. 12, pp. 1180–1191, Dec. 2014, doi: 10.1038/ncb3064.

[30] W. S. Yang *et al.*, 'Regulation of Ferroptotic Cancer Cell Death by GPX4', *Cell*, vol. 156, no. 1–2, pp. 317–331, Jan. 2014, doi: 10.1016/j.cell.2013.12.010.

[31] A. Meister, 'Selective Modification of Glutathione Metabolism', *Science*, vol. 220, no. 4596, pp. 472–477, Apr. 1983, doi: 10.1126/science.6836290.

[32] B. Proneth and M. Conrad, 'Ferroptosis and necroinflammation, a yet poorly explored link', *Cell Death Differ*, vol. 26, no. 1, pp. 14–24, Jan. 2019, doi: 10.1038/s41418-018-0173-9.

[33] M. Conrad and H. Sato, ‘The oxidative stress-inducible cystine/glutamate antiporter, system x c − : cystine supplier and beyond’, *Amino Acids*, vol. 42, no. 1, pp. 231–246, Jan. 2012, doi: 10.1007/s00726-011-0867-5.

[34] J. Burdo, R. Dargusch, and D. Schubert, ‘Distribution of the Cystine/Glutamate Antiporter System x ⁻ c in the Brain, Kidney, and Duodenum’, *J Histochem Cytochem.*, vol. 54, no. 5, pp. 549–557, May 2006, doi: 10.1369/jhc.5A6840.2006.

[35] S. Doll *et al.*, ‘FSP1 is a glutathione-independent ferroptosis suppressor’, *Nature*, vol. 575, no. 7784, pp. 693–698, Nov. 2019, doi: 10.1038/s41586-019-1707-0.

[36] K. Bersuker *et al.*, ‘The CoQ oxidoreductase FSP1 acts parallel to GPX4 to inhibit ferroptosis’, *Nature*, vol. 575, no. 7784, pp. 688–692, Nov. 2019, doi: 10.1038/s41586-019-1705-2.

[37] I. Buhaescu and H. Izzedine, ‘Mevalonate pathway: A review of clinical and therapeutical implications’, *Clinical Biochemistry*, vol. 40, no. 9–10, pp. 575–584, Jun. 2007, doi: 10.1016/j.clinbiochem.2007.03.016.

[38] J. L. Goldstein and M. S. Brown, ‘Regulation of the mevalonate pathway’, *Nature*, vol. 343, no. 6257, pp. 425–430, Feb. 1990, doi: 10.1038/343425a0.

[39] M. Wu, L.-G. Xu, X. Li, Z. Zhai, and H.-B. Shu, ‘AMID, an Apoptosis-inducing Factor-homologous Mitochondrion-associated Protein, Induces Caspase-independent Apoptosis’, *J. Biol. Chem.*, vol. 277, no. 28, pp. 25617–25623, Jul. 2002, doi: 10.1074/jbc.M202285200.

[40] K. R. Marshall *et al.*, ‘The Human Apoptosis-inducing Protein AMID Is an Oxidoreductase with a Modified Flavin Cofactor and DNA Binding Activity’, *J. Biol. Chem.*, vol. 280, no. 35, pp. 30735–30740, Sep. 2005, doi: 10.1074/jbc.M414018200.

[41] E. Mishima *et al.*, ‘DHODH inhibitors sensitize cancer cells to ferroptosis via FSP1 inhibition’, In Review, preprint, Oct. 2022. doi: 10.21203/rs.3.rs-2190326/v1.

[42] E. Mishima *et al.*, ‘A non-canonical vitamin K cycle is a potent ferroptosis suppressor’, *Nature*, vol. 608, no. 7924, pp. 778–783, Aug. 2022, doi: 10.1038/s41586-022-05022-3.

[43] J. K. Eaton *et al.*, ‘Selective covalent targeting of GPX4 using masked nitrile-oxide electrophiles’, *Nat Chem Biol*, vol. 16, no. 5, pp. 497–506, May 2020, doi: 10.1038/s41589-020-0501-5.

[44] M. Weïwer *et al.*, ‘Development of small-molecule probes that selectively kill cells induced to express mutant RAS’, *Bioorganic & Medicinal Chemistry Letters*, vol. 22, no. 4, pp. 1822–1826, Feb. 2012, doi: 10.1016/j.bmcl.2011.09.047.

[45] Y. Xie *et al.*, 'Ferroptosis: process and function', *Cell Death Differ*, vol. 23, no. 3, pp. 369–379, Mar. 2016, doi: 10.1038/cdd.2015.158.

[46] S. J. Dixon *et al.*, 'Pharmacological inhibition of cystine–glutamate exchange induces endoplasmic reticulum stress and ferroptosis', *eLife*, vol. 3, p. e02523, May 2014, doi: 10.7554/eLife.02523.

[47] M. Gao *et al.*, 'Role of Mitochondria in Ferroptosis', *Molecular Cell*, vol. 73, no. 2, pp. 354-363.e3, Jan. 2019, doi: 10.1016/j.molcel.2018.10.042.

[48] S. Neitemeier *et al.*, 'BID links ferroptosis to mitochondrial cell death pathways', *Redox Biology*, vol. 12, pp. 558–570, Aug. 2017, doi: 10.1016/j.redox.2017.03.007.

[49] H. Yuan, X. Li, X. Zhang, R. Kang, and D. Tang, 'CISD1 inhibits ferroptosis by protection against mitochondrial lipid peroxidation', *Biochemical and Biophysical Research Communications*, vol. 478, no. 2, pp. 838–844, Sep. 2016, doi: 10.1016/j.bbrc.2016.08.034.

[50] S. Papa *et al.*, 'The Oxidative Phosphorylation System in Mammalian Mitochondria', in *Advances in Mitochondrial Medicine*, vol. 942, R. Scatena, P. Bottoni, and B. Giardina, Eds. Dordrecht: Springer Netherlands, 2012, pp. 3–37. doi: 10.1007/978-94-007-2869-1_1.

[51] L. B. Sullivan and N. S. Chandel, 'Mitochondrial reactive oxygen species and cancer', *Cancer Metab*, vol. 2, no. 1, p. 17, Dec. 2014, doi: 10.1186/2049-3002-2-17.

[52] R. Brigelius-Flohé and M. Maiorino, 'Glutathione peroxidases', *Biochimica et Biophysica Acta (BBA) - General Subjects*, vol. 1830, no. 5, pp. 3289–3303, May 2013, doi: 10.1016/j.bbagen.2012.11.020.

[53] M. Dodson, R. Castro-Portuguez, and D. D. Zhang, 'NRF2 plays a critical role in mitigating lipid peroxidation and ferroptosis', *Redox Biology*, vol. 23, p. 101107, May 2019, doi: 10.1016/j.redox.2019.101107.

[54] A. Anandhan, M. Dodson, C. J. Schmidlin, P. Liu, and D. D. Zhang, 'Breakdown of an Ironclad Defense System: The Critical Role of NRF2 in Mediating Ferroptosis', *Cell Chemical Biology*, vol. 27, no. 4, pp. 436–447, Apr. 2020, doi: 10.1016/j.chembiol.2020.03.011.

[55] I. Bellezza, I. Giambanco, A. Minelli, and R. Donato, 'Nrf2-Keap1 signaling in oxidative and reductive stress', *Biochimica et Biophysica Acta (BBA) - Molecular Cell Research*, vol. 1865, no. 5, pp. 721–733, May 2018, doi: 10.1016/j.bbamcr.2018.02.010.

[56] K. Itoh *et al.*, 'An Nrf2/Small Maf Heterodimer Mediates the Induction of Phase II Detoxifying Enzyme Genes through Antioxidant Response Elements', *Biochemical and Biophysical Research Communications*, vol. 236, no. 2, pp. 313–322, Jul. 1997, doi: 10.1006/bbrc.1997.6943.

[57] M. Abdalkader, R. Lampinen, K. M. Kanninen, T. M. Malm, and J. R. Liddell, 'Targeting Nrf2 to Suppress Ferroptosis and Mitochondrial Dysfunction in Neurodegeneration', *Front. Neurosci.*, vol. 12, p. 466, Jul. 2018, doi: 10.3389/fnins.2018.00466.

[58] J. A. Johnson *et al.*, 'The Nrf2-ARE Pathway: An Indicator and Modulator of Oxidative Stress in Neurodegeneration', *Annals of the New York Academy of Sciences*, vol. 1147, no. 1, pp. 61–69, Dec. 2008, doi: 10.1196/annals.1427.036.

[59] S. C. Lu, 'Glutathione synthesis', *Biochimica et Biophysica Acta (BBA) - General Subjects*, vol. 1830, no. 5, pp. 3143–3153, May 2013, doi: 10.1016/j.bbagen.2012.09.008.

[60] D. Ross and D. Siegel, 'The diverse functionality of NQO1 and its roles in redox control', *Redox Biology*, vol. 41, p. 101950, May 2021, doi: 10.1016/j.redox.2021.101950.

[61] F. Sparla, G. Tedeschi, and P. Trost, 'NAD(P)H:(Quinone-Acceptor) Oxidoreductase of Tobacco Leaves Is a Flavin Mononucleotide-Containing Flavoenzyme', *Plant Physiology*, vol. 112, no. 1, pp. 249–258, 1996.

[62] T. Jarmi and A. Agarwal, 'Heme oxygenase and renal disease', *Current Science Inc*, vol. 11, no. 1, pp. 56–62, Feb. 2009, doi: 10.1007/s11906-009-0011-z.

[63] L.-C. Chang, S.-K. Chiang, S.-E. Chen, Y.-L. Yu, R.-H. Chou, and W.-C. Chang, 'Heme oxygenase-1 mediates BAY 11–7085 induced ferroptosis', *Cancer Letters*, vol. 416, pp. 124–137, Mar. 2018, doi: 10.1016/j.canlet.2017.12.025.

[64] B. Hassannia *et al.*, 'Nano-targeted induction of dual ferroptotic mechanisms eradicates high-risk neuroblastoma', *Journal of Clinical Investigation*, vol. 128, no. 8, pp. 3341–3355, Aug. 2018, doi: 10.1172/JCI99032.

[65] M.-Y. Kwon, E. Park, S.-J. Lee, and S. W. Chung, 'Heme oxygenase-1 accelerates erastin-induced ferroptotic cell death', *Oncotarget*, vol. 6, no. 27, pp. 24393–24403, Sep. 2015, doi: 10.18632/oncotarget.5162.

[66] X. Sun *et al.*, 'Activation of the p62-Keap1-NRF2 pathway protects against ferroptosis in hepatocellular carcinoma cells: Hepatobiliary Malignancies', *Hepatology*, vol. 63, no. 1, pp. 173–184, Jan. 2016, doi: 10.1002/hep.28251.

[67] D. M. Suttner and P. A. Dennery, ‘Reversal of HO-1 related cytoprotection with increased expression is due to reactive iron’, *FASEB j.*, vol. 13, no. 13, pp. 1800–1809, Oct. 1999, doi: 10.1096/fasebj.13.13.1800.

[68] B. N. Chorley *et al.*, ‘Identification of novel NRF2-regulated genes by ChIP-Seq: influence on retinoid X receptor alpha’, *Nucleic Acids Research*, vol. 40, no. 15, pp. 7416–7429, Aug. 2012, doi: 10.1093/nar/gks409.

[69] P. Koppula *et al.*, ‘A targetable CoQ-FSP1 axis drives ferroptosis- and radiation-resistance in KEAP1 inactive lung cancers’, *Nat Commun*, vol. 13, no. 1, p. 2206, Dec. 2022, doi: 10.1038/s41467-022-29905-1.

[70] The Cancer Genome Atlas Research Network, ‘Comprehensive molecular profiling of lung adenocarcinoma’, *Nature*, vol. 511, no. 7511, pp. 543–550, Jul. 2014, doi: 10.1038/nature13385.

[71] The Cancer Genome Atlas Research Network, ‘Comprehensive genomic characterization of squamous cell lung cancers’, *Nature*, vol. 489, no. 7417, pp. 519–525, Sep. 2012, doi: 10.1038/nature11404.

[72] J. A. Hellyer, S. K. Padda, M. Diehn, and H. A. Wakelee, ‘Clinical Implications of KEAP1-NFE2L2 Mutations in NSCLC’, *Journal of Thoracic Oncology*, vol. 16, no. 3, pp. 395–403, Mar. 2021, doi: 10.1016/j.jtho.2020.11.015.

[73] R. Venugopal and A. K. Jaiswal, ‘Nrf1 and Nrf2 positively and c-Fos and Fra1 negatively regulate the human antioxidant response element-mediated expression of NAD(P)H:quinone oxidoreductase $_1$ gene’, *Proc. Natl. Acad. Sci. U.S.A.*, vol. 93, no. 25, pp. 14960–14965, Dec. 1996, doi: 10.1073/pnas.93.25.14960.

[74] K. Shimada *et al.*, ‘Global survey of cell death mechanisms reveals metabolic regulation of ferroptosis’, *Nat Chem Biol*, vol. 12, no. 7, pp. 497–503, Jul. 2016, doi: 10.1038/nchembio.2079.

[75] M. M. Gaschler *et al.*, ‘FINO2 initiates ferroptosis through GPX4 inactivation and iron oxidation’, *Nat Chem Biol*, vol. 14, no. 5, pp. 507–515, May 2018, doi: 10.1038/s41589-018-0031-6.

[76] R. P. Abrams, W. L. Carroll, and K. A. Woerpel, ‘Five-Membered Ring Peroxide Selectively Initiates Ferroptosis in Cancer Cells’, *ACS Chem. Biol.*, vol. 11, no. 5, pp. 1305–1312, May 2016, doi: 10.1021/acschembio.5b00900.

[77] N. Eling, L. Reuter, J. Hazin, A. Hamacher-Brady, and N. R. Brady, ‘Identification of artesunate as a specific activator of ferroptosis in pancreatic cancer cells’, *Oncoscience*, vol. 2, p. 517, May 2015, doi: 10.18632/oncoscience.160.

[78] M. Jennis *et al.*, 'An African-specific polymorphism in the *TP53* gene impairs p53 tumor suppressor function in a mouse model', *Genes Dev.*, vol. 30, no. 8, pp. 918–930, Apr. 2016, doi: 10.1101/gad.275891.115.

[79] J. Guo *et al.*, 'Ferroptosis: A Novel Anti-tumor Action for Cisplatin', *Cancer Res Treat*, vol. 50, no. 2, pp. 445–460, Apr. 2018, doi: 10.4143/crt.2016.572.

[80] Y. Zhang *et al.*, 'Imidazole Ketone Erastin Induces Ferroptosis and Slows Tumor Growth in a Mouse Lymphoma Model', *Cell Chemical Biology*, vol. 26, no. 5, pp. 623-633.e9, May 2019, doi: 10.1016/j.chembiol.2019.01.008.

[81] B. R. Stockwell *et al.*, 'Ferroptosis: A Regulated Cell Death Nexus Linking Metabolism, Redox Biology, and Disease', *Cell*, vol. 171, no. 2, pp. 273–285, Oct. 2017, doi: 10.1016/j.cell.2017.09.021.

[82] N. Mobarra *et al.*, 'A Review on Iron Chelators in Treatment of Iron Overload Syndromes', *International Journal of Hematology-Oncology and Stem Cell Research*, vol. 10, no. 4, p. 9, Aug. 2019, doi: 10.1038/s41586-019-1426-6.

[83] V. A. N. Kraft *et al.*, 'GTP Cyclohydrolase 1/Tetrahydrobiopterin Counteract Ferroptosis through Lipid Remodeling', *ACS Cent. Sci.*, vol. 6, no. 1, pp. 41–53, Jan. 2020, doi: 10.1021/acscentsci.9b01063.

[84] M. Soula *et al.*, 'Metabolic determinants of cancer cell sensitivity to canonical ferroptosis inducers', *Nat Chem Biol*, vol. 16, no. 12, pp. 1351–1360, Dec. 2020, doi: 10.1038/s41589-020-0613-y.

[85] U. Barayeu *et al.*, 'Hydropersulfides inhibit lipid peroxidation and ferroptosis by scavenging radicals', *Nat Chem Biol*, Sep. 2022, doi: 10.1038/s41589-022-01145-w.

[86] H. Sato *et al.*, 'Redox Imbalance in Cystine/Glutamate Transporter-deficient Mice', *Journal of Biological Chemistry*, vol. 280, no. 45, pp. 37423–37429, Nov. 2005, doi: 10.1074/jbc.M506439200.

[87] G. J. McBean, 'The transsulfuration pathway: a source of cysteine for glutathione in astrocytes', *Amino Acids*, vol. 42, no. 1, pp. 199–205, Jan. 2012, doi: 10.1007/s00726-011-0864-8.

[88] S. Gupta *et al.*, 'Mouse models of cystathionine β-synthase deficiency reveal significant threshold effects of hyperhomocysteinemia', *FASEB j.*, vol. 23, no. 3, pp. 883–893, Mar. 2009, doi: 10.1096/fj.08-120584.

[89] M. Watanabe *et al.*, 'Mice Deficient in Cystathionine β-Synthase: Animal Models for Mild and Severe Homocyst(e) inemia', *Proceedings of the National Academy of Sciences of the United States of America*, vol. 92, no. 5, pp. 1585–1589, 1995.

[90] L. Wang *et al.*, 'A pharmacological probe identifies cystathionine β-synthase as a new negative regulator for ferroptosis', *Cell Death Dis*, vol. 9, no. 10, p. 1005, Oct. 2018, doi: 10.1038/s41419-018-1063-2.

[91] L. J. Yant *et al.*, 'The selenoprotein GPX4 is essential for mouse development and protects from radiation and oxidative damage insults', *Free Radical Biology and Medicine*, vol. 34, no. 4, pp. 496–502, Feb. 2003, doi: 10.1016/S0891-5849(02)01360-6.

[92] H. Liang, S.-E. Yoo, R. Na, C. A. Walter, A. Richardson, and Q. Ran, 'Short Form Glutathione Peroxidase 4 Is the Essential Isoform Required for Survival and Somatic Mitochondrial Functions', *Journal of Biological Chemistry*, vol. 284, no. 45, pp. 30836–30844, Nov. 2009, doi: 10.1074/jbc.M109.032839.

[93] I. Ingold *et al.*, 'Expression of a Catalytically Inactive Mutant Form of Glutathione Peroxidase 4 (Gpx4) Confers a Dominant-negative Effect in Male Fertility', *Journal of Biological Chemistry*, vol. 290, no. 23, pp. 14668–14678, Jun. 2015, doi: 10.1074/jbc.M115.656363.

[94] S.-E. Yoo *et al.*, 'Gpx4 ablation in adult mice results in a lethal phenotype accompanied by neuronal loss in brain', *Free Radical Biology and Medicine*, vol. 52, no. 9, pp. 1820–1827, May 2012, doi: 10.1016/j.freeradbiomed.2012.02.043.

[95] T. P. Dalton, M. Z. Dieter, Y. Yang, H. G. Shertzer, and D. W. Nebert, 'Knockout of the Mouse Glutamate Cysteine Ligase Catalytic Subunit (Gclc) Gene: Embryonic Lethal When Homozygous, and Proposed Model for Moderate Glutathione Deficiency When Heterozygous', *Biochemical and Biophysical Research Communications*, vol. 279, no. 2, pp. 324–329, Dec. 2000, doi: 10.1006/bbrc.2000.3930.

[96] Z.-Z. Shi *et al.*, 'Glutathione synthesis is essential for mouse development but not for cell growth in culture', *Proc. Natl. Acad. Sci. U.S.A.*, vol. 97, no. 10, pp. 5101–5106, May 2000, doi: 10.1073/pnas.97.10.5101.

[97] L. A. McConnachie *et al.*, 'Glutamate Cysteine Ligase Modifier Subunit Deficiency and Gender as Determinants of Acetaminophen-Induced Hepatotoxicity in Mice', *Toxicological Sciences*, vol. 99, no. 2, pp. 628–636, Oct. 2007, doi: 10.1093/toxsci/kfm165.

[98] A. Winkler *et al.*, 'Glutathione is essential for early embryogenesis – Analysis of a glutathione synthetase knockout mouse', *Biochemical and Biophysical Research Communications*, vol. 412, no. 1, pp. 121–126, Aug. 2011, doi: 10.1016/j.bbrc.2011.07.056.

[99] I. S. Harris *et al.*, 'Glutathione and Thioredoxin Antioxidant Pathways Synergize to Drive Cancer Initiation and Progression', *Cancer Cell*, vol. 27, no. 2, pp. 211–222, Feb. 2015, doi: 10.1016/j.ccell.2014.11.019.

[100] M. D. Arensman *et al.*, 'Cystine–glutamate antiporter xCT deficiency suppresses tumor growth while preserving antitumor immunity', *Proc. Natl. Acad. Sci. U.S.A.*, vol. 116, no. 19, pp. 9533–9542, May 2019, doi: 10.1073/pnas.1814932116.

[101] S. Kshattry *et al.*, 'Enzyme-mediated depletion of l-cyst(e)ine synergizes with thioredoxin reductase inhibition for suppression of pancreatic tumor growth', *npj Precis. Onc.*, vol. 3, no. 1, p. 16, Dec. 2019, doi: 10.1038/s41698-019-0088-z.

[102] M. A. Badgley *et al.*, 'Cysteine depletion induces pancreatic tumor ferroptosis in mice', *Science*, vol. 368, no. 6486, pp. 85–89, Apr. 2020, doi: 10.1126/science.aaw9872.

[103] E. Dai *et al.*, 'Ferroptotic damage promotes pancreatic tumorigenesis through a TMEM173/STING-dependent DNA sensor pathway', *Nat Commun*, vol. 11, no. 1, p. 6339, Dec. 2020, doi: 10.1038/s41467-020-20154-8.

[104] I. Poursaitidis *et al.*, 'Oncogene-Selective Sensitivity to Synchronous Cell Death following Modulation of the Amino Acid Nutrient Cystine', *Cell Reports*, vol. 18, no. 11, pp. 2547–2556, Mar. 2017, doi: 10.1016/j.celrep.2017.02.054.

[105] P. S. Hole *et al.*, 'Ras-induced reactive oxygen species promote growth factor–independent proliferation in human CD34+ hematopoietic progenitor cells', *Blood*, vol. 115, no. 6, pp. 1238–1246, Feb. 2010, doi: 10.1182/blood-2009-06-222869.

[106] H.-J. Cho *et al.*, 'Oncogenic H-Ras Enhances DNA Repair through the Ras/Phosphatidylinositol 3-Kinase/Rac1 Pathway in NIH3T3 Cells: EVIDENCE FOR ASSOCIATION WITH REACTIVE OXYGEN SPECIES', *J. Biol. Chem.*, vol. 277, no. 22, pp. 19358–19366, May 2002, doi: 10.1074/jbc.M200933200.

[107] Y. Adachi, Y. Shibai, J. Mitsushita, W. H. Shang, K. Hirose, and T. Kamata, 'Oncogenic Ras upregulates NADPH oxidase 1 gene expression through MEK-ERK-dependent phosphorylation of GATA-6', *Oncogene*, vol. 27, no. 36, pp. 4921–4932, Aug. 2008, doi: 10.1038/onc.2008.133.

[108] M.-T. Park *et al.*, 'Novel signaling axis for ROS generation during K-Ras-induced cellular transformation', *Cell Death Differ*, vol. 21, no. 8, pp. 1185–1197, Aug. 2014, doi: 10.1038/cdd.2014.34.

[109] H.-Q. Ju *et al.*, 'Mutant Kras- and p16-regulated NOX4 activation overcomes metabolic checkpoints in development of pancreatic ductal adenocarcinoma', *Nat Commun*, vol. 8, no. 1, p. 14437, Apr. 2017, doi: 10.1038/ncomms14437.

[110] M. Liu *et al.*, 'Selective killing of cancer cells harboring mutant RAS by concomitant inhibition of NADPH oxidase and glutathione biosynthesis', *Cell Death Dis*, vol. 12, no. 2, p. 189, Feb. 2021, doi: 10.1038/s41419-021-03473-6.

[111] V. Aggarwal *et al.*, 'Role of Reactive Oxygen Species in Cancer Progression: Molecular Mechanisms and Recent Advancements', *Biomolecules*, vol. 9, no. 11, p. 735, Nov. 2019, doi: 10.3390/biom9110735.

[112] C. C. Woo, A. Hsu, A. P. Kumar, G. Sethi, and K. H. B. Tan, 'Thymoquinone Inhibits Tumor Growth and Induces Apoptosis in a Breast Cancer Xenograft Mouse Model: The Role of p38 MAPK and ROS', *PLoS ONE*, vol. 8, no. 10, p. e75356, Oct. 2013, doi: 10.1371/journal.pone.0075356.

[113] X. Dai *et al.*, 'A novel benzimidazole derivative, MBIC inhibits tumor growth and promotes apoptosis via activation of ROS-dependent JNK signaling pathway in hepatocellular carcinoma', *Oncotarget*, vol. 8, no. 8, pp. 12831–12842, Feb. 2017, doi: 10.18632/oncotarget.14606.

[114] J. D. Hayes, A. T. Dinkova-Kostova, and K. D. Tew, 'Oxidative Stress in Cancer', *Cancer Cell*, vol. 38, no. 2, pp. 167–197, Aug. 2020, doi: 10.1016/j.ccell.2020.06.001.

[115] G. M. DeNicola *et al.*, 'Oncogene-induced Nrf2 transcription promotes ROS detoxification and tumorigenesis', *Nature*, vol. 475, no. 7354, pp. 106–109, Jul. 2011, doi: 10.1038/nature10189.

[116] T. Nguyen, P. Nioi, and C. B. Pickett, 'The Nrf2-Antioxidant Response Element Signaling Pathway and Its Activation by Oxidative Stress', *J. Biol. Chem.*, vol. 284, no. 20, pp. 13291–13295, May 2009, doi: 10.1074/jbc.R900010200.

[117] Y. Yu *et al.*, 'The ferroptosis inducer erastin enhances sensitivity of acute myeloid leukemia cells to chemotherapeutic agents', *Molecular & Cellular Oncology*, vol. 2, no. 4, p. e1054549, Oct. 2015, doi: 10.1080/23723556.2015.1054549.

[118] C. Schott, U. Graab, N. Cuvelier, H. Hahn, and S. Fulda, 'Oncogenic RAS Mutants Confer Resistance of RMS13 Rhabdomyosarcoma Cells to Oxidative Stress-Induced Ferroptotic Cell Death', *Front. Oncol.*, vol. 5, Jun. 2015, doi: 10.3389/fonc.2015.00131.

[119] J. K. M. Lim *et al.*, 'Cystine/glutamate antiporter xCT (SLC7A11) facilitates oncogenic RAS transformation by preserving intracellular redox balance', *Proc. Natl.*

Acad. Sci. U.S.A., vol. 116, no. 19, pp. 9433–9442, May 2019, doi: 10.1073/pnas.1821323116.

[120] E. M. Kerr, E. Gaude, F. K. Turrell, C. Frezza, and C. P. Martins, 'Mutant Kras copy number defines metabolic reprogramming and therapeutic susceptibilities', *Nature*, vol. 531, no. 7592, pp. 110–113, Mar. 2016, doi: 10.1038/nature16967.

[121] K. Kawada, K. Toda, and Y. Sakai, 'Targeting metabolic reprogramming in KRAS-driven cancers', *Int J Clin Oncol*, vol. 22, no. 4, pp. 651–659, Aug. 2017, doi: 10.1007/s10147-017-1156-4.

[122] J. Wu *et al.*, 'Intercellular interaction dictates cancer cell ferroptosis via NF2–YAP signalling', *Nature*, vol. 572, no. 7769, pp. 402–406, Aug. 2019, doi: 10.1038/s41586-019-1426-6.

[123] D. Pan, 'The Hippo Signaling Pathway in Development and Cancer', *Developmental Cell*, vol. 19, no. 4, pp. 491–505, Oct. 2010, doi: 10.1016/j.devcel.2010.09.011.

[124] B. Zhao, Q.-Y. Lei, and K.-L. Guan, 'The Hippo–YAP pathway: new connections between regulation of organ size and cancer', *Current Opinion in Cell Biology*, vol. 20, no. 6, pp. 638–646, Dec. 2008, doi: 10.1016/j.ceb.2008.10.001.

[125] J. Wu *et al.*, 'Intercellular interaction dictates cancer cell ferroptosis via NF2–YAP signalling', *Nature*, vol. 572, no. 7769, pp. 402–406, Aug. 2019, doi: 10.1038/s41586-019-1426-6.

[126] M. Malumbres and M. Barbacid, 'RAS oncogenes: the first 30 years', *Nat Rev Cancer*, vol. 3, no. 6, pp. 459–465, Jun. 2003, doi: 10.1038/nrc1097.

[127] A. Hall, C. J. Marshall, N. K. Spurr, and R. A. Weiss, 'Identification of transforming gene in two human sarcoma cell lines as a new member of the ras gene family located on chromosome 1', *Nature*, vol. 303, no. 5916, pp. 396–400, Jun. 1983, doi: 10.1038/303396a0.

[128] K. Shimizu, M. Goldfarb, M. Perucho, and M. Wigler, 'Isolation and preliminary characterization of the transforming gene of a human neuroblastoma cell line.', *Proc. Natl. Acad. Sci. U.S.A.*, vol. 80, no. 2, pp. 383–387, Jan. 1983, doi: 10.1073/pnas.80.2.383.

[129] G. A. Hobbs, C. J. Der, and K. L. Rossman, 'RAS isoforms and mutations in cancer at a glance', *J Cell Sci*, vol. 129, no. 7, pp. 1287–1292, Apr. 2016, doi: 10.1242/jcs.182873.

[130] A. D. Cox and C. J. Der, ‘Ras history: The saga continues’, *Small GTPases*, vol. 1, no. 1, pp. 2–27, Jul. 2010, doi: 10.4161/sgtp.1.1.12178.

[131] J. Cherfils and M. Zeghouf, ‘Regulation of Small GTPases by GEFs, GAPs, and GDIs’, *Physiological Reviews*, vol. 93, no. 1, pp. 269–309, Jan. 2013, doi: 10.1152/physrev.00003.2012.

[132] C. Herrmann and N. Nassar, ‘Ras and its effectors’, *Progress in Biophysics and Molecular Biology*, vol. 66, no. 1, pp. 1–41, 1996, doi: 10.1016/S0079-6107(96)00015-6.

[133] A. K. Murugan, M. Grieco, and N. Tsuchida, ‘RAS mutations in human cancers: Roles in precision medicine’, *Seminars in Cancer Biology*, vol. 59, pp. 23–35, Dec. 2019, doi: 10.1016/j.semcancer.2019.06.007.

[134] A. Wittinghofer, Ed., *Ras Superfamily Small G Proteins: Biology and Mechanisms 1*. Vienna: Springer Vienna, 2014. doi: 10.1007/978-3-7091-1806-1.

[135] I. R. Vetter and A. Wittinghofer, ‘The Guanine Nucleotide-Binding Switch in Three Dimensions’, *Science*, vol. 294, no. 5545, pp. 1299–1304, Nov. 2001, doi: 10.1126/science.1062023.

[136] D. K. Simanshu, D. V. Nissley, and F. McCormick, ‘RAS Proteins and Their Regulators in Human Disease’, *Cell*, vol. 170, no. 1, pp. 17–33, Jun. 2017, doi: 10.1016/j.cell.2017.06.009.

[137] M. I. Parker, J. E. Meyer, E. A. Golemis, and R. L. Dunbrack, ‘Delineating the RAS Conformational Landscape’, *Cancer Research*, vol. 82, no. 13, pp. 2485–2498, Jul. 2022, doi: 10.1158/0008-5472.CAN-22-0804.

[138] M. Schwab, Ed., *Encyclopedia of Cancer*. Berlin, Heidelberg: Springer Berlin Heidelberg, 2011. doi: 10.1007/978-3-642-16483-5.

[139] L. Buday and J. Downward, ‘Many faces of Ras activation’, *Biochimica et Biophysica Acta (BBA) - Reviews on Cancer*, vol. 1786, no. 2, pp. 178–187, Dec. 2008, doi: 10.1016/j.bbcan.2008.05.001.

[140] J. Downward, ‘Targeting RAS signalling pathways in cancer therapy’, *Nat Rev Cancer*, vol. 3, no. 1, pp. 11–22, Jan. 2003, doi: 10.1038/nrc969.

[141] T. Tanaka and T. H. Rabbitts, ‘Interfering with protein-protein interactions: Potential for cancer therapy’, *Cell Cycle*, vol. 7, no. 11, pp. 1569–1574, Jun. 2008, doi: 10.4161/cc.7.11.6061.

[142] C. Wellbrock, M. Karasarides, and R. Marais, 'The RAF proteins take centre stage', *Nat Rev Mol Cell Biol*, vol. 5, no. 11, pp. 875–885, Nov. 2004, doi: 10.1038/nrm1498.

[143] U. R. Rapp *et al.*, 'Structure and biological activity of v-raf, a unique oncogene transduced by a retrovirus.', *Proc. Natl. Acad. Sci. U.S.A.*, vol. 80, no. 14, pp. 4218–4222, Jul. 1983, doi: 10.1073/pnas.80.14.4218.

[144] A. S. Dhillon, 'Regulation of Raf-1 activation and signalling by dephosphorylation', *The EMBO Journal*, vol. 21, no. 1, pp. 64–71, Jan. 2002, doi: 10.1093/emboj/21.1.64.

[145] O. Tatli and G. Dinler Doganay, 'Recent Developments in Targeting RAS Downstream Effectors for RAS-Driven Cancer Therapy', *Molecules*, vol. 26, no. 24, p. 7561, Dec. 2021, doi: 10.3390/molecules26247561.

[146] T. L. Yuan and L. C. Cantley, 'PI3K pathway alterations in cancer: variations on a theme', *Oncogene*, vol. 27, no. 41, pp. 5497–5510, Sep. 2008, doi: 10.1038/onc.2008.245.

[147] J. Á. F. Vara, E. Casado, J. de Castro, P. Cejas, C. Belda-Iniesta, and M. González-Barón, 'PI3K/Akt signalling pathway and cancer', *Cancer Treatment Reviews*, vol. 30, no. 2, pp. 193–204, Apr. 2004, doi: 10.1016/j.ctrv.2003.07.007.

[148] I. A. Prior, F. E. Hood, and J. L. Hartley, 'The Frequency of Ras Mutations in Cancer', *Cancer Research*, vol. 80, no. 14, pp. 2969–2974, Jul. 2020, doi: 10.1158/0008-5472.CAN-19-3682.

[149] K. Rajalingam, R. Schreck, U. R. Rapp, and Š. Albert, 'Ras oncogenes and their downstream targets', *Biochimica et Biophysica Acta (BBA) - Molecular Cell Research*, vol. 1773, no. 8, pp. 1177–1195, Aug. 2007, doi: 10.1016/j.bbamcr.2007.01.012.

[150] I. A. Prior, P. D. Lewis, and C. Mattos, 'A Comprehensive Survey of Ras Mutations in Cancer', *Cancer Research*, vol. 72, no. 10, pp. 2457–2467, May 2012, doi: 10.1158/0008-5472.CAN-11-2612.

[151] M. E. Salem *et al.*, 'Landscape of *KRAS* ^{G12C} , Associated Genomic Alterations, and Interrelation With Immuno-Oncology Biomarkers in *KRAS* -Mutated Cancers', *JCO Precision Oncology*, no. 6, p. e2100245, May 2022, doi: 10.1200/PO.21.00245.

[152] A. D. Cox, S. W. Fesik, A. C. Kimmelman, J. Luo, and C. J. Der, 'Drugging the undruggable RAS: Mission Possible?', *Nat Rev Drug Discov*, vol. 13, no. 11, pp. 828–851, Nov. 2014, doi: 10.1038/nrd4389.

[153] T. Maurer *et al.*, 'Small-molecule ligands bind to a distinct pocket in Ras and inhibit SOS-mediated nucleotide exchange activity', *Proc. Natl. Acad. Sci. U.S.A.*, vol. 109, no. 14, pp. 5299–5304, Apr. 2012, doi: 10.1073/pnas.1116510109.

[154] Q. Sun *et al.*, 'Discovery of Small Molecules that Bind to K-Ras and Inhibit Sos-Mediated Activation', *Angew. Chem. Int. Ed.*, vol. 51, no. 25, pp. 6140–6143, Jun. 2012, doi: 10.1002/anie.201201358.

[155] F. Shima *et al.*, '*In silico* discovery of small-molecule Ras inhibitors that display antitumor activity by blocking the Ras–effector interaction', *Proc. Natl. Acad. Sci. U.S.A.*, vol. 110, no. 20, pp. 8182–8187, May 2013, doi: 10.1073/pnas.1217730110.

[156] A. D. Cox, C. J. Der, and M. R. Philips, 'Targeting RAS Membrane Association: Back to the Future for Anti-RAS Drug Discovery?', *Clinical Cancer Research*, vol. 21, no. 8, pp. 1819–1827, Apr. 2015, doi: 10.1158/1078-0432.CCR-14-3214.

[157] A. A. Samatar and P. I. Poulikakos, 'Targeting RAS–ERK signalling in cancer: promises and challenges', *Nat Rev Drug Discov*, vol. 13, no. 12, pp. 928–942, Dec. 2014, doi: 10.1038/nrd4281.

[158] D. A. Fruman and C. Rommel, 'PI3K and cancer: lessons, challenges and opportunities', *Nat Rev Drug Discov*, vol. 13, no. 2, pp. 140–156, Feb. 2014, doi: 10.1038/nrd4204.

[159] C. V. Pecot *et al.*, 'Therapeutic Silencing of KRAS Using Systemically Delivered siRNAs', *Molecular Cancer Therapeutics*, vol. 13, no. 12, pp. 2876–2885, Dec. 2014, doi: 10.1158/1535-7163.MCT-14-0074.

[160] T. L. Yuan *et al.*, 'Development of siRNA Payloads to Target *KRAS* -Mutant Cancer', *Cancer Discovery*, vol. 4, no. 10, pp. 1182–1197, Oct. 2014, doi: 10.1158/2159-8290.CD-13-0900.

[161] Y. Zhang, J.-A. Ma, H.-X. Zhang, Y.-N. Jiang, and W.-H. Luo, 'Cancer vaccines: Targeting KRAS-driven cancers', *Expert Review of Vaccines*, vol. 19, no. 2, pp. 163–173, Feb. 2020, doi: 10.1080/14760584.2020.1733420.

[162] J. M. Ostrem, U. Peters, M. L. Sos, J. A. Wells, and K. M. Shokat, 'K-Ras(G12C) inhibitors allosterically control GTP affinity and effector interactions', *Nature*, vol. 503, no. 7477, pp. 548–551, Nov. 2013, doi: 10.1038/nature12796.

[163] J. C. Hunter *et al.*, 'In situ selectivity profiling and crystal structure of SML-8-73-1, an active site inhibitor of oncogenic K-Ras G12C', *Proc. Natl. Acad. Sci. U.S.A.*, vol. 111, no. 24, pp. 8895–8900, Jun. 2014, doi: 10.1073/pnas.1404639111.

[164] J. Canon *et al.*, 'The clinical KRAS(G12C) inhibitor AMG 510 drives anti-tumour immunity', *Nature*, vol. 575, no. 7781, pp. 217–223, Nov. 2019, doi: 10.1038/s41586-019-1694-1.

[165] J. Hallin *et al.*, 'The KRASG12C Inhibitor MRTX849 Provides Insight toward Therapeutic Susceptibility of KRAS-Mutant Cancers in Mouse Models and Patients', *Cancer Discovery*, vol. 10, no. 1, pp. 54–71, Jan. 2020, doi: 10.1158/2159-8290.CD-19-1167.

[166] Z. Zhang, K. Z. Guiley, and K. M. Shokat, 'Chemical acylation of an acquired serine suppresses oncogenic signaling of K-Ras(G12S)', *Nat Chem Biol*, vol. 18, no. 11, pp. 1177–1183, Nov. 2022, doi: 10.1038/s41589-022-01065-9.

[167] J. Hallin *et al.*, 'Anti-tumor efficacy of a potent and selective non-covalent KRASG12D inhibitor', *Nat Med*, vol. 28, no. 10, pp. 2171–2182, Oct. 2022, doi: 10.1038/s41591-022-02007-7.

[168] A. Ashkenazi *et al.*, 'Safety and antitumor activity of recombinant soluble Apo2 ligand', *J. Clin. Invest.*, vol. 104, no. 2, pp. 155–162, Jul. 1999, doi: 10.1172/JCI6926.

[169] H. Walczak *et al.*, 'Tumoricidal activity of tumor necrosis factor–related apoptosis–inducing ligand in vivo', *Nat Med*, vol. 5, no. 2, pp. 157–163, Feb. 1999, doi: 10.1038/5517.

[170] N. V. Koshkina, C. Khanna, A. Mendoza, H. Guan, L. DeLauter, and E. S. Kleinerman, 'Fas-Negative Osteosarcoma Tumor Cells Are Selected during Metastasis to the Lungs: The Role of the Fas Pathway in the Metastatic Process of Osteosarcoma', *Molecular Cancer Research*, vol. 5, no. 10, pp. 991–999, Oct. 2007, doi: 10.1158/1541-7786.MCR-07-0007.

[171] M. J. Smyth *et al.*, 'Tumor Necrosis Factor–related Apoptosis-inducing Ligand (TRAIL) Contributes to Interferon ⁄–dependent Natural Killer Cell Protection from Tumor Metastasis', 2001.

[172] K. Takeda *et al.*, 'Involvement of tumor necrosis factor-related apoptosis-inducing ligand in surveillance of tumor metastasis by liver natural killer cells', *Nat Med*, vol. 7, no. 1, pp. 94–100, Jan. 2001, doi: 10.1038/83416.

[173] D. Yang, T. J. Stewart, K. K. Smith, D. Georgi, S. I. Abrams, and K. Liu, 'Downregulation of IFN-γR in association with loss of Fas function is linked to tumor progression: Cooperative Loss of IFN-γR and Fas in Tumor Escape', *Int. J. Cancer*, vol. 122, no. 2, pp. 350–362, Jan. 2008, doi: 10.1002/ijc.23090.

[174] J. Lemke, S. von Karstedt, J. Zinngrebe, and H. Walczak, 'Getting TRAIL back on track for cancer therapy', *Cell Death Differ*, vol. 21, no. 9, pp. 1350–1364, Sep. 2014, doi: 10.1038/cdd.2014.81.

[175] B. C. Barnhart, P. Legembre, E. Pietras, C. Bubici, G. Franzoso, and M. E. Peter, 'CD95 ligand induces motility and invasiveness of apoptosis-resistant tumor cells', *EMBO J*, vol. 23, no. 15, pp. 3175–3185, Aug. 2004, doi: 10.1038/sj.emboj.7600325.

[176] A. Trauzold *et al.*, 'CD95 and TRAF2 promote invasiveness of pancreatic cancer cells', *FASEB j.*, vol. 19, no. 6, pp. 1–24, Apr. 2005, doi: 10.1096/fj.04-2984fje.

[177] A. Trauzold *et al.*, 'TRAIL promotes metastasis of human pancreatic ductal adenocarcinoma', *Oncogene*, vol. 25, no. 56, pp. 7434–7439, Nov. 2006, doi: 10.1038/sj.onc.1209719.

[178] S. Kleber *et al.*, 'Yes and PI3K Bind CD95 to Signal Invasion of Glioblastoma', *Cancer Cell*, vol. 13, no. 3, pp. 235–248, Mar. 2008, doi: 10.1016/j.ccr.2008.02.003.

[179] M. E. Peter, P. Legembre, and B. C. Barnhart, 'Does CD95 have tumor promoting activities?', *Biochimica et Biophysica Acta (BBA) - Reviews on Cancer*, vol. 1755, no. 1, pp. 25–36, May 2005, doi: 10.1016/j.bbcan.2005.01.001.

[180] M. E. Peter *et al.*, 'The CD95 Receptor: Apoptosis Revisited', *Cell*, vol. 129, no. 3, pp. 447–450, May 2007, doi: 10.1016/j.cell.2007.04.031.

[181] E. Varfolomeev *et al.*, 'Molecular Determinants of Kinase Pathway Activation by Apo2 Ligand/Tumor Necrosis Factor-related Apoptosis-inducing Ligand', *Journal of Biological Chemistry*, vol. 280, no. 49, pp. 40599–40608, Dec. 2005, doi: 10.1074/jbc.M509560200.

[182] L. L. Belyanskaya *et al.*, 'TRAIL-induced survival and proliferation of SCLC cells is mediated by ERK and dependent on TRAIL-R2/DR5 expression in the absence of caspase-8', *Lung Cancer*, vol. 60, no. 3, pp. 355–365, Jun. 2008, doi: 10.1016/j.lungcan.2007.11.005.

[183] F. J. H. Hoogwater *et al.*, 'Oncogenic K-Ras Turns Death Receptors Into Metastasis-Promoting Receptors in Human and Mouse Colorectal Cancer Cells', *Gastroenterology*, vol. 138, no. 7, pp. 2357–2367, Jun. 2010, doi: 10.1053/j.gastro.2010.02.046.

[184] S. von Karstedt *et al.*, 'Cancer Cell-Autonomous TRAIL-R Signaling Promotes KRAS-Driven Cancer Progression, Invasion, and Metastasis', *Cancer Cell*, vol. 27, no. 4, pp. 561–573, Apr. 2015, doi: 10.1016/j.ccell.2015.02.014.

[185] W.-H. Yang and J.-T. Chi, 'Hippo pathway effectors YAP/TAZ as novel determinants of ferroptosis', *Molecular & Cellular Oncology*, vol. 7, no. 1, p. 1699375, Jan. 2020, doi: 10.1080/23723556.2019.1699375.

[186] S. Gysin, P. Rickert, K. Kastury, and M. McMahon, 'Analysis of genomic DNA alterations and mRNA expression patterns in a panel of human pancreatic cancer cell lines', *Genes Chromosom. Cancer*, vol. 44, no. 1, pp. 37–51, Sep. 2005, doi: 10.1002/gcc.20216.

[187] X. Jiang, B. R. Stockwell, and M. Conrad, 'Ferroptosis: mechanisms, biology and role in disease', *Nat Rev Mol Cell Biol*, vol. 22, no. 4, pp. 266–282, Apr. 2021, doi: 10.1038/s41580-020-00324-8.

[188] L. Li, H. Dong, E. Song, X. Xu, L. Liu, and Y. Song, 'Nrf2/ARE pathway activation, HO-1 and NQO1 induction by polychlorinated biphenyl quinone is associated with reactive oxygen species and PI3K/AKT signaling', *Chemico-Biological Interactions*, vol. 209, pp. 56–67, Feb. 2014, doi: 10.1016/j.cbi.2013.12.005.

[189] M. Ogrunc *et al.*, 'Oncogene-induced reactive oxygen species fuel hyperproliferation and DNA damage response activation', *Cell Death Differ*, vol. 21, no. 6, pp. 998–1012, Jun. 2014, doi: 10.1038/cdd.2014.16.

[190] J. Mitsushita, J. D. Lambeth, and T. Kamata, 'The Superoxide-Generating Oxidase Nox1 Is Functionally Required for Ras Oncogene Transformation', *Cancer Research*, vol. 64, no. 10, pp. 3580–3585, May 2004, doi: 10.1158/0008-5472.CAN-03-3909.

[191] Tauskela JS., 'MitoQ-a mitochondria-targeted antioxidant.', *IDrugs.*, no. 2007 Jun;10(6), pp. 399–412.

[192] M. E. Solesio *et al.*, 'The mitochondria-targeted anti-oxidant MitoQ reduces aspects of mitochondrial fission in the 6-OHDA cell model of Parkinson's disease', *Biochimica et Biophysica Acta (BBA) - Molecular Basis of Disease*, vol. 1832, no. 1, pp. 174–182, Jan. 2013, doi: 10.1016/j.bbadis.2012.07.009.

[193] P. Storz, 'KRas, ROS and the initiation of pancreatic cancer', *Small GTPases*, vol. 8, no. 1, pp. 38–42, Jan. 2017, doi: 10.1080/21541248.2016.1192714.

[194] C. Bartolacci, C. Andreani, Y. El-Gammal, and P. P. Scaglioni, 'Lipid Metabolism Regulates Oxidative Stress and Ferroptosis in RAS-Driven Cancers: A Perspective on Cancer Progression and Therapy', *Front. Mol. Biosci.*, vol. 8, p. 706650, Aug. 2021, doi: 10.3389/fmolb.2021.706650.

[195] N. Santana-Codina *et al.*, 'Oncogenic KRAS supports pancreatic cancer through regulation of nucleotide synthesis', *Nat Commun*, vol. 9, no. 1, p. 4945, Dec. 2018, doi: 10.1038/s41467-018-07472-8.

[196] K. O. Alfarouk *et al.*, 'The Pentose Phosphate Pathway Dynamics in Cancer and Its Dependency on Intracellular pH', *Metabolites*, vol. 10, no. 7, p. 285, Jul. 2020, doi: 10.3390/metabo10070285.

[197] K. Shimada, M. Hayano, N. C. Pagano, and B. R. Stockwell, 'Cell-Line Selectivity Improves the Predictive Power of Pharmacogenomic Analyses and Helps Identify NADPH as Biomarker for Ferroptosis Sensitivity', *Cell Chemical Biology*, vol. 23, no. 2, pp. 225–235, Feb. 2016, doi: 10.1016/j.chembiol.2015.11.016.

[198] W. Kuo, J. Lin, and T. K. Tang, 'Human glucose-6-phosphate dehydrogenase (G6PD) gene transforms NIH 3T3 cells and induces tumors in nude mice', *Int. J. Cancer*, vol. 85, no. 6, pp. 857–864, Mar. 2000, doi: 10.1002/(SICI)1097-0215(20000315)85:6<857::AID-IJC20>3.0.CO;2-U.

[199] H. P. Nguyen *et al.*, 'Aifm2, a NADH Oxidase, Supports Robust Glycolysis and Is Required for Cold- and Diet-Induced Thermogenesis', *Molecular Cell*, vol. 77, no. 3, pp. 600-617.e4, Feb. 2020, doi: 10.1016/j.molcel.2019.12.002.

[200] S. Ganapathy-Kanniappan and J.-F. H. Geschwind, 'Tumor glycolysis as a target for cancer therapy: progress and prospects', *Mol Cancer*, vol. 12, no. 1, p. 152, 2013, doi: 10.1186/1476-4598-12-152.

[201] A. Nickless, J. M. Bailis, and Z. You, 'Control of gene expression through the nonsense-mediated RNA decay pathway', *Cell Biosci*, vol. 7, no. 1, p. 26, Dec. 2017, doi: 10.1186/s13578-017-0153-7.

[202] S. Lykke-Andersen and T. H. Jensen, 'Nonsense-mediated mRNA decay: an intricate machinery that shapes transcriptomes', *Nat Rev Mol Cell Biol*, vol. 16, no. 11, pp. 665–677, Nov. 2015, doi: 10.1038/nrm4063.

[203] J. A. Hurt, A. D. Robertson, and C. B. Burge, 'Global analyses of UPF1 binding and function reveal expanded scope of nonsense-mediated mRNA decay', *Genome Res.*, vol. 23, no. 10, pp. 1636–1650, Oct. 2013, doi: 10.1101/gr.157354.113.

[204] A. Nickless, A. Cheruiyot, K. C. Flanagan, D. Piwnica-Worms, S. A. Stewart, and Z. You, 'p38 MAPK inhibits nonsense-mediated RNA decay in response to persistent DNA damage in noncycling cells', *Journal of Biological Chemistry*, vol. 292, no. 37, pp. 15266–15276, Sep. 2017, doi: 10.1074/jbc.M117.787846.

[205] M. A. Coelho *et al.*, 'Oncogenic RAS Signaling Promotes Tumor Immunoresistance by Stabilizing PD-L1 mRNA', *Immunity*, vol. 47, no. 6, pp. 1083-1099.e6, Dec. 2017, doi: 10.1016/j.immuni.2017.11.016.

[206] L. Munoz, Y. T. Yeung, and T. Grewal, 'Oncogenic Ras modulates p38 MAPK-mediated inflammatory cytokine production in glioblastoma cells', *Cancer Biology & Therapy*, vol. 17, no. 4, pp. 355–363, Apr. 2016, doi: 10.1080/15384047.2016.1139249.

[207] W. J. van Houdt *et al.*, 'Oncogenic K-Ras Activates p38 to Maintain Colorectal Cancer Cell Proliferation during MEK Inhibition', *Analytical Cellular Pathology*, vol. 32, no. 4, pp. 245–257, Jan. 2010, doi: 10.1155/2010/120143.

[208] G. Ramadori *et al.*, 'Diet-Induced Unresolved ER Stress Hinders KRAS-Driven Lung Tumorigenesis', *Cell Metabolism*, vol. 21, no. 1, pp. 117–125, Jan. 2015, doi: 10.1016/j.cmet.2014.11.020.

[209] Z. Li, J. K. Vuong, M. Zhang, C. Stork, and S. Zheng, 'Inhibition of nonsense-mediated RNA decay by ER stress', *RNA*, vol. 23, no. 3, pp. 378–394, Mar. 2017, doi: 10.1261/rna.058040.116.

[210] H. Yoshioka *et al.*, 'Identification of a Small Molecule That Enhances Ferroptosis via Inhibition of Ferroptosis Suppressor Protein 1 (FSP1)', *ACS Chem. Biol.*, vol. 17, no. 2, pp. 483–491, Feb. 2022, doi: 10.1021/acschembio.2c00028.

[211] O. Kakhlon, Y. Gruenbaum, and Z. I. Cabantchik, 'Repression of ferritin expression modulates cell responsiveness to H-ras-induced growth', *Biochemical Society Transactions*, vol. 30, no. 4, pp. 777–780, Aug. 2002, doi: 10.1042/bst0300777.

[212] N. Takahashi *et al.*, '3D Culture Models with CRISPR Screens Reveal Hyperactive NRF2 as a Prerequisite for Spheroid Formation via Regulation of Proliferation and Ferroptosis', *Molecular Cell*, vol. 80, no. 5, pp. 828-844.e6, Dec. 2020, doi: 10.1016/j.molcel.2020.10.010.

[213] G. C. Forcina *et al.*, 'Ferroptosis regulation by the NGLY1/NFE2L1 pathway', *Proc. Natl. Acad. Sci. U.S.A.*, vol. 119, no. 11, p. e2118646119, Mar. 2022, doi: 10.1073/pnas.2118646119.

[214] M. Conlon *et al.*, 'A compendium of kinetic modulatory profiles identifies ferroptosis regulators', *Nat Chem Biol*, vol. 17, no. 6, pp. 665–674, Jun. 2021, doi: 10.1038/s41589-021-00751-4.

[215] Q. Ong, S. Guo, K. Zhang, and B. Cui, ‘U0126 Protects Cells against Oxidative Stress Independent of Its Function as a MEK Inhibitor’, *ACS Chem. Neurosci.*, vol. 6, no. 1, pp. 130–137, Jan. 2015, doi: 10.1021/cn500288n.

[216] G. Sharbeen *et al.*, ‘Cancer-Associated Fibroblasts in Pancreatic Ductal Adenocarcinoma Determine Response to SLC7A11 Inhibition’, *Cancer Research*, vol. 81, no. 13, pp. 3461–3479, Jul. 2021, doi: 10.1158/0008-5472.CAN-20-2496.

[217] J. Lewerenz *et al.*, ‘The Cystine/Glutamate Antiporter System x_c^- in Health and Disease: From Molecular Mechanisms to Novel Therapeutic Opportunities’, *Antioxidants & Redox Signaling*, vol. 18, no. 5, pp. 522–555, Feb. 2013, doi: 10.1089/ars.2011.4391.

[218] M. Schneider *et al.*, ‘Absence of Glutathione Peroxidase 4 Affects Tumor Angiogenesis through Increased 12/15-Lipoxygenase Activity’, *Neoplasia*, vol. 12, no. 3, pp. 254–263, Mar. 2010, doi: 10.1593/neo.91782.

[219] W.-H. Yang *et al.*, ‘The Hippo Pathway Effector TAZ Regulates Ferroptosis in Renal Cell Carcinoma’, *Cell Reports*, vol. 28, no. 10, pp. 2501-2508.e4, Sep. 2019, doi: 10.1016/j.celrep.2019.07.107.

[220] W.-H. Yang, Z. Huang, J. Wu, C.-K. C. Ding, S. K. Murphy, and J.-T. Chi, ‘A TAZ–ANGPTL4–NOX2 Axis Regulates Ferroptotic Cell Death and Chemoresistance in Epithelial Ovarian Cancer’, *Molecular Cancer Research*, vol. 18, no. 1, pp. 79–90, Jan. 2020, doi: 10.1158/1541-7786.MCR-19-0691.

[221] M. Vucetic, B. Daher, S. Cassim, W. Meira, and J. Pouyssegur, ‘Together we stand, apart we fall: how cell-to-cell contact/interplay provides resistance to ferroptosis’, *Cell Death Dis*, vol. 11, no. 9, p. 789, Sep. 2020, doi: 10.1038/s41419-020-02994-w.

[222] E. Donato, F. Biagioni, A. Bisso, M. Caganova, B. Amati, and S. Campaner, ‘YAP and TAZ are dispensable for physiological and malignant haematopoiesis’, *Leukemia*, vol. 32, no. 9, pp. 2037–2040, Sep. 2018, doi: 10.1038/s41375-018-0111-3.

EIDESSTATTLICHE ERKLÄRUNG ZUR DISSERTATION

gemäß der Promotionsordnung vom 12. März 2020

Hiermit versichere ich an Eides statt, dass ich die vorliegende Dissertation selbstständig und ohne die Benutzung anderer als der angegebenen Hilfsmittel und Literatur angefertigt habe. Alle Stellen, die wörtlich oder sinngemäß aus veröffentlichten und nicht veröffentlichten Werken dem Wortlaut oder dem Sinn nach entnommen wurden, sind als solche kenntlich gemacht. Ich versichere an Eides statt, dass diese Dissertation noch keiner anderen Fakultät oder Universität zur Prüfung vorgelegen hat; dass sie - abgesehen von unten angegebenen Teilpublikationen und eingebundenen Artikeln und Manuskripten - noch nicht veröffentlicht worden ist sowie, dass ich eine Veröffentlichung der Dissertation vor Abschluss der Promotion nicht ohne Genehmigung des Promotionsausschusses vornehmen werde. Die Bestimmungen dieser Ordnung sind mir bekannt. Darüber hinaus erkläre ich hiermit, dass ich die Ordnung zur Sicherung guter wissenschaftlicher Praxis und zum Umgang mit wissenschaftlichem Fehlverhalten der Universität zu Köln gelesen und sie bei der Durchführung der Dissertation zugrundeliegenden Arbeiten und der schriftlich verfassten Dissertation beachtet habe und verpflichte mich hiermit, die dort genannten Vorgaben bei allen wissenschaftlichen Tätigkeiten zu beachten und umzusetzen. Ich versichere, dass die eingereichte elektronische Fassung der eingereichten Druckfassung vollständig entspricht.

Teilpublikationen:

Müller F, Lim JKM, Bebber CM, Seidel E, Tishina S, Dahlhaus A, Stroh J, Beck J, Yapici FI, Nakayama K, Torres Fernández L, Brägelmann J, Leprivier G, von Karstedt S.
Elevated FSP1 protects KRAS-mutated cells from ferroptosis during tumor initiation
Cell Death Differ. 2022 Nov 29. doi: 10.1038/s41418-022-01096-8. PMID: 36443441

Fabienne Müller
Köln, 19.12.2022

ACKNOWLEDGEMENT

First of all, I would like to thank my supervisor Prof. Dr. Silvia von Karstedt, who gave me the opportunity to complete my PhD in her lab. Thank you for your big support over the past 4 years, for the excellent guidance, the motivational support, and the constant encouragement. You pushed me through good and hard times, and you gave me the possibility to evolve and grow as a scientist.

I also would like to thank Prof. Dr. Manolis Pasparakis and Prof. Dr. Martin Sos for their support and scientific guidance during my PhD thesis. Moreover, I would like to thank Prof. Dr. Jan Riemer who kindly agreed to take part in my dissertation defense as a member of my thesis advisory committee.

Mostly, I would like to thank the whole von Karstedt lab who supported me over all these years. Especially, I want to thank Alina Dahlhaus, Jenny Stroh, Christina Bebber, Isil Yapici, Sofya Tishnia, Eric Seidel, Ariadne Androulidaki, Fanyu Liu and Julia Beck for their contribution to my project, for listening to my problems, for fruitful discussions and for working in a great atmosphere. Moreover, a special thank-you goes to Alina Dahlhaus, who really helped and supported me in the past year and Christina Bebber for proofreading my PhD thesis.

Zum Schluss möchte ich meiner Familie danken, allen voran meinen Eltern. Ohne eure bedingungslose, großartige Unterstützung während der Promotion und meines gesamten Studiums hätte ich es nicht bis hierhin geschafft. Ein großes Dankeschön gilt auch meinen Schwestern und all meinen Freundinnen und Freunden, die mich auf diesem Weg immer begleitet haben, die mir zugehört haben, die mich gestärkt haben und die mir Mut und Kraft gegeben haben. Ohne euch hätte ich die Promotionsphase nicht so gut überstanden. Danke, dass ihr immer für mich da wart.

Insbesondere möchte ich Hannah danken. Danke, dass du dir all meine Sorgen angehört hast. Danke, dass du mich verstanden hast und mir mit Rat und Tat zur Seite standest. Danke, dass du immer für mich da warst. Danke, dass wir diese Zeit gemeinsam gemeistert haben. Ich wüsste nicht, was ich ohne dich gemacht hätte.